11. RADIONUCLIDE TRANSPORT IN THE UNSATURATED ZONE

11.1 INTRODUCTION

This section describes process model results, related uncertainties, and total system performance assessment (TSPA) model abstractions concerning radionuclide transport between the potential repository and the water table. The following analysis model reports provide documentation associated with this subject:

- *UZ Flow Models and Submodels* (CRWMS M&O 2000 [DIRS 122797]) provides three-dimensional site-scale transport results for technetium and neptunium using different flow models and climate scenarios

- *Radionuclide Transport Models under Ambient Conditions* (CRWMS M&O 2000 [DIRS 144331]) describes the basis for process transport models and transport sensitivity results for two and three-dimensional site-scale models, including colloid-facilitated radionuclide transport

- *Analysis of Base-Case Particle Tracking Results of the Base-Case Flow Fields (ID: U0160)* (CRWMS M&O 2000 [DIRS 134732]) describes sensitivity studies using the TSPA transport model for the three-dimensional site-scale transport problem, including comparisons between the TSPA transport model and a process transport model

- *Analysis Comparing Advective-Dispersive Transport Solution to Particle Tracking* (CRWMS M&O 2000 [DIRS 141389]) provides comparisons of the particle-tracking transport models and a direct-solution process model for transport in a one-dimensional system

- *Fault Displacement Effects on Transport in the Unsaturated Zone* (CRWMS M&O 2000 [DIRS 151953]) describes sensitivity studies concerning the effects of variations in fracture characteristics on transport

- *Particle Tracking Model and Abstraction of Transport Processes* (CRWMS M&O 2000 [DIRS 141418])–describes the TSPA model for unsaturated zone (UZ) transport

- *UZ Colloid Transport Model* (CRWMS M&O 2000 [DIRS 122799]) presents process-model results for colloid-facilitated radionuclide transport

- *Unsaturated Zone Flow and Transport Model Process Model Report* (CRWMS M&O 2000 [DIRS 151940]) provides a summary of all UZ processes and TSPA abstractions, including UZ transport.

Radionuclides released from the engineered barrier system (EBS) would enter the natural environment in the UZ. The primary mechanism by which radionuclides can migrate through the UZ is aqueous transport (CRWMS M&O 2000 [DIRS 151940], Section 3.3.11). Water carrying radionuclides is expected to generally move downwards, with some component of lateral motion caused by flow diversion around low-permeability horizons (e.g., where perched water flows into fault zones) (CRWMS M&O 2000 [DIRS 151940], Figure 3.7-8b). Diffusion, sorption, dispersion, decay, and colloid interactions are additional processes that influence general advective radionuclide movement.

UZ transport modeling follows the general concepts used for development of the UZ flow model (CRWMS M&O 2000 [DIRS 151940], Section 3.7). Transport in fractured rock is approximated by a dual continuum model in which solute transport can occur in both the fracture continuum and the matrix continuum, with dynamic exchange between these continua through advective and diffusive transport. The transport models for radionuclide movement to the water table use the same grid as the site-scale UZ flow model. Radionuclide sorption is modeled using an infinite-capacity linear equilibrium model.

Colloid-facilitated radionuclide transport is modeled using a combination of two modes of interaction between aqueous radionuclides and radionuclides associated with colloids (CRWMS M&O 2000 [DIRS 151940], Sections 3.11.7 and 3.11.13). Radionuclides can either sorb to colloids following a linear sorption model (termed the reversible colloid-facilitated radionuclide transport model), or they can be permanently bound to the colloid (termed the irreversible colloid-facilitated radionuclide transport model). In the TSPA transport model (CRWMS M&O 2000 [DIRS 151940], Section 3.11.13), colloid filtration was limited to physical straining at tuff layer interfaces. Process model calculations for transport treated colloid filtration as a linear kinetic process. Dispersion was included using a standard Fickian representation. Radioactive decay, including chain decay, was included in the models.

11.2 TREATMENT OF UNSATURATED ZONE TRANSPORT ISSUES

This section identifies the set of five model refinements that have been evaluated for modeling radionuclide transport through the UZ from the potential repository to the water table. Subsequent subsections describe the methods used to perform these evaluations and the implications the model refinements have for modeling radionuclide transport to support TSPA evaluations of potential repository system performance. These sections represent new work and extensions of existing work. Table 11-1 identifies the primary reason for development of each section and indicates which of these analyses have been included in TSPA calculations.

11.2.1 Transport in the Drift Shadow

Process Description–The hydrologic conditions beneath waste emplacement drifts are affected by the diversion of seepage around the drift. This diversion of seepage results in a zone of reduced water saturations and flow beneath waste emplacement drifts.

An important aspect of radionuclide transport in the vicinity of the drift is how radionuclides enter the rock. Radionuclides can enter the rock from waste emplacement drifts as a result of diffusive transport or a combination of advection and diffusion. If seepage into the drift is substantial, the radionuclides will be advected out of the drift, predominantly into the rock fractures. If seepage into the drift is sufficiently small, radionuclides will either advect or diffuse, predominantly into the rock matrix. Diffusive releases of radionuclides from the drift will predominantly enter the rock matrix because its water content is considerably larger than the water content of the fractures, providing a greater cross section for diffusion. Initiating transport

Table 11-1. Summary of Supplemental Models and Analyses

			Reason For Supplemental Scientific Model or Analysis				Performance Assessment Treatment of Supplemental Scientific Model or Analysis[a]	
Key Attributes of System	**Process Model (Section of S&ER)**	**Topic of Supplemental Scientific Model or Analysis**	**Unquantified Uncertainty Analysis**	**Update in Scientific Information**	**Lower-Temperature Operating Mode Analysis**	**Section of Volume 1**	**TSPA Sensitivity Analysis**	**Included in Supplemental TSPA Model**
Delay and Dilution of Radionuclide Concentrations by the Natural Barriers	Unsaturated Zone Radionuclide Transport (Advective Pathways; Retardation; Dispersion; Dilution) (4.2.8)	Effect of drift shadow zone - advection/diffusion splitting	X		X	11.3.1	X	X
		Effect of drift shadow zone – concentration boundary condition on EBS release rates	X			11.3.1		
		Effect of matrix diffusion	X			11.3.2 11.3.3		
		3-D transport			X	11.3.2		
		Effect of coupled Thermo-Hydrologic, Thermo-Hydro-Chemical, and Thermo-Hydro-Mechanical processes on transport		X	X	11.3.5		

NOTE: S&ER = *Yucca Mountain Science and Engineering Report* (DOE 2001 [DIRS 153849]).
[a] Performance assessment treatment of supplemental scientific model or analysis discussed in SSPA Volume 2 (McNeish 2001 [DIRS 155023]).

in the rock matrix, rather than the fractures, can substantially reduce the rate of radionuclide movement away from the drift. This is caused primarily by the limited contact between the fractures and the matrix, which is consistent (see Section 11.3.1.7) with the calibration of the UZ flow model and geochemical observations. The result is long residence times in the slow-flowing matrix. Furthermore, the reduction in water saturation in the fractures beneath the drift enhances the retention of radionuclides in the matrix.

Current Modeling Approach and Uncertainties–Transport calculations for the analysis model reports listed in Section 11.1 were based on the release of radionuclides from the EBS into fracture flow, undisturbed by the presence of the waste emplacement drift, as calculated using the site-scale UZ flow model. Any effects of the drift shadow on transport were not considered. In the current approach, the shadow zone is considered directly in the process model calculations. Radionuclide releases are modeled from the emplacement drift to the rock matrix and fractures according to the physical processes that govern radionuclide movement. The effects of reduced water saturations and flow rates beneath the emplacement drift are considered in process model calculations for radionuclide transport away from the drifts. Uncertainties concerning seepage diversion, which leads to the drift shadow, are discussed in Section 4. Uncertainties in fracture-matrix interaction are estimated through calibration of hydrologic properties (CRWMS M&O 2000 [DIRS 144426]) using a range of infiltration rates.

11.2.2 Matrix Block Discretization Effects

Process Description–Dual-permeability models of UZ radionuclide transport in fractured rock commonly use a single matrix gridblock associated with each fracture gridblock. The single-matrix grid model must approximate radionuclide concentration gradients leading to diffusion between the fractures and the matrix in terms of a single matrix concentration. In reality, a continuous range of concentrations in the matrix will result from radionuclide concentration differences between the fractures and the matrix. This continuous range of concentrations can be more accurately captured using multiple-matrix gridblocks associated with each fracture grid.

Current Modeling Approach and Uncertainties–A comparison of transport calculations using a single-matrix grid model and a multiple-matrix grid model (see Section 11.3.2) shows that the leading edge of a radionuclide breakthrough curve will arrive significantly earlier using the single-matrix grid model. Transport at later times in the breakthrough are not appreciably affected by the single-matrix grid approximation. Thus, the results indicate that a single-matrix grid model is a conservative predictor of radionuclide transport behavior. More refined approaches to evaluating radionuclide transport include multiple-matrix gridblock models for both flow and transport, models for transport but not for flow, and alternative calculation schemes, such as particle tracking methods (see Section 11.2.3).

Transport calculations for performance assessment are performed using a different calculation scheme (see the discussion of FEHM V2.10 in Sections 11.2.3 and 11.3.3) that avoids the spatial discretization problem discussed here. However, the TSPA transport calculation method introduces other approximations that generally underestimate fracture-matrix interaction due to diffusion. Because of the difficulties in implementing a uniformly accurate transport calculation method in the TSPA, a precise evaluation of the significance of the differences in these methods to overall repository performance has yet to be determined.

11.2.3 Calculation Methods for Radionuclide Transport

Process Description–Calculation schemes for radionuclide transport include particle tracking methods and direct numerical solutions of the conservation equations. The different schemes can result in different model predictions, particularly because of differences in the approaches used for matrix diffusion.

Current Modeling Approach and Uncertainties–This section describes results from three different simulation methods for UZ transport: FEHM V2.10, DCPT V1.0, and T2R3D V1.4. All three methods use the same dual-permeability grid consisting of overlapped meshes that represent fracture and matrix continua. FEHM V2.10 uses a node-based particle tracking approach with simplifying assumptions for fracture-matrix diffusive exchange. It is the only transport calculation method used in the *Total System Performance Assessment for the Site Recommendation* (TSPA-SR) (CRWMS M&O 2000 [DIRS 153246], Section 3.7.2) and in the current analyses. DCPT V1.0 uses a random walk particle tracking method that more directly implements the dual-permeability conceptual model. T2R3D V1.4 uses an integrated finite difference method to solve the conservation equations for a dual-permeability system. Although the three simulation methods tested agree for certain problems, differences between the FEHM V2.10 particle tracking method used for the TSPA and for the process-level models were found for transport calculations involving dual-permeability systems. These differences are attributable to simplifying assumptions used in the FEHM V2.10 particle tracking algorithm that provide a more efficient calculation scheme for capturing concentration gradients in the matrix (see Section 11.3.3.3). Improvements in DCPT V1.0 also provide a more accurate representation of matrix concentration gradients for fracture-matrix diffusive exchange than the baseline version.

11.2.4 Effects of Potential Repository Footprint on Three-Dimensional Transport

Process Description–Radionuclide transport in the UZ between the potential repository and the water table depends on the location, size, and shape of the potential repository (i.e., the repository footprint). This results from the unpredictable, location-specific geologic and hydrologic variability present in a natural system. These variabilities include hydrogeologic and mineralogical characteristics, hydrogeologic unit thicknesses, faulting, and surface infiltration.

Current Modeling Approach and Uncertainties–Sensitivity calculations were performed (see Section 11.3.4) to investigate the changes in radionuclide transport behavior that would result if the baseline repository footprint were extended to the south. The investigation found that radionuclide transport in the extended footprint was slower than in the baseline potential repository block, although the differences were not large (e.g., mean breakthrough times differ by less than a factor of two). Uncertainties with regard to footprint effects on radionuclide transport are primarily caused by uncertainties in the footprint itself (i.e., the potential repository design) and in the geologic characterization of regions that lie outside the baseline footprint. This uncertainty is treated by using a range of flow models. A statistical characterization is made of flow focusing as it could occur in the Topopah Spring welded hydrogeologic unit (i.e., the potential repository horizon). Also, a series of perched water conceptual models were constructed for variable characteristics of the Calico Hills nonwelded hydrogeologic unit (e.g., degree of fracturing and zeolite content) to evaluate the potential for perched water table buildup underneath the potential repository.

11.2.5 Effects of Thermally-Driven Coupled Processes

Process Description–Thermal energy from the potential repository will induce thermal-hydrologic (TH) and thermal-hydrologic-mechanical (THM) couplings that affect flow, as well as thermal-hydrologic-chemical (THC) couplings that affect flow and geochemical conditions. All of these coupled processes affect the conditions for radionuclide transport. Because the heat source is located in the emplacement drifts, the effects of these coupled processes tend to be more pronounced in the vicinity of the drifts. The TH flow coupling is primarily caused by vaporization/condensation phenomena that result in redistribution of water and changes in flow patterns. The THM coupling affects flow behavior through changes in hydrologic characteristics resulting from induced mechanical strain in the rock. The THC coupling can cause changes to hydrologic properties through precipitation and dissolution of minerals, as well as aqueous and mineralogical changes that can affect radionuclide sorption and colloid behavior.

Current Modeling Approach and Uncertainties–Process model evaluations concerning TH effects on mountain-scale flow indicate that effects on radionuclide transport should be minimal (see Section 11.3.5). However, the dryout in the vicinity of the emplacement drift may result in significant delays in radionuclide transport in the higher-temperature operating mode. The effects of THM coupled processes on radionuclide transport were found to cause relatively small changes in hydrologic properties; hence, the effects on flow and transport should be minimal (see Section 11.3.5). Similarly, THC coupled processes were found to cause relatively small changes in hydrologic properties and, therefore, should not have much effect on radionuclide transport (see Section 11.3.5). Geochemical changes have not been fully analyzed; however, the results to date indicate only minimal effects on radionuclide transport. Uncertainties regarding coupled processes include thermal operating modes, modification of hydrologic properties resulting from precipitation/dissolution and mechanical effects, and formation-specific thermal dependency for radionuclide diffusion and sorption characteristics. These uncertainties have been treated by investigating a range of thermal operating modes, performing sensitivity studies on hydrologic properties, and collecting thermodynamic and chemical kinetic data.

11.3 INTRODUCTION TO UNCERTAINTY ANALYSIS

11.3.1 Transport in the Drift Shadow Zone

11.3.1.1 Introduction

Flow in the UZ tends to be diverted by an opening such as an emplacement drift. The underlying reason for the diversion of unsaturated flow around a drift is that capillary forces in the rock prevent water entry into the drift unless the capillary pressure in the rock decreases sufficiently for gravity forces to overcome the capillary barrier (Philip et al. 1989 [DIRS 105743]).

However, water tends to drain laterally around the drift, due to capillary and gravity forces, as saturations rise at the drift boundary. Thus, flow tends to be deflected around the cavity.

The degree to which percolation flux is deflected by the presence of the drift is the subject of Section 4. The absence of downward flow beneath the drift results in a shadow zone of reduced water flux and water saturation. Moving downward, away from the drift, the shadow zone asymptotically re-equilibrates to the undisturbed flow conditions due to capillary forces. This section discusses the consequences of the shadow zone relative to radionuclide transport behavior, not including the effects of repository heat.

11.3.1.1.1 Drift Shadow with Zero Seepage

The phenomenon of flow diversion around a cavity was investigated for a nonspecific homogeneous porous medium by Philip et al. (1989 [DIRS 105743]). The key feature of this phenomenon with respect to the transport of dissolved or colloidal material from the drift is that flow velocities in a zone beneath the drift are reduced relative to the undisturbed flow velocities away from the drift. In particular, the flow velocity at the base of the drift is exactly zero. The zone beneath the drift was also found to have lower water saturation than the undisturbed zone. This region of reduced flow velocity and water saturation beneath the drift is known as the drift shadow (Philip et al. 1989 [DIRS 105743]).

For a quasi-linear representation of the hydrogeologic properties, Philip et al. (1989 [DIRS 105743], p. 18) found that the extent of the drift shadow is a function of a characteristic sorptive length scale and the drift radius. Capillary pressure, expressed in units of length, is proportional to the logarithm of relative permeability in the quasi-linear flow formulation. The sorptive length scale is two times the constant of proportionality in this relationship. The quasi-linear model is a special case in which the logarithm of the effective water permeability is linearly proportional to the capillary pressure. The shape of the drift shadow is governed by the ratio of the drift radius to the sorptive length scale. The ratio of the drift radius to the sorptive length scale is a measure of the relative importance of gravitational forces compared with the capillary forces that define flow patterns around the drift. Philip showed that the drift shadow becomes more elongated (relative to coordinates scaled by the drift radius) as the dimensionless ratio increases (i.e., the gravitational gradient becomes more dominant). Diagrams showing contours of equal flow velocity are given in Philip et al. (1989 [DIRS 105743]). Outside the shadow, near the edge of the drift, a zone of enhanced flow occurs where the diverted flow from the top of the drift is focused.

The results of Philip et al. (1989 [DIRS 105743]) may be used as independent corroboration for the expected behavior in fractured, porous rock using the dual-permeability concept of a fracture continuum and a matrix continuum (see Section 3). Because this work was for a single continuum, this evaluation requires the approximation that, in the vicinity of the drift, the flow behavior in the fracture and matrix continua can be treated as flow in two independent and noninteracting continua. Although this is not exactly correct, interaction between the two continua is weak, as evidenced by the necessity to severely reduce fracture-matrix interaction area in the UZ flow model (CRWMS M&O 2000 [DIRS 141187], Section 6.1.3; Liu et al. 1998 [DIRS 105729]). Furthermore, additional analyses presented here that allow for interacting fracture-matrix continua verify this concept. The expected behavior of fractured rock can be represented by this approximation in conjunction with the results from Philip et al. (1989 [DIRS 105743]) for a gravity-dominated flow system (e.g., the fracture continuum) and a capillary-dominated flow system (e.g., the matrix continuum). The reduction in flow below the drift is much more severe for the fracture continuum than for the matrix continuum. Furthermore, the very low water content of the fracture continuum below the drift, due to very low saturation and porosity (as compared with the matrix continuum), means that the vast majority of the water in the rock immediately below the drift will be in the rock matrix. This results in diffusive radionuclide releases from a waste emplacement drift into the rock, which will preferentially go into the rock matrix.

11.3.1.1.2 Drift Shadow with Nonzero Seepage

Although seepage into a drift can occur if the flow rate is sufficiently large, in many cases the drifts are expected to deflect all of the percolation flux (CRWMS M&O 2000 [DIRS 153314]). Previous calculations for the base case (CRWMS M&O 2000 [DIRS 153246], Section 4.1.2) predict that 87 percent of the drifts will not receive seepage over the first 100,000 years. The analysis given below does not extend to the case for drifts with seepage, and the effects of the drift shadow in these cases are less certain. Even drifts that receive seepage will divert some of the percolation flux, which will result in some reduction in the percolation rate immediately below the drift. However, uncertainty exists with respect to the distribution of flux coming out of the drift into rock fractures versus rock matrix. As discussed in Section 11.3.1.5.3, initiating transport in the matrix versus the fractures has a large (several orders of magnitude) effect on transport time; however, the overall significance on performance has yet to be determined.

11.3.1.1.3 The Role of Fracture/Matrix Interaction

As stated previously, the fracture and matrix continua appear to be only weakly connected. This observation is based on information from the UZ flow model calibration (CRWMS M&O 2000 [DIRS 141187], Section 6.1.3) and from geochemical comparisons of perched water (water from the fracture continuum) and matrix pore water (BSC 2001 [DIRS 154874], Section 7.5). The UZ flow model requires severely reduced fracture-matrix interaction areas for calibration against field measurements of water saturation and potential (CRWMS M&O 2000 [DIRS 144426]). Perched water and matrix pore waters are found to be significantly different in composition, indicating a lack of geochemical equilibrium between the fracture and matrix continua. Although the hydrologic and geochemical evidence indicates that the fracture and matrix continua are only weakly coupled, quantitative estimates of parameters reflecting this aspect of the fractured rock system are uncertain. Furthermore, this aspect of the system has a large impact on radionuclide transport in the drift shadow and further from the drifts. However, the overall significance on performance has yet to be determined.

11.3.1.2 Goal of the Models

The goal of the drift shadow model is to incorporate the effects of the drift shadow on radionuclide releases from the EBS and the subsequent transport of radionuclides in the flow field disturbed by the presence of the emplacement drift. This goal is achieved through the following analyses:

- Process model evaluation of the flow field below the drifts with zero seepage
- Process model evaluation of radionuclide release transport from drifts with zero seepage
- Model abstraction to be used in the Volume 2 TSPA (McNeish 2001 [DIRS 155023]) for the radionuclide concentration boundary condition at the edge of the drift if no seepage occurs
- Model abstraction to be used in the Volume 2 TSPA (McNeish 2001 [DIRS 155023]) for radionuclide transport in the drift shadow.

11.3.1.3 Discussion of Total System Performance Assessment-Site Recommendation Results

Although detailed process model calculations relating to drift seepage were performed and model abstractions developed and used in the TSPA-SR (CRWMS M&O 2000 [DIRS 153246]), the results did not include any discussion of drift shadow effects. The TSPA-SR computed seepage into the drifts, and as stated previously, TSPA-SR calculations for the base case (CRWMS M&O 2000 [DIRS 153246], Section 4.1.2) predict that 87 percent of the drifts will not receive seepage over the first 100,000 years. Furthermore, releases during the first 40,000 years are dominated by diffusion. In terms of releases from the drift, the radionuclides were assumed to be instantaneously transported from the drift. The result was a zero-concentration boundary condition at the drift wall. This condition was used for diffusive radionuclide releases from the EBS, where diffusion occurs between the radionuclide source and the drift wall. A zero-concentration boundary condition at the drift wall for the EBS diffusion model is the most conservative boundary condition that could be implemented because zero concentration gives the highest possible diffusive flux. Furthermore, all radionuclide releases into the rock were released to the fracture continuum. The flow in the fracture and matrix continua (for radionuclide transport) was assumed to be undisturbed by the presence of the drifts.

The abstractions used in the TSPA-SR (CRWMS M&O 2000 [DIRS 153246]) resulted in large, rapid, diffusive releases of radionuclides into fractures immediately below the emplacement drifts. This approach clearly overestimates the ability of radionuclides to move from the drifts into fractures immediately below for those cases without drift seepage, resulting in conservative dose estimates.

11.3.1.4 Model Developments Since the Total System Performance Assessment-Site Recommendation

The drift shadow model (CRWMS M&O 2000 [DIRS 122894]) is conceptually similar to the drift seepage process model used to support the TSPA-SR, but extends the analysis to the zone beneath the drift. The computer codes iTOUGH2 V4.0, iTOUGH2 V4.4, and TOUGH2 V1.11, MEOS9nT V1.0 were used for this evaluation. The iTOUGH2 V4.0 code can be used for either forward calculations (as performed with TOUGH2 V1.11 MEOS9nT V1.0) or inverse calculations involving parameter estimation. In this analysis, iTOUGH2 V4.0 was used only for forward model calculations.

11.3.1.4.1 Model Grid and Hydrologic Property Sets

The calculations reported here are for a two-dimensional, homogeneous, dual-permeability model of an emplacement drift. Figure 11.3.1-1 shows the grid employed in the calculations. The area around the 5-m diameter drift uses a refined grid of 0.2 m by 0.2 m. Farther from the drift, the grid coarsens to roughly 2 m by 2 m. The property set for the tsw35 hydrogeologic unit (CRWMS M&O 2000 [DIRS 144426], Table 13), which corresponds to the lower lithophysal unit of the Topopah Spring Tuff, is used in the flow calculations. The mountain-scale property sets were used because the drift shadow extends well beyond the length scale of measurements used to define the drift-scale property sets. However, the appropriate scale of properties to be used should be considered an uncertainty in the calculation. The question of property sets is not considered to be a major uncertainty because the drift-scale and mountain-scale property sets differ primarily in their fracture permeabilities. Although the drift-scale property sets have fracture permeabilities that are roughly one order of magnitude less than the mountain-scale property sets, the effects on water flow and aqueous transport are expected to be small because for both property sets, the capacity for gravity flow in the fracture continuum is orders of magnitude greater than the existing water flow rates.

11.3.1.4.2 Boundary Conditions

The flow model requires the specification of boundary conditions. As Figure 11.3.1-1 shows, the model uses a no-flow symmetry condition along the centerline of the drift. Similarly, the far lateral boundary is also a no-flow symmetry condition reflecting the periodic, 81-m drift spacing. Flow is introduced at the top boundary at a prescribed flow rate. For the dual continuum model calculations, flow rates are prescribed separately for the fracture and matrix continua. This is necessary to develop a flow field compatible with results from the mountain-scale UZ flow model. The bottom boundary condition is simply free gravity drainage.

Guidance on how to distribute the flow into the fractures and matrix is available from model predictions given in *UZ Flow Models and Submodels* (CRWMS M&O 2000 [DIRS 122797], Section 6.6), in which the fractures in the potential repository were found to carry between 84 and 97 percent of the total flow. These percentages represent the average distribution of flow for average infiltration rates over the UZ flow model that vary from about 5 mm/yr to 33 mm/yr (CRWMS M&O 2000 [DIRS 122797], Section 6.6). The computed variations in flow rate are a function not only of the total flow rate, but also of other conditions, such as the characteristics of infiltration at the ground surface. Therefore, in the calculations that follow, the fraction of flow introduced to the fracture continuum at the top of the model is investigated for a range of values. Putting more of the flow in the fractures is conservative because matrix water content will be reduced and fracture water content will be increased. This tends to allow more releases from the drift to enter the fractures, and also results in a larger fracture/matrix contact area through the active fracture model. This area is a function of the effective water saturation of the fracture continuum. However, it is not conservative with respect to matrix advection rates, as discussed in Section 11.3.1.5. For higher percolation rates, the percentage is adjusted to allow for more flow in the matrix than found at the lower percolation rates, short of saturating the matrix.

The center of the drift is 17.5 m below the top of the model domain, and the drift has a radius of 2.5 m. Hydrologic properties are assigned to the drift such that the capillary pressure is zero for all values of water saturation and the relative permeability is zero over nearly the entire saturation range (until water saturations exceed 0.9999999). Relative permeability is the ratio of permeability at partial saturation to permeability at full saturation.

11.3.1.4.3 Transport Parameters

Transport calculations require the specification of matrix diffusion and sorption parameters. These parameters have been chosen to be the expected values used in the TSPA-SR base case (CRWMS M&O 2000 [DIRS 153246], Tables 3.7-1 and 3.7-2). The drift shadow transport calculations presented here consider nonsorbing technetium and moderately sorbing neptunium. The transport of these radionuclides is calculated without including the effects of radioactive decay. The active fracture model, which specifies fracture-matrix area and other relevant parameters for fracture-matrix interaction, is also used for defining the corresponding properties needed to compute advective and diffusive exchange between fractures and the matrix.

11.3.1.5 Results of Analysis

11.3.1.5.1 Consistency with the Philip Analytical Model

Two calculations were performed for the problem of flow around a drift using a single continuum to compare the results of the Philip et al. (1989 [DIRS 105743]) analytical model with the results of iTOUGH2 V4.4. This comparison provides confirmation that the specific implementation of iTOUGH2 V4.4 for flow around a drift is suitable. The analytical model uses the Gardner relationship (Bear 1988 [DIRS 101379], p. 492), in which relative permeability is an exponential function of capillary pressure. The Gardner relative permeability model is not available in iTOUGH2 V4.0, but is included in iTOUGH2 V4.4, which was used for these comparison calculations only. The iTOUGH2 V4.4 calculations used the van Genuchten capillary-pressure relationship and base permeability parameters from the tsw35 property set (CRWMS M&O 2000 [DIRS 144426], Table 13). Comparisons were made for two values of the dimensionless parameter, s, in the Gardner model. A value of s equal to 0.25 is representative of the matrix continuum, where capillarity dominates gravity. A value of 8 for s corresponds to gravity-dominated flow, as expected in the fracture continuum (Philip et al. 1989 [DIRS 105743]). The comparisons were performed using a percolation rate of 10 mm/yr for the gravity-dominated system (i.e., the fracture continuum) and 0.32 mm/yr for the capillary-dominated system (i.e., the matrix continuum). These are the most representative values of s for the tsw35 fracture continuum and matrix continuum in the calculations presented in Philip et al. (1989 [DIRS 105743]).

Figures 11.3.1-2a and 11.3.1-2b compare vertical flow velocity contours for iTOUGH2 V4.4 and the analytical Philip solution using capillary coefficients of 8 and 0.25, respectively. Some discrepancies between the solutions are found farther from the drift, where grid discretization effects contribute to discrepancies. Overall, iTOUGH2 V4.4 reproduces the analytical model results with sufficient precision, given the magnitude of other uncertainties about flow and transport in performance assessment.

11.3.1.5.2 Flow Field Results

Unsaturated flow calculations were performed for a dual continuum model using the tsw35 (lower lithophysal unit) property set (CRWMS M&O 2000 [DIRS 144426], Table 13) and the unsaturated flow code iTOUGH2 V4.0. The current repository design locates about 70 percent of the emplacement drifts in this unit (DOE 2001 [DIRS 153849], Section 2.3.4.1.3). The assumed total percolation flux is 10 mm/yr, with 97 percent introduced to the fracture continuum and 3 percent to the matrix continuum at the upper boundary of the model. Fracture-matrix interaction is described by the active fracture model. Flow calculations for tsw35 are shown in Figures 11.3.1-3 to 11.3.1-6. Figures 11.3.1-3 and 11.3.1-4 show the flow velocity and water saturation, respectively, for the fracture continuum. Figures 11.3.1-5 and 11.3.1-6 show the flow velocity and water saturation, respectively, for the matrix continuum.

The results are qualitatively similar to those found for a single continuum using the Gardner relative permeability model. In particular, the drift shadow is seen to be long and narrow for gravity-dominated fracture flow, resulting in a substantial decrease in fracture flow below the drift and for several drift diameters below the drift. For example, the flow rate within about three drift diameters, on the drift centerline below the emplacement drift, is less than 50 percent of the undisturbed flow rate. The matrix, on the other hand, has a much shorter drift shadow. The flow rate in the matrix is less than 50 percent of the undisturbed flow rate within approximately 0.2 drift diameters on the centerline below the bottom of the drift.

An important aspect of the drift shadow flow field is its effect on water saturation. The fracture flow field shows a large decrease in fracture water saturation. For the 10-mm/yr case with a 0.3-mm/yr rate in the matrix, the fracture water saturation drops 35 percent. This reduction in fracture water saturation is even larger in terms of effective water saturation, S_e, defined as:

$$S_e = \frac{S_f - S_{fr}}{1 - S_{fr}} \qquad \text{(Eq. 11.3.1-1)}$$

where S_f is the fracture water saturation and S_{fr} ($S_{fr} = 0.01$) is the residual fracture water saturation (CRWMS M&O 2000 [DIRS 145771]; DTN: LB997141233129.001 [DIRS 104055]). The effective water saturation in the fractures drops to about 15 percent of its undisturbed value. The drop in water saturation is significant with respect to diffusion from the emplacement drift and rock matrix to the fracture continuum and from the fracture continuum to the rock matrix. For diffusive exchange between the fracture and matrix continua, the active fracture model area reduction factor is $S_e^{1+\gamma}$, where S_e is the effective fracture water saturation and the active fracture model parameter, γ, is 0.41. This reduction factor ranges from about 9×10^{-4} to 6×10^{-5} in the undisturbed zone and immediately below the drift. These reduction factors can be deduced from the formula for effective fracture water saturation and the plot of fracture water saturation provided (Figure 11.3.1-4b). Conversely, for the matrix, the reductions in water saturation are relatively small, ranging from 0.83 below the drift to 0.85 in the undisturbed zone. Because of the low values of flow and water saturation in the drift shadow immediately below the drift, transport from the drift is dominated by diffusive releases to the rock matrix and very restricted diffusion from the rock matrix to the fractures.

11.3.1.5.3 Transport in the Drift Shadow

Transport calculations were run for a dual-permeability flow and transport system using TOUGH2 V1.11 module MEOS9nT V1.0. The transport calculations were performed using the same cross-sectional model grid shown in Figure 11.3.1-1 in the tsw35. These calculations were performed for technetium and neptunium, but without radioactive decay. For each radionuclide, 1 kg was released from two drift cells connected to all the fracture and matrix cells in contact with the drift within 1 m of the drift centerline.

An important process for transport modeling is molecular diffusion in both the matrix and the fractures. Diffusion in TOUGH2 V1.11, MEOS9nT V1.0 is set through specification of the free water diffusion coefficient, roughly 1.6×10^{-9} m^2/s for strong electrolytes (Weast 1972 [DIRS 127163]), and the tortuosity. The values of matrix diffusion used here are the same values implemented for performance assessment (CRWMS M&O 2001 [DIRS 154024], Section 6.6.3). The value for technetium is 3.2×10^{-11} m^2/s, and the value for neptunium is 1.6×10^{-10} m^2/s. For the fracture continuum, tortuosity is taken to be equal to the water content of the fractures. Much lower values of tortuosity are implied by measured data (CRWMS M&O 1997 [DIRS 100401], Section VI). Diffusion in the fracture continuum is important primarily for diffusive releases from the drift to the rock. Immediately below the drift, the tortuosity is 1.3×10^{-4}, using a value of 0.011 for fracture porosity (CRWMS M&O 2000 [DIRS 145771]) and a saturation of 0.012, as seen in Figure 11.3.1-4b.

Breakthrough curves for transport to the bottom of the model (45 m below the bottom of the emplacement drift, as seen in Figure 11.3.1-1) are shown for technetium and neptunium in Figures 11.3.1-7a and 11.3.1-7b, respectively. These figures compare the technetium and neptunium transport results for a percolation rate of 10 mm/yr for two matrix percolation cases that bracket the expected ranges, from a low percolation rate of 0.3 mm/yr to a high percolation rate of 1.6 mm/yr (CRWMS M&O 2000 [DIRS 122797], Section 6.6.3). Because of the diffusive release of radionuclides from the drift to the rock matrix and the restricted fracture-matrix diffusion in the active fracture model, radionuclides are transported primarily in the matrix. The transport is dominated by advection if the 0.5 fraction arrives at the bottom of the model at the time expected for transport due to matrix advection. For the case of technetium, a 0.3 mm/yr percolation rate in the matrix, and a water content of about 0.11, the travel time for pure matrix advection is about 6,200 years, or a $\log_{10}$ value of 3.8. For the 1.6-mm/yr matrix percolation rate, the travel time for pure matrix advection is about 3,500 years, or a $\log_{10}$ time of 3.5. In this case, the travel time of the 0.5 cumulative breakthrough fraction is close to the travel time for pure matrix advection. The long tail leading up to the main breakthrough is caused by diffusive release of the radionuclides from the matrix to the fractures. Diffusive release from the matrix to the fractures dominates transport for the 0.3-mm/yr case. The plot also shows reference results using direct release to undisturbed flow in the fractures, as in the TSPA-SR transport model (CRWMS M&O 2000 [DIRS 153246], Section 3.7.2). The TSPA transport model uses the FEHM V2.10 particle tracking method for transport calculations, which was not used in this analysis. The vast difference in transport (more than three orders of magnitude) results directly from the difference between transport through fractures and transport through the matrix. Fracture-matrix exchange is not large for either calculation, resulting in extremely rapid transport of releases to the fracture continuum compared with releases to the matrix continuum.

A comparison of the two matrix-percolation cases for neptunium transport is shown in Figure 11.3.1-7b. Neptunium transport differs from technetium transport because of sorption (K_d = 0.3 ml/g for neptunium, 0 for technetium [CRWMS M&O 2000 [DIRS 143665], Table 3.7-1]) and a matrix diffusion coefficient that is 5 times larger (1.6×10^{-10} m^2/s for neptunium versus 3.2×10^{-11} m^2/s for technetium (CRWMS M&O 2000 [DIRS 143665], Table 3.7-2). Although the higher matrix diffusion rate will cause earlier release to the fractures from the matrix, sorption helps retain neptunium in the matrix; in addition, transport through the matrix is slowed by sorption. The net effect is slower transport for neptunium than for technetium.

Transport calculations were also carried out for a percolation flux of 100 mm/yr to investigate sensitivity to percolation rate. The results of these transport calculations are shown in Figures 11.3.1-8a and 11.3.1-8b. Higher overall percolation rates result in more rapid release of radionuclides to the fractures, represented by the gently rising portion of the breakthrough curve. This is primarily a result of higher fracture water saturations and a larger fracture-matrix contact area, as computed with the active fracture model. However, the breakthrough times for the 0.5 breakthrough fractions are still dominated by matrix advection in the higher matrix percolation rate case. This can be roughly deduced by comparing the time for breakthrough of the 0.5 fraction with the time for matrix advection from the drift to the bottom of the model. The range of matrix percolation rates is more difficult to define for future climates. To address this uncertainty, a lower matrix percolation rate of 0.3 mm/yr was used. The upper percolation flux rate was taken to be 3 mm/yr and resulted in a matrix water saturation in excess of 0.99 in the undisturbed flow region.

11.3.1.5.4 Effects of the Drift Shadow on Colloid-Facilitated Radionuclide Transport

Although colloid transport is not quantitatively evaluated here, the drift shadow will have a significant impact on colloid-facilitated radionuclide transport. Because of their large size, colloids can only diffuse slowly. Furthermore, only very small colloids will be able to diffuse into the rock matrix because of size exclusion effects. Colloid diffusion in the fractures will be further restricted by the low water saturations in the drift shadow. Using a fracture tortuosity of 1.3×10^{-4} (see above), the colloid diffusion coefficient in the fractures will vary from about 10^{-16} m^2/s to 10^{-14} m^2/s for a range of colloids from 450 nm to 6 nm in diameter, respectively (CRWMS M&O 2000 [DIRS 144331], Table 6.18). Colloids will therefore tend to be trapped, to a large extent, in the emplacement drift by the drift shadow effects.

11.3.1.6 Abstraction for Total System Performance Assessment

In previous TSPA calculations (CRWMS M&O 2000 [DIRS 153246]), contaminant flux from the near-field/EBS simulated by GoldSim V6.04.007 was introduced into the fracture domain of the FEHM V2.10 UZ particle tracking model (CRWMS M&O 2000 [DIRS 153246]). The results presented in Section 11.3.1.5 indicate that a significant portion of the contaminant flux from the EBS may enter the rock matrix rather than fractures. This occurs because, in the absence of seepage, releases from the EBS are diffusive and will enter the rock matrix and fractures roughly in proportion to the water content of the two continua. The water content of the rock matrix is on the order of 0.1, whereas the fractures have water content on the order of 10^{-4}. Therefore, nearly all of the EBS releases will go into the matrix. The FEHM V2.10 particle tracking routine was modified to account for this partitioning of contaminant flux into the fracture and matrix domains (CRWMS M&O 2000 [DIRS 141418]). The basic idea is that the mass advected through the EBS cells via seepage is released into the fracture nodes, and the mass diffused through the EBS cells is released into the matrix nodes.

11.3.1.6.1 Abstraction for Transport in the Drift Shadow

FEHM V2.10 interfaces with GoldSim V6.04.007 through collector cells that provide the contaminant flux leaving the EBS. There are five collector cells, which correspond to each infiltration bin. The five separate infiltration bins are based on the multiscale thermal-hydrologic model (CRWMS M&O 2000 [DIRS 153246], Section 3.7.2). Specifically, the model is based on the percolation flux derived from the multiscale model nodes that are 5 m above the drift crown. The advective and diffusive mass from the EBS is combined into a GoldSim V6.04.007 collector cell, then passed to FEHM V2.10 as a boundary condition. GoldSim V6.04.007 also passes an advection-diffusion flow fraction for each of the cells that represents the ratio of the advective and diffusive mass fluxes entering the collector cell. The flow fraction is used to calculate the proportion of mass entering the fracture and matrix domains. Masses from each of the collector cells are then sent to the corresponding spatial location in the FEHM V2.10 model. The FEHM V2.10 particle tracking routine partitions particles between the fracture and matrix nodes, using the flow fractions such that advective releases from the drift are passed to fracture nodes in the transport calculation and diffusive releases from the drift are passed to matrix nodes.

FEHM V2.10 does not allow radionuclides that have entered the matrix to diffuse to the fractures. Therefore, radionuclides that enter the matrix must either advect from the matrix to the fractures or travel through the matrix to the water table. This should be recognized as a nonconservative feature of TSPA calculations that incorporate the drift shadow abstraction. However, this implementation of the drift shadow provides an estimate of the potential range of results between the TSPA base case (CRWMS M&O 2000 [DIRS 153246]), which does not account for the drift shadow, and a TSPA that includes the drift shadow effect.

11.3.1.6.2 Abstraction for the Engineered Barrier System Boundary Condition

A radionuclide concentration boundary condition at the drift wall may be established based on continuity of radionuclide concentration and flux exiting the drift and entering the rock. This model abstraction is developed for the situation in which radionuclide flux is entirely diffusive in the EBS invert and advective in the rock matrix. Neglecting diffusion in the rock matrix, in combination with the assumption that advective velocities in the rock matrix are at undisturbed levels, should be acceptable (i.e., conservative) as long as the drift shadow keeps the radionuclides moving in the matrix for a few meters. The transport results in Section 11.3.1.5 support the idea that most radionuclides will transport away from the drift in the matrix for at least a few meters before entering fractures.

EBS diffusion is modeled as a one-dimensional steady-state diffusion through two different domains, the waste package and the invert (CRWMS M&O 2000 [DIRS 153246], Table 3.6-1). For steady-state diffusion in the waste package and invert:

$$\frac{d^2 c_{wf}}{dx^2} = 0 \text{ and } \frac{d^2 c_{in}}{dx^2} = 0 \qquad \text{(Eq. 11.3.1-2)}$$

where c_{wf} is the concentration in the waste form domain and c_{in} is the concentration in the invert domain. The general solutions to these two equations are (Crank 1975 [DIRS 122990], p. 44):

$$c_{wf}(x) = F_{11}x + F_{12} \text{ and } c_{in}(x) = F_{21}x + F_{22} \qquad \text{(Eq. 11.3.1-3)}$$

where F_{ij} are the integration constants. The boundary conditions consist of the source concentration condition and continuity of concentration and flux across the boundaries:

$$\begin{aligned}
& c_{wf}(0) = c_s \\
& c_{wf}(L_{wf}) = c_{in}(L_{wf}) \\
& -\phi_{wf} S_{wf} D_{wf}(S_{wf}) \frac{dc_{wf}}{dx}(L_{wf}) = -\phi_{in} S_{in} D_{in}(S_{in}) \frac{dc_{in}}{dx}(L_{wf}) \\
& -\phi_{in} S_{in} D_{in}(S_{in}) \frac{dc_{in}}{dx}(L_{wf} + L_{in}) = v_D c_{in}(L_{wf} + L_{in})
\end{aligned} \qquad \text{(Eq. 11.3.1-4)}$$

where

ϕ_{wf} and ϕ_{in} = porosities of the waste form and invert

S_{wf} and S_{in} = water saturations of the waste form and invert

$D_{wf}(S_{wf})$ and $D_{in}(S_{in})$ = effective diffusion coefficients for the waste form and invert

L_{wf} and L_{in} = diffusion path lengths in the waste form and invert

v_D = specific discharge in the rock matrix.

The interface areas between the waste form and invert and between the invert and the rock matrix are equal. The effective diffusion coefficients may be functions of water saturation, but the water saturations must be spatially uniform within each domain.

Solving these equations for F_{ij} and evaluating $c_{in}(L_{wf}+L_{in})$ (the concentration at the invert–rock matrix boundary) gives:

$$c_{in}(L_{wf} + L_{in}) = \frac{c_s}{1 + Pe_{wf} + Pe_{in}} \qquad \text{(Eq. 11.3.1-5)}$$

where the waste form and invert Peclet numbers are, respectively:

$$Pe_{wf} = \frac{v_D L_{wf}}{\phi_{wf} S_{wf} D_{wf}(S_{wf})}$$

and (Eq. 11.3.1-6)

$$Pe_{in} = \frac{v_D L_{in}}{\phi_{in} S_{in} D_{in}(S_{in})}$$

This model results in concentrations at the drift boundary that are greater than zero. The boundary concentration may be large (relative to the source concentration) for regions where the waste form and invert Peclet numbers are small.

11.3.1.7 Multiple Lines of Evidence

Evidence for fracture/matrix disequilibrium is available from field and laboratory tests (CRWMS M&O 2000 [DIRS 141187], Section 6.1.3; Liu et al. 1998 [DIRS 105729]; BSC 2001 [DIRS 154874], Section 7.5). Hydrologic measurements of matrix water potential and saturation, combined with model results, lead to the conclusion that the products of the effective interface permeability, the geometric interface area, and the driving force for fracture-matrix flow (i.e., the capillary pressure differential between fractures and the matrix) must be reduced to match field measurements (CRWMS M&O 2000 [DIRS 144426]; Liu et al. 1998 [DIRS 105729]). Although the effects of these factors are difficult to distinguish based on hydrologic observations alone, geochemical observations of matrix water composition and fracture water composition from perched water zones suggest that the fractures and matrix are not in geochemical equilibrium (BSC 2001 [DIRS 154874], Section 7.5). The only way to achieve the observed level of disequilibrium without invoking special characteristics for fractures or the matrix that are inconsistent with existing data and conceptual models is to have a severely reduced fracture-matrix contact area.

11.3.1.8 Summary of Remaining Uncertainties

The main areas of uncertainty concern the aspects of the flow and transport problem in the vicinity of the emplacement drift that have a large influence on the calculated behavior. These aspects are related primarily to fracture-matrix interaction for diffusive exchange between fractures and the matrix. The reduction in fracture-matrix interface area in the flow and transport models is supported by a combination of hydrologic and geochemical observations (Section 11.3.1.7).

The reduction in fracture-matrix interaction area in the flow model is represented through the active fracture model (CRWMS M&O 2000 [DIRS 141187], Section 6.4.5; Liu et al. 1998 [DIRS 105729]), which must be calibrated to field data to determine an empirical parameter introduced by the model. However, there is an additional effective reduction in fracture-matrix interaction because of the weighting scheme used for fracture-matrix flow calculations. Fracture-matrix flow uses upstream weighting of the relative permeability combined with downstream weighting of the saturated permeability to define the interface permeability. Typically, flow is from fracture to matrix because of the disequilibrium of capillary pressures.

Therefore, fracture to matrix flow is computed using the matrix saturated permeability and the fracture relative permeability. Given the extremely low saturations characteristic of flow in the fractures, the fracture relative permeability is typically orders of magnitude lower than the matrix relative permeability. The effective permeability of the matrix controls imbibition from fractures to the matrix; hence, the true interface permeability is biased to be lower by the ratio of the fracture relative permeability to the matrix relative permeability. This is equivalent to a fracture-matrix area reduction factor. Because the flow model is calibrated to field data, explicit recognition of this reduction factor is not critical to the flow model. However, it is important to recognize this factor when determining the area reduction factor to be used for matrix diffusion. This reduction factor is not accounted for with respect to matrix diffusion in the current drift shadow transport model. The neglect of this effect is conservative for radionuclides that initially enter the matrix because neglecting this factor gives a larger fracture/matrix interface area, leading to more fracture/matrix diffusion, shorter retention of radionuclides in the matrix and, therefore, shorter transport times. Clearly, for radionuclides that initially enter the fractures, the opposite is true and transport is more rapid. However, because the model results in most of the radionuclides initially entering the matrix, the overall effect of neglecting the additional reduction in the fracture/matrix interface area is conservative.

The variation in transport behavior investigated as a function of total percolation rate, as well as the distribution of percolation between fractures and the matrix, represents another element of uncertainty. In this case, the combination of the climate and infiltration uncertainty coupled with site-scale flow model uncertainty can capture the main aspects of this element for the drift shadow transport problem.

Additional uncertainties include drift seepage and parameter uncertainty and variability (heterogeneity). The treatment of the drift shadow for the TSPA calculations in this report captures some aspects of parameter uncertainty directly and conservatively treats the effects of drift seepage. However, the overall significance on performance remains to be determined. The input parameters for flow and transport are uncertain: the propagation of uncertainties through transport models could demonstrate the significance for these uncertainties on performance assessment. The main uncertainties for the drift shadow transport model are summarized in Table 11.3.1-1. Because of this approach, it is likely that a more realistic incorporation of seepage processes, and further development of the process models evaluating the effects of drift seepage, would result in TSPA model calculations that have lower radionuclide releases than those in the TSPA-SR (CRWMS M&O 2000 [DIRS 153246]).

11.3.1.9 Summary and Conclusions

The effects of the drift shadow have a dramatic impact on radionuclide transport times in a limited region below the waste emplacement drifts. The transport times for technetium in the drift shadow model are roughly three to four orders of magnitude longer than transport times over the same domain when computed using the transport assumptions from the TSPA-SR transport model (CRWMS M&O 2000 [DIRS 153246], Section 3.7.2). It is important to recognize that the breakthrough curves presented here are for a boundary 45 m below the potential repository, whereas the water table is an average of about 300 m below the potential repository (DOE 2001 [DIRS 153849], Section 4.3.3.1). The main portions of the radionuclide transport breakthrough curves are dominated by matrix advection for the higher matrix percolation cases. The simulation results show that for these cases, most of the radionuclide mass still remains in the matrix at breakthrough. Therefore, the effects of the drift shadow model on transport extend beyond the zone of reduced flow beneath the waste emplacement drift and, in some cases, beyond the existing model boundary. The effect of the drift shadow transport model on breakthrough curves at the water table has not been investigated. For radionuclide releases from drifts without seepage, the results presented in this section indicate that transport times to the water table will be thousands to tens of thousands of years. The drift shadow analysis presented is a preliminary and exploratory investigation of flow and transport processes not previously included in process models or TSPA analyses of Yucca Mountain. Further justification in terms of additional analyses and field or laboratory experiments are needed prior to incorporating the complete drift shadow flow and transport analysis into the TSPA baseline.

11.3.2 Matrix Block Discretization and Its Effects on Unsaturated Zone Flow and Transport Simulations

In this section, the effects of matrix block discretization schemes on UZ flow and transport simulations are evaluated.

11.3.2.1 Introduction

Within the context of the continuum approach for modeling flow and transport in unsaturated fractured rock, a numerical gridblock generally includes a fracture block and a matrix block. Depending on the matrix block discretization scheme used for a numerical simulation, the matrix block can be treated as a single matrix gridblock or subdivided into a number of matrix gridblocks. Each matrix gridblock generally corresponds to a matrix continuum.

Because fractures and the matrix have different hydraulic properties, flow and transport between them significantly affects the overall flow and transport behavior in the UZ. Consequently, the accuracy with which flow and transport between them is calculated, which is largely determined by the matrix block discretization scheme, is a critical issue for simulating overall flow and transport processes and for assessing the performance of the potential repository.

As discussed in *Conceptual and Numerical Models for UZ Flow and Transport* (CRWMS M&O 2000 [DIRS 141187], Section 6.4), a dual-permeability model (DKM) has been used as the baseline approach for modeling UZ flow and transport processes. This approach was based on considerations regarding flow and transport behavior in the UZ, the scale of the problem, data availability, and computational feasibility (CRWMS M&O 2000 [DIRS 141187], Section 6.4.2).

Because the matrix is orders of magnitude less permeable than the fracture network, very steep gradients (sharp fronts) may develop in the matrix near fractures. In the DKM, the matrix is treated as a single continuum. As a result, capillary pressure gradients (which drive imbibition) and concentration gradients (which drive diffusion) cannot be fully described. Use of the DKM, therefore, may introduce uncertainty into simulations of UZ flow and transport. To evaluate the effect of the uncertainty, this section compares DKM simulation results to results obtained using the multiple interacting continua (MINC) discretization scheme, which was devised specifically to eliminate this source of uncertainty by using multiple matrix blocks per fracture block (Pruess and Narasimhan 1985 [DIRS 101707], pp. 14 to 16).

11.3.2.2 Goals of the Modeling Study

This modeling study evaluates the DKM for UZ flow and transport and associated uncertainties. Specifically, the goals of this study are:

1. Compare simulation results for UZ flow and transport obtained using the DKM with simulation results obtained using MINC, a more accurate matrix block discretization scheme.

2. Make recommendations for improving the current matrix discretization scheme (DKM) based on the simulation results presented in this study (Bodvarsson 2001 [DIRS 154669], Attachment 7, pp. 129 to 141).

11.3.2.3 Matrix Block Discretization

Typical schemes for matrix discretization include the effective continuum model (Pruess et al. 1990 [DIRS 100819]), the dual porosity model (Warren and Root 1963 [DIRS 100611]), the DKM (Doughty 1999 [DIRS 135997], pp. 74 to 79), and the MINC scheme (Pruess and Narasimhan 1985 [DIRS 101707], pp. 14 to 16). A diagram of these schemes for a one-dimensional column of gridblocks is illustrated in Figure 11.3.2-1.

In the effective continuum model (Figure 11.3.2-1a), liquid saturation is partitioned into the matrix and fractures in accordance with the principle of thermodynamic equilibrium, which requires equal capillary pressure in the matrix and fracture components of a gridblock. This is equivalent to assuming that flow and transport between fractures and the matrix occurs instantaneously; thus, fractures and the matrix are combined as a single continuum in a numerical simulation.

In the dual porosity model (Figure 11.3.2-1b), each gridblock includes a fracture gridblock and a matrix gridblock. Unlike the effective continuum model, the fracture and matrix gridblocks need not be in thermodynamic equilibrium. In this approach, flow and transport occurs between fractures and the matrix, but is ignored between matrix gridblocks. The DKM (Figure 11.3.2-1c) is the same as the dual-porosity model, except that it allows for global flow and transport between matrix blocks. The DKM is valid when the capillary pressure and concentration gradients near fracture-matrix interfaces are not steep.

The schemes mentioned above can give poor solutions for flow and transport involving steep fronts near fracture-matrix interfaces in unsaturated fractured rock. This happens because of the thermodynamic equilibrium assumption (in the effective continuum model) or the use of one matrix gridblock (in the other two schemes) (Doughty 1999 [DIRS 135997], pp. 74 to 79). To solve this problem, Pruess and Narasimhan (1985 [DIRS 101707], pp. 14 to 16) proposed the MINC scheme (Figure 11.3.2-1d), which is similar to the DKM except that the matrix is further subdivided into several continua, each at a different distance from the fracture-matrix interface. Thus, the MINC scheme is able to more accurately resolve sharp gradients near the fracture-matrix interfaces.

Although the MINC is known to be the most accurate of these schemes (CRWMS M&O 2000 [DIRS 141187], Section 6.4), it needs more computational effort because several matrix gridblocks are involved for each fracture block. For this reason, the DKM has been used as the baseline approach in the UZ flow and transport models. As discussed below, a comparison of the simulation results from the DKM and MINC models indicates that the MINC results are relatively conservative. A more detailed discussion of the usefulness and limitations of the matrix block discretization schemes is given in *Conceptual and Numerical Models for UZ Flow and Transport* (CRWMS M&O 2000 [DIRS 141187]).

11.3.2.4 Modeling Approaches

To evaluate the accuracy of the DKM in modeling flow and transport in the UZ, simulation results obtained from the DKM were compared with those obtained from a MINC model. In the MINC model, a fracture network is conceptualized as two perpendicular sets of vertical fractures and the matrix is divided into five matrix gridblocks (continua) (Figure 11.3.2-2). Ratios of the distances (i.e., from interfaces between matrix continua to the fracture-matrix interface) to the corresponding fracture spacing are set at 0.004, 0.032, 0.108, and 0.256, respectively. Fine discretization is used near the fracture-matrix interface, and relatively coarse discretization is used for matrix blocks away from the interface. This is because steep gradients generally occur near the interface, as previously discussed. All the matrix continua are globally connected in the vertical direction. In nonvertical directions, only the first (outermost) matrix continuum is globally connected, while the connection parameters (e.g., node distance and interface area) are the same as those in the DKM for the same fracture configuration. All the matrix continua in Figure 11.3.2-2 have identical hydraulic properties.

Because MINC simulations are computationally intensive, a site-scale, two-dimensional cross section was used for all the simulations in this study (Figures 11.3.2-3 and 11.3.2-4). This cross section was selected because it does not contain the vitric Calico Hills Formation, where fracture-matrix interaction is not important. Fracture flow is a major flow mechanism below the potential repository, and matrix diffusion is expected to be a significant mechanism for radionuclide transport between fractures and the matrix below the potential repository (CRWMS M&O 2000 [DIRS 141187], Sections 6.1.2 and 6.2.2). Simulation results were compared for the DKM and the MINC matrix block discretization schemes. The initial conditions, boundary conditions, and rock properties (discussed below) are identical in both simulations.

The top model boundary for the two-dimensional vertical cross-sectional model domain coincides with the bedrock surface of the mountain. Net infiltration at the surface of the mountain is applied to the top boundary. The present-day infiltration map (DTN: GS000308311221.005 [DIRS 147613]) and the calibrated, base case UZ property set (DTN: LB997141233129.001 [DIRS 104055]) determined from one-dimensional inverse modeling studies were used in this study. The bottom boundary is located at the water table. The left and right boundaries are no-flow boundaries in the horizontal direction. Steady-state flow fields were simulated with the EOS9 module of TOUGH2 V1.4. Transport runs were carried out by the T2R3D V1.4 code. The active fracture model documented in *Conceptual and Numerical Models for UZ Flow and Transport* (CRWMS M&O 2000 [DIRS 141187], Section 6.4.5) was used for describing flow and transport in fractures.

In the tracer-transport simulations, a conservative (nonadsorbing) component is transported from the potential repository to the water table under steady-state flow conditions. At time zero, tracer concentration is zero everywhere in the matrix, and a predetermined tracer concentration is applied to water in the fractures in the potential repository host rock. The simulation results for tracer transport are represented by the cumulative mass of tracer arriving at the water table over time, normalized by the total initial mass introduced at the potential repository. Hydrodynamic dispersion has no significant effect on solute transport through the unsaturated fracture-matrix system, as discussed in *UZ Flow Models and Submodels* (CRWMS M&O 2000 [DIRS 122797], Section 6.8.1), and was therefore ignored in this study. Two molecular diffusion coefficients, 0 and 3.2×10^{-11} m^2/s, were used in the simulations for all model layers. The latter value is the average matrix molecular diffusion coefficient for TcO_4^- reported in *Unsaturated Zone and Saturated Zone Transport Properties (U0100)* (CRWMS M&O 2001 [DIRS 154024], Table 16).

11.3.2.5 Results of Analysis

Figures 11.3.2-5 and 11.3.2-6 compare simulated results obtained with the DKM (solid line) and the MINC (circles), respectively, for the two columns (a14 and a23) from the two-dimensional cross section (Figure 11.3.2-4). The simulated matrix saturations are in good agreement with the two schemes of matrix block discretization under steady-state flow conditions, indicating that the whole matrix block can be treated as a single continuum (as used in the DKM). This is further supported by an observation that for a given MINC gridblock, the five matrix continua have almost identical water saturations and potentials (Figure 11.3.2-7). In other words, all five matrix continua of the MINC are in hydraulic equilibrium, consistent with the assumption used in the DKM. This is not surprising because the matrix has small van Genuchten α (i.e., strong capillarity), and flow between different matrix continua is determined purely by capillary forces. The gravity term is not involved in a connection between matrix continua for a given matrix block (Figure 11.3.2-2).

Figures 11.3.2-5 and 11.3.2-6 compare simulated distributions of water flux in fractures for the two columns from the two discretization schemes. While the DKM and the MINC agree fairly well, the DKM overestimates fracture flux (i.e., liquid flux in the fractures) in the PTn unit compared to the MINC. This is because a steep gradient of capillary pressure exists near the fracture-matrix interface, despite the uniform capillary pressure distribution that occurs within a matrix block (e.g., Figure 11.3.2-7). In a DKM, the connection distance between nodes corresponding to the fracture and matrix gridblocks is set to one-eighth (0.125) of the fracture spacing for a fracture network given in Figure 11.3.2-2 (Warren and Root 1963 [DIRS 100611]; Pruess 1983 [DIRS 100605], Table 1). This value is considerably larger than the connection distance between the fracture gridblock and the matrix gridblock corresponding to Matrix Continuum #1 in the MINC (Figure 11.3.2-7). Because the calculated water flux from fractures to matrix varies inversely with this connection distance, the DKM underestimates the flux from fractures to the matrix and overestimates the fracture flux.

While the DKM and the MINC yield similar fracture-flux distributions in the TSw unit, the DKM overestimates fracture fluxes in the CHn and CFu units (Figures 11.3.2-5 and 11.3.2-6) compared to the MINC. Compared with the TSw unit, these units have relatively small fracture permeabilities and large effective fracture-matrix interface areas, as indicated by small values of the active fracture parameter (γ) (DTN: LB997141233129.001 [DIRS 104055]). A combination of these factors and the fine discretization of the matrix block results in a larger flux from fractures to the matrix, and consequently a smaller fracture flux, for the MINC scheme than for the DKM. The differences in fracture flux result from these factors, not from lateral flow, because the total simulated water fluxes at the water table (for both columns), including contributions from the matrix and fractures, are similar for the DKM and the MINC.

Figure 11.3.2-8 shows simulated tracer transport results with and without molecular diffusion ($D_m = 3.2 \times 10^{-11}$ m^2/s and $D_m = 0$). The use of $D_m = 0$ allows for investigation of pure advection effects. In this case (Figure 11.3.2-8a), the DKM and the MINC give similar breakthrough times (less than 10 years) but different values for the tracer cumulative flux. This results from the differences in fracture fluxes in the CHn and CFu units, as discussed above. In the DKM, the majority of tracer mass is transported through fractures from the potential repository (within TSw) to the water table, as implied by the relatively uniform fracture-flux distributions within the TSw unit and below (Figures 11.3.2-5 and 11.3.2-6). In contrast, a relatively small portion of the tracer mass is transported through the fractures to the water table in the MINC scheme.

Comparisons between simulated transport results for the two molecular diffusion coefficients further confirm the importance of the matrix diffusion indicated by the Alcove 1 test and modeling study discussed in *UZ Flow Models and Submodels* (CRWMS M&O 2000 [DIRS 122797], Section 6.8.1). The DKM and MINC schemes produce significantly different breakthrough curves in simulations using the different molecular diffusion coefficients. The comparisons also suggest the necessity to accurately consider the solute-concentration gradient near the fracture-matrix interface. For example, similar breakthrough times are simulated for both matrix-block discretization schemes using $D_m = 0$, but significantly different breakthrough times are simulated using $D_m = 3.2 \times 10^{-11}$ m^2/s. This results mainly from using different discretization schemes. Matrix diffusion is underestimated by the DKM at the early time for radionuclide transport, when there is a large concentration gradient near the fracture-matrix interface. Because the MINC scheme is expected to provide more accurate results, it is likely that the DKM underestimates the breakthrough time (i.e., it predicts earlier breakthrough) for radionuclide transport from the potential repository to the water table.

11.3.2.6 Abstraction for Total System Performance Assessment

As stated in Section 11.3.2.2, the modeling study is devoted to evaluating the DKM for modeling UZ flow and transport in general. The results indicate that the DKM conservatively predicts shorter breakthrough times than the MINC. The simulation results from this study are not directly used for TSPA abstraction; nevertheless, the results imply that it may be important to improve fracture-matrix interaction as modeled with a single matrix grid method. As discussed in Section 11.3.3, the comparisons between simulation results indicate that the effects of matrix diffusion in reducing the initial breakthrough time is not as significant in three dimensions as it seems to be in one dimension. However, the relatively significant impact found here for a two-dimensional system, and possibly more significant effects for the MINC solution, suggest that these effects could also be important for transport in the three-dimensional site-scale model.

11.3.2.7 Multiple Lines of Evidence

The simulation results indicate that the DKM might overestimate fracture flow in the nonwelded units (see comparisons between simulation results for the PTn in Figures 11.3.2-5 and 11.3.2-6). This is consistent with experimental observations from the Busted Butte site (CRWMS

M&O 2000 [DIRS 152773], Section 6.8.9). For the vitric part of the Calico Hills Formation, the current UZ model predicts that about 20 percent of the liquid water occurs in fractures (CRWMS M&O 2000 [DIRS 151940], Figure 3.6.9). In Phase 1A testing at Busted Butte, tracer was injected from a point in the vitric part of the Calico Hills formation. The observed tracer plume clearly indicates that flow and transport occurs only in the matrix of the vitric Calico Hills formation. During Phase 1B testing, in which liquid was injected immediately adjacent to a fracture, water imbibed quickly into the surrounding matrix. Details of these tests can be found in *Unsaturated Zone and Saturated Zone Transport Properties (U0100)* (CRWMS M&O 2001 [DIRS 154024], Section 6.8.9).

Observations at a number of analogue sites generally support the concept that radionuclides transported from fractures to the matrix are distributed near fracture-matrix interfaces (CRWMS M&O 2000 [DIRS 151945], Sections 13.4 and 13.6). Therefore, steep concentration gradients exist near fracture-matrix interfaces. At the Nopal I site in Peña Blanca, Mexico, and the Poços de Caldas site in Brazil, uranium has been transported small distances (almost completely along fractures) and sorbed onto ferric oxides and calcites (CRWMS M&O 2000 [DIRS 151945], Sections 13.4 and 13.6). Matrix diffusion appears to have been inconsequential at Nopal I, with evidence of uranium generally extending only a few centimeters away from the fracture-matrix interface (CRWMS M&O 2000 [DIRS 151945], Section 13.4). While advective transport along fractures has been identified as an important transport mechanism in the analogue sites, matrix diffusion is an important mechanism attributed to the loss of lead in uraninites at Oklo and Cigar Lake (Janeczek and Ewing 1992 [DIRS 125262]).

11.3.2.8 Summary of Remaining Uncertainties

The focus of this modeling study is the evaluation of the DKM, the matrix discretization scheme currently used in the UZ flow and transport model, and the associated uncertainties in modeling flow and transport in UZ. It was found that the DKM can overestimate liquid flow in fractures within nonwelded units and underestimate matrix diffusion for radionuclide transport from the potential repository to the water table at the early time, when there is a large concentration gradient near the fracture-matrix interface. These uncertainties can be eliminated by using numerical schemes that account for steep gradients near fracture-matrix interfaces (see Section 11.3.2.9).

Table 11.3.2-1 summarizes the key uncertainties related to the calculation of flow and transport between fractures and the matrix. This evaluation is based on a conceptual model that the continuum approach can be used for adequately modeling UZ flow and transport. All the uncertainties associated with using the continuum approach to model UZ flow and transport still exist. The reason for using the continuum approach for the UZ flow and transport model is documented in *Conceptual and Numerical Models for UZ Flow and Transport* (CRWMS M&O 2000 [DIRS 141187], Section 6.4).

The upstream weighting scheme was used to determine flow and transport between fractures and the matrix; that is, the relative permeability in fractures was used as the relative permeability for the connection between fractures and the matrix. Because the relative permeability for the fracture continuum is defined for flow along the fracture-matrix interface, rather than flow between fractures and the matrix, using the relative permeability for the matrix is expected to be more appropriate for flow between fractures and the matrix. While this issue was partially accounted for in the estimation of effective parameters for flow during model calibration, its effects on overall flow and transport behavior in the UZ remain uncertain.

In this study, properties determined from a one-dimensional model calibration were used. Hence, perched water below the potential repository was not considered. While additional consideration of perched water may result in different flow and transport behavior, the evaluation results are expected to remain qualitatively unchanged. This is because the mechanisms governing flow and transport between fractures and the matrix are the same for both cases (i.e., with and without perched water).

11.3.2.9 Conclusions and Recommendations

The MINC simulation results show that under steady-state flow conditions, the matrix continua within a given gridblock have almost identical water saturations and potentials, indicating that the matrix can be treated as a single continuum. Thus, the dual-permeability concept is valid for modeling steady-state flow processes in the Yucca Mountain UZ.

Comparisons between simulation results indicate that the current dual-permeability approach overestimates fracture fluxes in some units, resulting in too large a connection distance between the fracture and matrix gridblocks. This is consistent with the noted discrepancy between the previously simulated fracture fluxes in the vitric Calico Hills Formation and those implied from the tracer-test results at the Busted Butte site (CRWMS M&O 2001 [DIRS 154024], Section 6.8.9). It is recommended that a reduced connection distance be used in generating the DKM grids for future flow simulations. The exact value of this reduced distance remains to be determined.

Simulation results demonstrate the importance of accurately representing the concentration gradients near fracture-matrix interfaces in simulating the overall radionuclide transport processes in the UZ. Because the DKM underestimates matrix diffusion during early time periods, it is likely that this model provides conservative estimates of the breakthrough time for radionuclide transport from the potential repository to the water table. This issue can be resolved using one of the following three approaches:

- Use the MINC for flow and transport in the site-scale UZ model. This approach is computationally intensive.

- Take advantage of the finding that the DKM is valid for modeling steady-state flow processes if the reduced connection distance is used. In this case, flow fields are simulated with the DKM and then mapped into a MINC grid. Radionuclide transport is simulated for the MINC grid using the computationally efficient T2R3D V1.4 code, which solves only the solute-transport equation. However, further investigations are needed to determine the reduced connection distance in this approach.

- Improve the existing particle trackers so they can handle sharp concentration gradients for a DKM grid and the corresponding flow fields. Section 11.3.3 contains a detailed discussion of current particle trackers and their capabilities.

11.3.3 A Comparison of Radionuclide Transport Calculation Methods

11.3.3.1 Introduction

This section summarizes the comparison of three transport modeling codes used in predicting radionuclide transport from the potential repository to the water table at Yucca Mountain and the discussions of the unquantified and quantified uncertainties in modeling using these three codes. Because of the differences of the modeling approaches used, the predictions of radionuclide transport for the same case may not be consistent among the codes. Therefore, a comparison study is necessary to assess the uncertainties and the suitability of each code as a modeling tool for predicting radionuclide transport in the Yucca Mountain UZ. In particular, FEHM V2.10 was used in TSPA, DCPT (Dual Continuum Particle Tracker) V1.0 was used in *Analysis of Base-Case Particle-Tracking Results of the Base-Case Flow Fields (ID: U0160)* (CRWMS M&O 2000 [DIRS 134732]) and *Analysis Comparison Advective-Dispersive Transport Solution to Particle Tracking* (CRWMS M&O 2000 [DIRS 141389]), and T2R3D V1.4 was used in *Analysis Comparison Advective-Dispersive Transport Solution to Particle Tracking* (CRWMS M&O 2000 [DIRS 141389]) and *Unsaturated Zone Flow and Transport Model Process Model Report* (CRWMS M&O 2000 [DIRS 151940]). Uncertainties in conceptual models and code implementations are presented in *Analysis Comparison Advective-Dispersive Transport Solution to Particle Tracking* (CRWMS M&O 2000 [DIRS 141389]) and *Particle Tracking Model and Abstraction of Transport Processes* (CRWMS M&O 2000 [DIRS 141418]) and summarized in Section 11.3.3.8.

Modeling three-dimensional chemical transport in unsaturated, heterogeneous, and fractured porous media such as the Yucca Mountain UZ is a challenging task, in terms of both the scientific basis and the required computational resources. The models developed using the three codes (FEHM V2.10, DCPT V1.0, and T2R3D V2.10) are based on the same dual-permeability grid formulation, with the same steady-state flow field calculated using TOUGH2 V1.4. The dual-permeability grid provides one mesh for the fractures and a second mesh for the matrix. Because each mesh occupies the entire spatial domain for a given problem, the fractures and matrix can be thought of as overlapping continua in the spatial domain. In the dual continuum approach, flow and transport in fractured porous media are conceptualized as two spatially overlapping and interactive subprocesses. Global flow and transport can take place in both fracture and matrix continua, while mass transfer between the two continua can occur locally in each grid cell. The major advantage of the dual continuum model is its capability to capture the major features of flow and transport in fractured porous rock with a minimum of computational resources. In terms of the transport calculation method, T2R3D V1.4 is based on the integral finite difference method of solving the advection-dispersion equations, FEHM V2.10 uses the node-based particle tracking method, and DCPT V1.0 uses the random-walk particle tracking method. In this comparison study, simulations were done in which all parameters (i.e., grid, flow field, and transport parameters) were exactly the same; the only difference was in the transport calculation methods used.

Uncertainties about the effect of the flow field on transport results from the dual continuum approach are presented in Section 11.3.2.8. The simulations produced by the three transport calculation methods are examined in the following sections.

11.3.3.2 Goal of Code Comparison for Modeling Unsaturated Zone Transport

The goal of the T2R3D V1.4, FEHM V2.10, and DCPT V1.0 is to predict the transport of radionuclides from the potential repository to the water table at Yucca Mountain. The goals of the code comparison were:

- Evaluate the advantages and disadvantages of the three transport simulators relative to each other
- Identify the conceptual and implementation uncertainties in the three transport simulators
- Evaluate the suitability of the three transport simulators with respect to the Yucca Mountain site.

11.3.3.3 Discussion of Total System Performance Assessment-Site Recommendation Results

A dual continuum approach with steady-state water flow was used for all three transport simulators, using the same dual-permeability grid and steady-state flow field calculated using TOUGH2 V1.4. This approach was considered appropriate because:

- The dual continuum model is capable of capturing the major features of flow and transport in fractured porous rock with a minimum of computational resources (Pan et al. 2001 [DIRS 154916], Section 3).
- Detailed prediction of transport at the discrete fracture level is not necessary for the intended use of the transport models in terms of predicting the breakthrough of radionuclides at the water table.
- A steady-state water flow field is a reasonable approximation of flow beneath the potential repository at Yucca Mountain because the long-term flow regime is approximately at a steady state under ambient condition. For comparison of different transport simulation codes, a steady-state water flow field makes the comparison simpler and allows a focus on the transport aspects.

All three simulators agree well with the analytical solutions for a dual porosity transport system approximated as a dual continuum model in which water flows only in the fractures (CRWMS M&O 2000 [DIRS 141389], Section 6.4.1; CRWMS M&O 2000 [DIRS 141418], Section 6.3.1. T2R3D V1.4 and DCPT V1.0 agree well in predicting breakthrough curves at the water table (CRWMS M&O 2000 [DIRS 141389], Sections 6.4.3 and 6.4.4) for the case of dual-permeability transport systems, which is likely to be the situation within the Yucca Mountain UZ (CRWMS M&O 2000 [DIRS 151940]). T2R3D V1.4 requires more computation time than DCPT V1.0, especially for the site-scale three-dimensional model (CRWMS M&O 2000 [DIRS 141389], Section 6.4.4). FEHM V2.10 can predict either faster or slower breakthrough of radionuclides at the water table than the other transport simulation codes, depending on the specific case (CRWMS M&O 2000 [DIRS 141418], Section 6.3). The conceptual models and their implementations, as well as advantages and disadvantages, are described in:

- FEHM V2.10
- DCPT V1.0
- T2R3D V1.4.

Differences in the results found for FEHM V2.10 compared with T2R3D V1.4 and DCPT V1.0 are a result of the difference in implementing the diffusion process between fractures and the matrix.

T2R3D V1.4 directly simulates the mass flux between the fracture and matrix continua and uses a finite-difference approximation to calculate the concentration gradient at the fracture-matrix interface. However, after the radionuclides are released into the fractures, the concentration gradient at the fracture-matrix interface is sharper near the front of a plume than farther back in the plume. But the finite-difference approximation of the concentration gradient at the fracture-matrix interface used in T2R3D V1.4 does not distinguish this difference; instead, it uses a fixed node distance and the average concentration in the matrix block to calculate the concentration gradient through the fracture-matrix interface. Such average values account for the average behavior of the fracture-matrix mass exchange, but the small-scale features of the concentration gradient are missed.

In DCPT V1.0, the mass exchange between the fractures and the matrix is simulated as a random switch process between two continua controlled by the particle transfer probabilities. This model is based on analogies between the particle transfer probabilities (either from fracture to matrix or vice versa) and the mass flux through the fracture-matrix interface with respect to the mass amount in each continuum. The approach is similar to the residence time/transfer function method used in the particle tracking algorithm of FEHM V2.10. The difference is that DCPT V1.0 calculates the probability of a particle leaving the current continuum after a given duration, while FEHM V2.10 calculates the probability of how much time a particle will spend in the given cell. Although continuum switching of particles is statistically independent of each particle, the calculation of the particle transfer probabilities requires parameters describing the fracture-matrix system that are based on an approximation of the concentration gradient at the fracture-matrix interface. In this regard, the concentration gradient at the interface will decrease as the particles further diffuse into the matrix with time. DCPT V1.0 does not consider this dynamic feature, and uses the same approximation of the concentration gradient at the interface as T2R3D V1.4 to derive the solution of the particle transfer probability. Thus, it has the same problem as T2R3D V1.4 with a dual-permeability grid. The transport calculation results found for these codes are in good agreement (CRWMS M&O 2000 [DIRS 141389], Sections 6.4.3 and 6.4.4).

FEHM V2.10 uses the residence time/transfer function approach for tracking particles, which calculates the probability of the residence time for a particle in a cell (as well as the probability of which adjacent cell the particle will enter after staying in the current cell). This approach is based on analogies between the cumulative probability distribution function of the residence time and the relative concentration as a function of time for a cell with a given flow path length to account for diffusion and dispersion. In FEHM V2.10, particles can move between nodes only via advection. A residence time of a particle in a cell is first calculated as the ratio of the fluid mass in the cell over the sum of the outlet mass flow rates from the cell. The residence time is then used as a scaling factor to calculate a new residence time from a dimensionless residence time to account for the diffusion and dispersion processes between nodes in the same continuum. The dimensionless residence time is determined randomly, based on a cumulative probability distribution function of the residence time that is equivalent to a one-dimensional analytical solution of the advection-dispersion equation for the cell with a step-input.

A similar approach is used to determine the modified residence time that accounts for the effects of the fracture-matrix diffusion process for the particles in the fracture continuum. The cumulative probability distribution function used in this step is based on an analytical solution of a dual porosity system (i.e., where there is no water flow through the matrix or the fracture-matrix interface). The reason for this two-step modification approach in FEHM V2.10 is to provide a more rapid calculation method that avoids the discretization errors associated with large matrix grid cells. Note that the residence time from the first modification step (accounting for diffusion and dispersion in the same continuum) is a random value, but it will be used to characterize the fracture-matrix transport system (i.e., the ratio of travel length along a fracture over the pore water velocity in the fracture) in the second modification step (accounting for diffusion between fracture and matrix). This implies that there are different fracture-matrix transport systems for particles entering the same cell.

How the introduction of randomness into the fracture-matrix transport system affects the overall simulation of the transport is not theoretically clear. However, numerical experiments show that this effect may lead FEHM V2.10 to underestimate the residence time added by diffusion into the matrix of particles traveling in the fractures. For particles in the matrix continuum, the same fracture-matrix diffusion process is neglected in FEHM V2.10. In principle, the fracture-matrix diffusion process should increase the residence time for the particles traveling in the fracture continuum and decrease the residence time for the particles traveling in the matrix continuum. This process becomes critical when the pore water velocity in the fracture continuum is higher than that in the matrix continuum. (Velocities in the fractures are typically larger than those in the matrix by several orders of magnitude.)

The uncertainties of these three simulators and their possible effects on transport modeling in terms of the repository performance evaluation are summarized as follows:

- The finite-difference approximation used in T2R3D V1.4 may be subject to discretization errors for cases with large matrix blocks and a small diffusion coefficient, especially in the early periods. Its inability to capture the small-scale concentration gradient at the fracture-matrix interface leads it to underestimate the fracture-matrix diffusion flux in early periods and to overestimate an early breakthrough, provided that the mass is released directly into fractures and the pore water velocity in the fractures is much faster than that in the matrix. Therefore, with a dual continuum grid, it tends to be a conservative predictor (i.e., it predicts early breakthrough).

- DCPT V1.0 shares this problem with T2R3D V1.4 and tends to be a conservative predictor.

- Neglecting the effect of the fracture-matrix diffusion process on the residence time of the particles in the matrix continuum will lead FEHM V2.10 to overestimate the travel time of the particles in the matrix continuum because the pore water velocity in the fracture continuum is usually much greater than that in the matrix continuum. This effect would cause the FEHM V2.10 to become an optimistic predictor (i.e., it would predict late breakthrough).

- Assuming zero pore water velocity in the matrix continuum (dual porosity model) in deriving the second cumulative probability distribution function for particles in fractures will also lead FEHM V2.10 to overestimate the residence time of the particles in the fracture continuum. This effect would also cause FEHM V2.10 to become an optimistic predictor.

- The effects of water flow through the fracture-matrix interface and the randomizing of the parameters on the calculation of the second cumulative probability distribution function for particles in the fracture continuum are not clear. However, numerical experiments show that these effects might cause FEHM V2.10 to have a much shorter delay time for particles in the fracture continuum. In some cases, such an effect can be of greater magnitude than the previous two effects and lead FEHM V2.10 to become a conservative predictor, as was found for three-dimensional site-scale model transport calculations (CRWMS M&O 2000 [DIRS 134732], Section 6.2.5).

- The analysis presented here is based on the existing baseline UZ flow model. Uncertainty in the flow model, particularly with respect to flowing fracture spacing, may affect the results of the transport comparison.

11.3.3.4 Model Developments since the Total System Performance Assessment-Site Recommendation

To solve the problem associated with the large matrix block in a dual-permeability grid, a new method to calculate the fracture-matrix particle transfer probability has been developed to capture the small-scale features of the fracture-matrix diffusion process (Bodvarsson 2001 [DIRS 154669], Attachment 8).

A MINC grid could be used to further split the matrix gridblock into multiple connected subblocks (see Section 11.3.2) and capture the small-scale concentration gradient at the fracture-matrix interface. However, the MINC approach has the following disadvantages:

- It is computationally intensive because it usually requires 5 to 10 times the grid size for the same problem.

- It is conceptually difficult to represent the global water flow in the matrix continuum (i.e., to connect the subblocks between neighboring matrix cells in a MINC grid with global water flow existing in both the fractures and the matrix). It is also practically difficult to validate such representations.

As discussed in Section 11.3.3.3, the approach used in FEHM V2.10 introduces additional uncertainties to the transport model. It yields undesired features in terms of modeling radionuclide transport in a fractured porous medium in which water flow occurs in both fractures and the matrix, as well as through the fracture-matrix interface (i.e., case-dependency as a conservative or optimistic predictor).

Capturing the small-scale features of the concentration gradient at the fracture-matrix interface with the dual continuum model remains a difficult challenge. To solve this problem, a refined model of fracture-matrix mass transfer within the framework of the dual-continuum random walk particle method was developed and incorporated into DCPT V2.0. Unlike DCPT V1.0, the new version defines the fracture-matrix particle transfer probability as a function of the active range. The active range is defined for each individual pulse (a group of particles that enter the domain at the same time) such that the probability of finding a particle of that pulse outside of the range is practically zero. That is, all particles of that pulse will be confined to this spatial range over a time step. An analytical solution is derived for the active range as a function of the particle age (the time since the particle was released into the media) based on diffusion into the matrix. DCPT V2.0 is able to capture the small-scale features of the concentration gradient at the fracture-matrix interface without having to add additional subblocks for the matrix (as with the MINC approach).

Details of Model Development–The fracture-matrix mass transfer is simulated by tracking the particles transferred between the fractures and the matrix, which is governed by the particle transfer probability. Equivalent to the finite-difference approximation for calculation of the mass transfer rate between the fractures and the matrix, the particle transfer probability from Continuum 1 to Continuum 2 can be determined as (Pan et al. 2001 [DIRS 154916], Section 3.5):

$$P_{12} = \frac{F_{12}}{F_{\text{out}} + F_{12}}[1 - \exp(-\Delta t / T_c)] \qquad \text{(Eq. 11.3.3-1)}$$

where F_{12} is a parameter that describes the strength of the water flow from Continuum 1 to Continuum 2 and the diffusion process through the interface between two continua. It is defined as follows ($Q_{12} = q_{\text{fm}} A_{12}$):

$$F_{12} = \max(Q_{12}, 0) + \frac{D_{12} A_{12}}{S_{12}} \qquad \text{(Eq. 11.3.3-2)}$$

where the effective dispersion coefficient at the fracture-matrix interface is $D_{12} = D_{\text{fm}} \theta_{\text{m}}$, the fracture-matrix interface area is A_{12}, the characteristic distance of the fracture-matrix system is S_{12}, and θ_{m} is volumetric water content in the matrix. F_{out} is a parameter that is the sum of the total water outflow from the cell to adjacent cells and the strength of the dispersion process through their interfaces through Continuum 1. The strength of the dispersion process can be calculated like the second term of Equation 11.3.3-2, but for each interface with the adjacent cells in the same continuum instead of the fracture-matrix interface. T_c is the characteristic time of Continuum 1 and is defined as a function of the water body volume in the cell (V_0), the retardation factor (R), F_{12}, and F_{out} (of Continuum 1):

$$T_c = \frac{V_0 \, R}{F_{12} + F_{out}} \qquad \text{(Eq. 11.3.3-3)}$$

Equation 11.3.3-1 shows that the particle transfer probability is a function of the time step Δt, but not t itself. In other words, the particle transfer process is assumed to be a stationary random process (i.e., the probability density function is independent of time). This is because the concentration gradient at the fracture-matrix interface can be represented as the difference of the average concentrations in the fractures and the matrix divided by the node spacing (a fixed characteristic distance). In terms of particle walking, this is equivalent to assuming that the particles in a given pulse will have the same range to walk within the matrix over time. However, this is not a proper assumption at early times when a plume has just entered the domain. Physically, a pulse only has limited influence at early times; significant time will be needed for the pulse to have its full range of influence, especially for cases with larger fracture spacing. As depicted in Figure 11.3.3-1 (lower part), the probability density function of the particle becomes wider and flatter with increasing time (t_3 is greater than t_2 and t_2 is greater than t_1). To catch this dynamic feature, the particle transfer probability defined in Equation 11.3.3-1 with Equation 11.3.3-2 and Equation 11.3.3-3 has to be modified by introducing a new concept: the active range. The active range is defined for each pulse such that the probability of finding a particle of the pulse outside of the range is practically zero; that is, all particles are confined to this spatial range over a time step. This leads to the replacement of the characteristic distance S_{12} and the water body volume V_0 in Equations 11.3.3-2 and 11.3.3-3 with the effective distance $S_{12}(t)$ and the effective volume $V_0(t)$, both of which are related to the active range. For parallel fracture systems, they can be defined as:

$$S_{12}(t) = S_{12} \frac{B^*(t)}{B} \qquad \text{(Eq. 11.3.3-4)}$$

and

$$V_0(t) = V_0 \frac{B^*(t)}{B} \qquad \text{(Eq. 11.3.3-5)}$$

where $B^*(t)$ is the active range within the matrix at time t. B is defined such that $2B$ is the fracture spacing. The effective volume for the fractures is assumed to be constant because the fracture aperture is usually so small that the active range can quickly reach its full capacity.

To get a scheme for estimating the active range $B^*(t)$, consider the transport in a system of parallel-plate fractures separated by porous rock (Figure 11.3.3-2). By the superposition principle, only the one-dimensional governing equation (in fracture-matrix dimension) is needed to derive the active range (temporarily ignoring advection):

$$\frac{\partial}{\partial t}[RC] = \frac{\partial}{\partial s}\left(D_{12} \frac{\partial C}{\partial s} \right) \qquad \text{(Eq. 11.3.3-6)}$$

where s is the distance into the matrix. With sources (and ignoring the fracture aperture $2b$ because b is much smaller than B):

$$C(s,0) = M_s \; \delta(s - 2iB) \qquad \text{(Eq. 11.3.3-7)}$$

where $\delta(s - 2iB)$ is a Dirac delta function whose value is zero everywhere except for an infinite value at point zero, which makes initial concentrations nonzero at the fractures only. The term M_s is a scaling factor that makes the concentration, C, in the final solution become a dimensionless variable within a range between 0 and 1. The i is the index of the fracture (from 0 to infinite). The solution to Equation 11.3.3-6, subject to Equation 11.3.3-7, can be expressed as (for $s \geq 0$ and using symmetry):

$$C(s,t) = \frac{2M_s}{(4\pi D_{12}\, t/R)^{1/2}} \sum_{i=0}^{\infty} \exp\left(-\frac{(s-2iB)^2}{4D_{12}\, t/R}\right) \qquad \text{(Eq. 11.3.3-8)}$$

For very small time,

$$C(s,t) \approx \frac{2M_s}{(4\pi D_{12}\, t/R)^{1/2}} \exp\left(-\frac{s^2}{4D_{12}\, t/R}\right) \qquad \text{(Eq. 11.3.3-9)}$$

The concentration in Equation 11.3.3-9 can be interpreted as the probability of finding a particle (initially at $s = 0$) at location s and time t. Therefore, the probability a particle will be located in the active range $[0, B^*]$ is:

$$P(0 \leq s \leq B^*) = \mathrm{erf}\left(\frac{B^*}{\sqrt{4D_{12}\, t/R}}\right) \qquad \text{(Eq. 11.3.3-10)}$$

Equation 11.3.3-10 implies that B^* should be proportional to the square root of t. By definition, a B^* should be selected such that $P(0 \leq s \leq B^*)$ is close to 1. An adequate active range for short time can be expressed as (Bodvarsson 2001 [DIRS 154669], Attachment 8, p. 140):

$$B^*(t) = \min\left(4\sqrt{4D_{12}\, t/R},\, B\right) \qquad \text{(Eq. 11.3.3-11)}$$

The corresponding $P(0 \leq s \leq B^*)$ is about 1×10^{-7} and B is half of the fracture spacing, which is the maximum active range by definition.

For a longer time, B^* approaches B, and the other terms in Equation 11.3.3-8 cannot be ignored. There is no simple solution like Equation 11.3.3-9 for that case. However, because the purpose is to get a proper $B^*(t)$, it can be assumed that the relative effects of the other terms in Equation 11.3.3-8 on the active range are equal to their relative contributions to concentration. In other words, the active range can be modified as follows:

$$B^*(t) = \min\left(4\sqrt{4D_{12}\, t/R}\, W(t),\, B\right) \qquad \text{(Eq. 11.3.3-12)}$$

The weighting function $W(t)$ is obtained as the ratio of the two-term solution over the one-term solution as defined in Equation 11.3.3-8 at a given B^*, and can be approximated as:

$$W(t) \approx 1 + \frac{1}{1 + \dfrac{B\left(B - B^*\right)}{D_{12}\, t/R}} \qquad \text{(Eq. 11.3.3-13)}$$

The reason for taking only two terms in calculating the weighting function is because further terms are insignificant for typical values of B.

A similar approach can be used to incorporate the effects of fracture-matrix water flow on the active range. In a dual continuum model, the total water flow rate through the interface ($s = 0$) and at $s = B$ (where Q is zero) is known. One can take a linear interpolation and get the final scheme for the active range as:

$$B^*(t) = \min\left(4\sqrt{4\, D_{12}\, t/R}\, W(t) + \frac{Q_{12}\, t}{A_{12}}\left(1 - \frac{B^*}{B}\right),\ B \right) \qquad \text{(Eq. 11.3.3-14)}$$

Note that the time, t, used in the above equations is for a single pulse. Multiple initial values of time (i.e., $t = 0$) have to be defined for cases with multiple pulses. In other words, for the same pair of fracture and matrix cells at the same simulation time, the particle transfer probability may be different for different individual particles. The implementation in DCPT V2.0 tracks the age of each particle, which is defined as the time elapsed since the particle was released into the domain. Thus, the particle transfer probability is a function of the age of the particle.

The above derivation of the active range is valid only for particles initially released in the fractures. The active ranges for particles released into the matrix would be different, and depend on how far from the interface they are initially located, which is not known in practice. It is assumed that all particles initially released into the matrix are uniformly distributed within the matrix, and thus the active range will always be B. A parameter called "initial status" is assigned to each particle to distinguished which continuum it is released into initially (at $t_p = 0$).

11.3.3.5 Results of Analysis

Verification with Analytical Solutions (Parallel Fractures)–An analytical solution for solute transport in fractured porous media with parallel fractures (Figure 11.3.3-2) was derived by Sudicky and Frind (1982 [DIRS 105043]). This solution is based on the assumption that solute transport between fractures and the matrix occurs through matrix diffusion in the horizontal direction only, and that matrix advection and diffusion in the vertical direction can be ignored. Table 11.3.3-1 shows the relevant parameters for the two test cases. In particular, the two different fracture spacings of 1 m and 10 m were used for Case 1 and 2, respectively.

Figure 11.3.3-3 shows the results for Case 1. Breakthrough curves produced by DCPT V1.0 and DCPT V2.0 agree well with the analytical solution. DCPT V1.0 slightly overestimates the concentration at early times for the smaller fracture spacing (1 m) case. However, DCPT V1.0 seriously overestimates the breakthrough at early times for Case 2, which has a larger fracture spacing (10 m) (Figure 11.3.3-4). In particular, DCPT V1.0 estimates that more than 60 percent of solutes would have leached out of the system in about 0.1 yr if a plume had been injected into the top of the column. This error obviously is too large to be acceptable for predicting radionuclide transport at Yucca Mountain. Note that DCPT V1.0 agrees well with the analytical solution at much later times (i.e., after about 100,000 years), which clearly indicates that the finite-difference approximation is accurate only for later times. DCPT V2.0 agrees with the analytical solution for both cases because it catches the dynamic nature of the fracture-matrix mass transfer process (Figures 11.3.3-3 and 11.3.3-4). The dynamic concentration gradient between fractures and matrix depends on fracture spacing. At early times (up to 5,000 years), the analytical solutions for Case 1 and Case 2 shown in Figure 11.3.3-5 are almost identical. Therefore, the fracture spacing has little effect on the breakthrough during early periods of time.

Results for Transport in the Unsaturated Zone–UZ transport calculations for the site-scale model with the present-day mean infiltration map and perched water table model #1 (CRWMS M&O 2000 [DIRS 151940], Section 3.7) were used to assess the impact of different models of fracture-matrix mass transfer on overall simulated radionuclide transport behavior. Figure 11.3.3-6 shows the cumulative breakthrough curves of two radionuclides (technetium and neptunium) at the water table, as predicted by DCPT V1.0 and DCPT V2.0, respectively. DCPT V1.0 overestimates the early breakthrough for both radionuclides compared to DCPT V2.0. Technetium breaks through about 30 times faster than neptunium because it is not retarded by adsorption.

11.3.3.6 Abstraction for Total System Performance Assessment

DCPT V2.0 may be used for TSPA UZ transport calculations as an alternative particle tracking code to FEHM V2.10. DCPT has been modified to enable its use with GoldSim, the TSPA code. All connections between GoldSim V6.04.007 and DCPT V2.0 are analogous to those between GoldSim V6.04.007 and FEHM V2.10 in the TSPA-SR model (CRWMS M&O 2000 [DIRS 143665]). However, DCPT V2.0 was not used for SSPA Volume 2 calculations (McNeish 2001 [DIRS 155023]) because a version of GoldSim linked with DCPT V2.0 was not available when the TSPA calculations were performed.

11.3.3.7 Multiple Lines of Evidence

Because this section deals solely with the comparison of different software codes used in predicting radionuclide transport, multiple lines of evidence are not directly applicable.

11.3.3.8 Summary of Remaining Uncertainties

Several uncertainties concerning the suitability of the different codes for TSPA transport calculations are discussed below. Also, related uncertainties are identified in Section 11.3.2.8. The key uncertainty issues are summarized in Table 11.3.3-2.

Uncertainties Caused by Grid Discretization Effects–The current numerical model as described in Section 11.3.3.3 uses coarse grids (up to 60 m vertically and up to 200 m laterally) because of limitations on computational resources. Although numerical mixing/dispersion is not a serious problem for transport simulation in the Yucca Mountain UZ (as shown in numerical experiments reported in *Analysis Comparing Advective-Dispersive Transport Solution to*

Particle Tracking [CRWMS M&O 2000 [DIRS 141389]), any transport calculation method using a coarse grid may lack the resolution to capture the spatial variability of the flow field and transport properties. With respect to the flow solution, a coarse grid will cause TOUGH2 V1.4 to underestimate capillary effects where critical layers are thin. This will result in uncertainties in the flow-field and transport pathways for radionuclides. In a complex and heterogeneous media such as the UZ, the effects on radionuclide travel time could be very large. It is possible to reduce the uncertainty in predictions by developing numerical models of flow and transport with higher spatial resolution. Calculation of detailed flow fields for the UZ may require a supercomputer to run the TOUGH2 V1.4 code with parallel computing techniques. Considerable effort is also required to develop particle trackers that can efficiently simulate transport with large grids.

The uncertainties resulting from the grid discretization effect of matrix blocks with respect to diffusion through the fracture-matrix interface are discussed in Section 11.3.2.

Uncertainties Resulting from Limited Theoretical and Experimental Results to Support Dual Continuum Transport Calculation Methods in Fractured Porous Media–No analytical solution is currently available for transport in unsaturated, fractured porous media with global water flow occurring in both fracture and matrix continua. As a result, the transport code has been validated against analytical solutions for transport in fractured porous media assuming that water flow occurs in the fractures only (Section 11.3.3.5). Applicable field or experimental data are limited. Well-controlled experiments of transport in unsaturated, fractured porous rock would provide opportunities to verify the numerical model and further explore the nature of the fracture-matrix mass transfer process. An example of a well-controlled experiment would be a laboratory experiment of tracer with a 1-m^3 block of rock containing fractures. This type of experiment is important for building an accurate numerical model because many aspects of the fracture-matrix interaction process are still poorly understood. Many numerical experiments show that the fracture-matrix mass transfer is a critical process that controls how fast radionuclides migrate to the water table. An example of one such experiment is presented in *Analysis Comparing Advective-Dispersive Transport Solution to Particle Tracking* (CRWMS M&O 2000 [DIRS 141389], Section 6.4.3).

11.3.3.9 Summary and Conclusions

For transport in fractured porous media with water flow occurring in both continua, T2R3D V1.4 (with a dual continuum grid) or DCPT V1.0 may be a conservative predictor of radionuclide breakthrough at the Yucca Mountain water table, especially at early times. By using a residence time/transfer function approach based on analytical solutions for a simpler system, the FEHM V2.10 particle tracking algorithm does not have the discretization problem associated with large matrix blocks in a dual continuum grid. But it can be a conservative or optimistic predictor compared with T2R3D V1 or DCPT V1.0, depending on the particular case or portion of the breakthrough because of the uncertainties introduced in the implementing the fracture-matrix diffusion processes. In site-scale transport simulations performed so far (CRWMS M&O 2000 [DIRS 134732], Section 6.2.5), FEHM V2.10 is found to be generally conservative relative to DCPT V1.0. However, the implementation of the fracture-matrix diffusion processes for problems with water flow in both continua is complicated. By using the new method for calculating fracture-matrix particle transfer probability, DCPT V2.0 does not have the problems associated with the larger matrix block in a dual-permeability grid that T2R3D V1.4 and DCPT V1.0 do. It also does not have the uncertainties of FEHM V2.10.

Of the codes evaluated, DCPT V2.0 is the most suitable simulator for such a system, considering numerical accuracy, efficiency issues, and the current understanding of transport processes in fractured porous media. T2R3D V1.4 with a MINC grid can be an alternative, but with the associated cost of poorer numerical efficiency and more complicated validation requirements.

11.3.4 Effects of Change in Potential Repository Footprint on Three-Dimensional Transport Simulation

This section summarizes the results of modeling three-dimensional radionuclide transport (TOUGH2 V1.4) with the new southern extended flow model domain. The extended domain, additional hydrogeologic settings, and flow modeling results are provided in Section 3.3.4. The new UZ transport model examines the extended potential repository design for a lower-temperature operating mode (BSC 2001 [DIRS 154548]) with the southern and northern blocks (Figure 3.3.4-7). The objective of this section is to investigate the effects of the lower-temperature operating mode on radionuclide transport under ambient flow conditions. The simulations were conducted using a conservative radionuclide and a reactive radionuclide released from the extended potential repository and transported to the water table.

11.3.4.1 Introduction

The *Unsaturated Zone Flow and Transport Model Process Model Report* (CRWMS M&O 2000 [DIRS 151940]) presents a summary of models used to simulate flow and transport processes in the Yucca Mountain UZ in support of the TSPA-SR (CRWMS M&O 2000 [DIRS 153246]). The evaluation of radionuclide transport from the potential repository horizon to the groundwater in the saturated zone is critical to assessing the performance of the potential repository. The transport modeling efforts use the flow processes of the UZ flow model as a framework for the transport of aqueous and colloidal radionuclide species. Modeled mechanisms include transport inside and between fracture and matrix continua by advective and/or diffusive processes, as well as sorption in the matrix. Results of previous three-dimensional modeling (BSC 2001 [DIRS 144331]; CRWMS M&O 2000 [DIRS 122797]) were used to identify major transport mechanisms, breakthrough times through different hydrogeologic units, effects of major hydrogeologic features (faults and perched water), and transport characteristics (sorption and matrix diffusion).

As documented in the *Unsaturated Zone Flow and Transport Model Process Model Report* (CRWMS M&O 2000 [DIRS 151940]), the transport model evaluates a suite of factors that control potential radionuclide transport to determine their effects on radionuclide breakthrough times and concentrations at the groundwater table (CRWMS M&O 2000 [DIRS 151940], Section 3.11.1.1). More than 70 three-dimensional radionuclide transport simulations (CRWMS M&O 2000 [DIRS 151940], Section 3.11; CRWMS M&O 2000 [DIRS 122797], Section 6.7; CRWMS M&O 2000 [DIRS 144331], Sections 6.10 to 6.17) were conducted to obtain insight into the various impacts of infiltration rates, perched water conceptual models, faults, retardation, matrix diffusion, and colloidal effects on tracer and radionuclide migration through the UZ.

Modeling uncertainties are attributed primarily to the large variability in the flow and transport properties over the spatial and temporal scales that have been identified during site characterization and modeling studies. Other uncertainties are model parameters for sorption (K_d) coefficients in different tuffs and matrix diffusion coefficients.

11.3.4.2 Goals of the Model

The fundamental goals of the UZ transport model are to:

- Integrate the available geochemical and isotopic data from the UZ system into a single comprehensive model

- Develop an understanding of tracer and radionuclide transport mechanisms and identify controlling processes and factors

- Estimate groundwater travel and radionuclide transport times from the potential repository to the water table and breakthrough curves and collection areas at the water table under ambient hydrologic, thermal, and geochemical conditions, as well as predict system response to future climate conditions.

11.3.4.3 Discussion of Total System Performance Assessment-Site Recommendation Results

More than 40 three-dimensional modeling studies on groundwater travel times and tracer or radionuclide transport using more than 20 three-dimensional flow fields are documented in *UZ Flow Models and Submodels* (CRWMS M&O 2000 [DIRS 122797], Section 6.7). Simulation results for conservative and reactive tracers/radionuclides were used to obtain insights into groundwater travel times and radionuclide transport from the repository to the water table.

Another 30 three-dimensional radionuclide transport simulations were conducted in support of *Radionuclide Transport Models under Ambient Conditions* (CRWMS M&O 2000 [DIRS 144331], Sections 6.10 through 6.17). Technetium-99, neptunium-237, and plutonium-239 were investigated, as well as the important members in the decay chains of neptunium-237 and plutonium-239. Transport simulations of four colloids of different sizes were also documented (CRWMS M&O 2000 [DIRS 144331], Sections 6.16 to 6.17). The report examined the influence of three climatic scenarios, as well as perched water models and fault treatment, on radionuclide transport.

The model results present a quantitative evaluation of the effects of different perched water conceptual models, faults, infiltration rates, sorption, and matrix diffusion on radionuclide transport processes. In particular, the simulations indicate that faults and fractures are the main pathway of transport because they channel flow along their orientation and limit lateral transport across their orientation. In the simulations, diffusion from the fractures into the matrix is the main mechanism retarding the transport of nonsorbing radionuclides.

Figure 11.3.4-1 correlates average infiltration rates and tracer transport times at 50 percent mass breakthrough at the water table from the 42 three-dimensional tracer transport simulations, including 9 climatic scenarios and different perched water conceptual models. The correlations presented in Figure 11.3.4-1 indicate that:

- Radionuclide transport times decrease with increasing average surface infiltration (net water recharge) rate over the model domain. When an average infiltration rate increases from 5 to 35 mm/yr, average groundwater travel (50 percent breakthrough) times decrease by one to two orders of magnitude.

- Nonsorbing radionuclides (e.g., neptunium-237) migrate one to two orders of magnitude faster than sorbing radionuclides when traveling from the repository to the water table under the same infiltration conditions.

- Perched water conceptual models may also have a large effect on groundwater travel and transport times, but the overall impact on tracer breakthrough times at the water table is small compared to the effects of infiltration and sorption.

11.3.4.4 Model Development since Total System Performance Assessment-Site Recommendation

A new three-dimensional UZ flow model (see Section 3.3.4) has been developed to evaluate the performance of a potential expanded repository design (BSC 2001 [DIRS 154548]). The new model domain is enlarged to include a southern expansion area (i.e., a potential second southern repository block) (Figure 3.3.4-7). This extended UZ flow model was used to conduct transport studies of technetium-99 and neptunium-237 (Bodvarsson 2001 [DIRS 154669], Attachment 13, pp. 26 to 27).

11.3.4.5 Discussion and Comparison of New Flow Fields to Previous Results

This section summarizes results from the simulations of tracer and radionuclide transport using the new three-dimensional flow field for an extended southern model domain. These simulations represent transport processes for radionuclides from the potential repository to the water table given the current perched water conceptual model, mean infiltration scenarios, and steady-state ambient flow conditions described in Section 3.3.4.5.2.

In the modeling studies, a tracer or radionuclide is treated as a conservative (nonsorbing) or reactive (sorbing) component transported through the UZ. In both cases, the hydrodynamic dispersion effect through the fracture-matrix system is ignored. A constant molecular diffusion coefficient of 3.2×10^{-11} m^2/s is used for matrix diffusion for the conservative component technetium-99, and a coefficient of 1.6×10^{-10} m^2/s is used for the reactive component of neptunium-237 (CRWMS M&O 2001 [DIRS 154024], Section 6.6.3). In the case of a reactive (sorbing) tracer several K_d values, ranging from 1 to 3 ml/g, are selected to approximate those for neptunium-237 transport (CRWMS M&O 2001 [DIRS 154024], Table 2a). For a conservative tracer, K_d is set to zero. All transport simulations were run to 1 million years using a steady-state flow field generated by the new three-dimensional flow model and constant source concentration conditions at the repository fracture nodes. A total of six simulations were conducted for technetium and neptunium (neglecting radioactive decay) released from the entire potential repository, including the southern extension and the northern potential repository model domain used in the TSPA-SR (CRWMS M&O 2000 [DIRS 148384], Section 6.3.1.3).

Tracer transport times from the potential repository to the water table can be analyzed using a cumulative or fractional breakthrough curve (Figure 11.3.4-2). The fractional mass breakthrough in these figures is defined as the cumulative mass of tracers or radionuclides (normalized by the total initial mass of the component at the potential repository blocks) predicted to arrive at the water table over the entire bottom model boundary as a function of time. In Figure 11.3.4-2, solid- or dashed-line curves represent simulation results for conservative (technetium) and reactive (neptunium) tracers released from the fractured repository blocks in the new model grid and the TSPA grid. The symbols represent tracer results released from the southern and northern potential repository blocks using the new grid.

Figure 11.3.4-2 shows release scenarios grouped into sorbing and nonsorbing. The grid refinement in the new transport model produces longer or improved tracer transport times when compared with the TSPA results shown in Figure 11.3.4-2. Sorbing and nonsorbing tracer releases from the southern potential repository block are significantly longer because the southern block is situated over an area with lower average infiltration rates and a longer travel distance to the water table. Overall, the simulations of tracer transport in the extended potential repository domain give similar, but somewhat slower, breakthrough times than the TSPA-SR flow fields shown in Figure 11.3.4-2.

11.3.4.6 Field-Scale Model Validation Studies at Busted Butte

UZ tracer tests are being conducted at Busted Butte to determine solute and colloid movement through tuff horizons that underlie the potential repository location at Yucca Mountain. The Busted Butte test block consists of three stratigraphic units. Two of these are part of the Topopah Spring Tuff, which is subdivided into an upper moderately welded vitric tuff (Tptpv2) and a lower vitric and nonwelded tuff (Tptpv1); the third is the underlying vitric and nonwelded tuff of the Calico Hills Formation (Tac). The boundary between the Topopah Spring welded hydrostratigraphic unit (TSw) and the Calico Hills nonwelded vitric hydrostratigraphic unit in the UZ flow and transport model is defined as being between units Tptpv2 and Tptpv1 (CRWMS M&O 2000 [DIRS 151940], Table 3.2-2).

Test Phase 1A was designed to provide information regarding flow and transport in the Calico Hills hydrogeologic unit and an understanding of the influence of permeability contrasts on fluid movement. Phase 1B was designed to provide data on fracture flow and transport in the welded Topopah Spring hydrogeologic unit (CRWMS M&O 2001 [DIRS 154024]). Phase 2 (Dixon 2001 [DIRS 155048], p.1) was designed to test the larger-scale behavior of the two units, including:

- Validation of scaling assumptions at various scales
- Validation of laboratory determined sorption for field-scale tests
- Colloid migration behavior.

In October 2000, Phase 2 injection was terminated. Overcore samples were collected and a mineback is currently in progress (Dixon 2001 [DIRS 155048], p. 3).

Detailed numerical models have been developed for both Phase 1B and Phase 2. Computational grids have been generated and updated based on all available physical data. The increasing grid accuracy and complexity is used to address the question of how the quantity of site-specific data improves the ability of the model to predict flow and transport (Dixon 2001 [DIRS 155048]).

11.3.4.6.1 Phase 2 Test Results: Comparison of Model with Field Data

All modeling is being done using FEHM V2.10. The current grid has almost 2 million elements and reflects the most current information about fault and stratigraphic contacts in the test block. This grid accurately represents the injection and collection boreholes. Grid resolution ranges from 0.0625 m near features to 1 m. Hydrogeologic parameters are taken from measurements at Busted Butte, as available. These include porosity, hydraulic conductivity, van Genuchten parameters for relative permeability, and sorption coefficients. Simulations assume homogeneity within units.

Initial simulation results show very good agreement with bromide breakthrough data (Dixon 2001 [DIRS 155048], p. 9, Figure 5). The actual injection rate appears to be 10 to 20 percent lower than the original rate. The observation that the quality of fit uniformly decreases with change in injection rate suggests the possibility that the laboratory-measured hydrogeologic parameters do not accurately reflect the field behavior. For example, if reported laboratory conductivities are lower than the effective field conductivities, the model would underpredict breakthrough. These issues are currently being tested.

Sensitivity analyses of the various parameters have been run to attempt to best fit the experimental tracer data. In general, simulations tend to underpredict concentration at early times and overpredict at late times.

11.3.4.6.2 Phase 2 Test Results: Validation of Scaling Assumptions

In Phase 2, collection holes were placed at different distances from the injection holes to assess the influence of travel distance. Differing travel distances also provide a range of scales for studying transport, from tens of centimeters to meters.

The effect of travel distance on tracer transport in the hydrogeologic Calico Hills unit is demonstrated by tracer breakthrough (Dixon 2001 [DIRS 155048], pp. 10 to 11). Breakthrough times at the different distances scale approximately linearly with travel distance. The observed linearly increasing travel times suggest that at the scale of tens to hundreds of centimeters, the hydrogeologic response of the unit is relatively homogeneous.

The major uncertainty in capturing the tracer response in the Phase 2 simulations seems to be the representativeness of using the hydraulic properties obtained from small core samples to model field-scale flow and transport. The qualitatively good fit of the breakthrough curves for each borehole suggests that heterogeneity plays a less significant role. The problem is how to scale up the core data to represent the processes occurring at the Busted Butte test site or to collect data at the appropriate scale for site-scale models. Currently, an inverse modeling approach is being applied to best fit the test data to determine if it is possible to use inverse modeling results to test current approaches to upscaling (Dixon 2001 [DIRS 155048], p. 11).

11.3.4.6.3 Phase 2 Test Results: Effects of Sorption

The influence of sorption/retardation has been analyzed by comparing breakthrough curves for bromide versus lithium at various boreholes. This analysis indicates that, as expected, lithium breakthrough is retarded with respect to bromide (Dixon 2001 [DIRS 155048], p. 12). Laboratory sorption measurements calculate lithium K_d values between 0.4 and 1.1 ml. All other reactive tracers used have significantly higher K_d values and were not expected to break through at any of the boreholes within the injection time frame. Analyses of rock samples from overcoring and mineback, initiated in December 2000, should provide travel distances and concentrations for other reactive tracers. The computational model predicts nickel (K_d of 48 in Tptpv1, 430 in Tptpv2) will have moved only 6.25 cm from the upper injection holes over the period of the Phase 2 experiment. Model predictions will be compared to rock analyses as they become available.

11.3.4.6.4 Phase 2 Test Results: Colloid Transport

Field experiments at Busted Butte included the injection of latex microspheres to examine colloid transport in the field (Dixon 2001 [DIRS 155048], p. 12). Analysis of the collection pads for the microspheres was inconclusive as to whether colloids were being transported in the experiment. As a result, a series of laboratory-based column experiments was used to determine the likelihood of colloid transport at Busted Butte.

Core samples 5 cm in length from all three stratigraphic units were used in the experiments (Dixon 2001 [DIRS 155048], p. 13). The initial experiments used synthetic Busted Butte water with the field concentrations of LiBr and latex microspheres (190-nm and 55-nm diameter). Results showed that the breakthrough of microspheres was affected by ionic strength. In general, as the ionic strength of a solution increases, the double layer around particulates decreases, which can lead to coagulation and flocculation of particulates in solution. The synthetic Busted Butte water (0.01 M ionic strength) has a higher divalent cation concentration than observed in the J-13 well water or local groundwater, which affects the stability of the microspheres. In addition, there was not a supply of lower ionic strength water mixing with the tracer solution in the Busted Butte experiment. The combination of these two factors is one of the reasons breakthrough of the microspheres was not observed in the field experiment. Samples collected during overcoring of injection locations will be examined to qualitatively determine if any migration of the microspheres occurred away from the injection location.

Experiments were conducted to detect breakthrough of the microspheres through saturated Tac core samples as a function of ionic strength (Dixon 2001 [DIRS 155048], p. 13, Figure 8). The breakthrough curve at 0.01 M LiBr shows that the peak of the microsphere breakthrough occurs after tracer injection is stopped and 1.5 pore volume of water has been put through the column. This is not observed in the breakthrough curves of the other two experiments (0 and 0.0005 M LiBr), in which the peak of the microsphere breakthrough occurs when the injection is switched to a water flush. The late breakthrough for the 0.01 M solution suggests that colloids are aggregated due to the high ionic strength during the injection and are not transported. When the column is switched to the water flush, the ionic strength is reduced and some of the aggregated colloids are able to break apart and be transported through the column.

This set of experimental results illustrates two points. First, under saturated conditions, colloid transport is possible under steady-state conditions. This serves as an upper bound for modeling unsaturated colloid transport. The results indicate that some of the colloids are retained, but a significant percentage is transported. Second, localized chemistry is an important factor for colloid transport.

The effects of water saturation, pH changes, and divalent cation concentrations on the stability and transport of colloids remain an area of uncertainty in the modeling.

11.3.4.7 Abstraction for Total System Performance Assessment

The work reported in this section is devoted to evaluating process model sensitivities and uncertainties. Consequently, simulation results from this study are not used to support any abstraction model that directly supports the TSPA. The results found here indicate that the process model and associated model abstractions used to represent potential repository footprint effects on three-dimensional transport effects are representative (or conservative) with respect to the TSPA-SR baseline (CRWMS M&O 2000 [DIRS 153246]). Therefore, any future changes in model abstractions for this component will not diminish the performance represented in the total system performance baseline.

11.3.4.8 Multiple Lines of Evidence

This section presents information from ongoing and past analogue studies that provide indications of the rate of transport in unsaturated media over decades and millennia and the efficacy of sorbing minerals in retarding radionuclides.

11.3.4.8.1 Peña Blanca

Preliminary results from fiscal year 2000 uranium isotope studies at the Nopal I uranium deposit at Peña Blanca, Mexico, appear to indicate low actinide mobility in unsaturated siliceous tuffs under semiarid, oxidizing conditions. Uranium-thorium age data from fracture-filling minerals indicate that the primary transport of uranium away from the Nopal I deposit along fractures occurred more than 300,000 years ago (CRWMS M&O 2000 [DIRS 141407], Section 6.5.2.1.4.2). The radium-226/thorium-230 activity ratios indicate redistribution of radium within the last 5,000 years as a result of secondary fluid events. Therefore, the data demonstrate stability over 100,000-year time scales for uranium (uranium-235 and uranium-238), thorium, and protactinium in fracture-filling materials. In an analogous sense, this stability should extend to transuranics and the rare earth elements. The high mobility of radium can be considered analogous to transport of strontium and cesium because of a similar ionic radius. Because of similarities between Peña Blanca and Yucca Mountain in hydrogeologic setting, mineralogy, and term, the tuffs at Yucca Mountain should have similar retentive properties to impede oxidized uranium mobility.

In 2000, water samples were collected from the adit, a small borehole, and a neighboring well at Peña Blanca. Stable isotope data and semi-quantitative uranium concentration data were obtained for these samples.

Table 11.3.4-1 indicates that the stable isotope data for samples AS-5 and AS-6 (from a drill hole into a perched water horizon and from a well) have significantly lower values than the other samples. They fall on the global meteoric water line (Craig 1961 [DIRS 104753]) and probably represent the average composition for the precipitation at the site. The other samples were all collected from the adit. The isotopic signature of sample AS-1 lies on the global meteoric water line, but probably does not represent a rainwater sample, since it is relatively high for meteoric water at this latitude. The other three samples all fall significantly to the left of the global meteoric water line and may represent atmospheric water vapor that has diffused into the adit and condensed in the cooler, underground environment, followed by some period of evaporation in the collection bottles. The uranium data shown in Table 11.3.4-1 indicate a rapid decrease in uranium concentration with distance from the ore body, which is closest to sample AS-1.

Pickett and Murphy (1999 [DIRS 110009]) obtained uranium and thorium measurements for waters near the Peña Blanca uranium deposit. They analyzed three types of samples: perched water trapped in an old borehole at the +10 level (the same location as AS-5), seep water from an old adit about 8 m below the surface, and groundwater in the carbonate aquifer from a sample collection point about 1.3 km southeast of the deposit. Uranium concentrations range from 7.1×10^{-10} mol/L (0.13 dpm/L) for groundwater to a range of 8.3×10^{-10} to 37.2×10^{-10} mol/L (0.15 to 0.66 dpm/L) for seep water and a range of 2.0×10^{-8} to 2.4×10^{-8} mol/L (3.6 to 4.3 dpm/L) for perched water. Thorium concentrations range from 6.1×10^{-13} mol/L (3.5×10^{-5} dpm/L) for groundwater to a range of 1.9×10^{-12} to 5.3×10^{-12} mol/L (1.1×10^{-4} to 3.0×10^{-4} dpm/L) for seep water and a range of 6.7×10^{-10} to 11.6×10^{-10} mol/L (0.038 to 0.066 dpm/L) for perched water. Pickett and Murphy (1999 [DIRS 110009]) interpreted the results in terms of mineral solubility. They found that uranium in the perched water is close to the solubility for haiweeite (a calcium uranyl silicate mineral), whereas in other waters it is undersaturated with respect to uranium minerals. However, in all the waters thorium is supersaturated with respect to thorianite, and is likely present in colloidal form (less than 0.2 μm). The occurrence of undersaturation for uranium and supersaturation for thorium indicates that radionuclide transport in the UZ may be controlled by kinetic factors, such as rock dissolution and colloid formation, which complicate interpretations based on thermodynamic (solubility) considerations.

The uranium-series modeling described in Ku et al. (1992 [DIRS 109939]) provides a means to characterize the kinetically controlled radionuclide transport at Peña Blanca. Figure 11.3.4-3a plots uranium-234/uranium-238 versus 1/uranium-238 from the Pickett and Murphy (1999 [DIRS 110009]) data. The positive linear correlation shown by the plot is expected for samples from the UZ. The one sample from the carbonate aquifer in the saturated zone shows a much lower uranium-234/uranium-238 concentration, perhaps due to a prolonged interaction with old calcites in the aquifer, which allows uranium exchange between rock and solution and masks the alpha recoil-induced uranium-234 enrichment in the water. Using this model, the uranium-234 alpha-recoil rate into fluids is estimated to be 9 dpm/L/yr at Peña Blanca, versus dissolution rates of 8.3 dpm/L/yr for uranium-238 and uranium-234. The model also allows determination of fluid transit time in the UZ. As shown in Figure 11.3.4-3b, uranium-238 increases linearly with increasing transit time, while uranium-234/uranium-238 decreases. The transit time for the seep water infiltrated into the Level +00 adit 8 m below surface is estimated to be 6 to 29 days, and that for the perched water at 10.7-m depth in an old borehole is 0.4 to 0.5 years. The large values of transit time for the perched water may reflect the long residence time of water in the borehole.

It should be noted that although the water transit time in the UZ is short, significant dissolution of uranium from fractured rocks does occur in a low-water flux, high-uranium concentration setting near the Nopal I uranium deposit. This can be seen from the uranium data in Table 11.3.4-1, which indicates a rapid decrease in uranium concentration with distance from the ore body, which is closest to sample AS-1.

11.3.4.8.2 Little Movement of Metals in the Unsaturated Zone–Akrotiri, Santorini

The Akrotiri archeological site on the island of Santorini, Greece, provided conditions for the study of trace element transport in a setting similar to Yucca Mountain in its silicic volcanic rocks, dry climate, and oxidizing, hydrologically unsaturated subsurface conditions (Murphy et al. 1998 [DIRS 126105]). About 3,600 years ago, in 1645 B.C., the Minoan eruption buried settlements under 30 m of volcanic sediment (Murphy et al. 1998 [DIRS 126105]). Evidence for a plume of copper, tin, and lead was indicated through selective leaching of packed earth and bedrock samples collected directly beneath the site, where bronze and lead artifacts were excavated from a depth of 1.5 to 2 m. Field data indicated that little of the bronze material had been transported away from its primary location. Original textures and patterns were preserved in fine detail, even on artifacts that were apparently crushed by compacting volcanic ash. The total amount of copper predicted to have been removed from the artifacts is approximately 38 cm^3, roughly three orders of magnitude smaller than the volume of the artifacts (Murphy et al. 1998 [DIRS 126105], p. 273). Neither copper nor lead was detected below a depth of 45 cm from their sources, providing a rough estimate of migration over several thousand years.

11.3.4.8.3 Importance of Clays in Sorbing Radionuclides–Oklo and Cigar Lake

Oklo, Gabon, and Cigar Lake, Canada, are localities that host uranium deposits in saturated, reducing environments. In their entirety, attributes of both sites differ significantly from conditions that could be expected at Yucca Mountain (e.g., CRWMS 2000 [DIRS 151945], Section 13). However, at Oklo, which is situated in near-surface Lower Proterozoic metasediments, and Cigar Lake, located in deep Precambrian granite, clay haloes that surround the ore deposits are effective in retarding the migration of uranium away from the source. This suggests that clays found in altered vitrophyre and fracture fillings at Yucca Mountain will also be effective in retarding the migration of actinides.

11.3.4.8.4 Fast Paths, Perched Water, and Lateral Transport–Idaho National Engineering and Environmental Laboratory

Long-range subsurface transport near the subsurface disposal area of the radioactive waste management complex at the Idaho National Engineering and Environmental Laboratory (INEEL) was investigated in a tracer test in 1999 (Nimmo et al. 2001 [DIRS 154458]). A conservative tracer was applied in infiltration ponds 1.3 km away from the subsurface disposal area. The subsurface at INEEL consists of thick layers of fractured basalts interbedded with thinner layers of coarse- to fine-grained sediments. The unsaturated zone above the Snake River Plain aquifer is 200 m thick.

Samples were collected for tracer analysis from 24 wells within 3 km of the infiltration ponds for several months. Tracer was detected in 1 of 13 sampled aquifer wells 0.2 km away from the nearest spreading area and in 8 of 11 perched water wells completed within the uppermost 70 m of the UZ from 0.2 to 1.3 km away. One of these wells is directly under the subsurface disposal area. The results indicate that percolation from the infiltration ponds can reach the water table in less than nine days, an average rate of at least 22 m/day, and that water from this source can move horizontally in the UZ at an average rate of at least 14 m a day (Nimmo et al. 2001 [DIRS 154458], p. 82).

At least under ponded infiltration, the interbeds and dense basalt layers do not prevent rapid, high-volume vertical flow through fractured basalt. However, some impediments to flow are sufficient to cause substantial perching and horizontal diversion of flow. The fact that this horizontal flow moves quickly over considerable distances suggests that there must also be layers of high horizontal permeability in the zone of perching above the impeding layers. All of the UZ detections were east of the infiltration ponds, the direction in which the interbeds tilt with a slope of 0.004. Transport along such a slope at the observed rates is plausible through extensive horizontal fractures or rubbly layers if they are nearly saturated. A combination of a low-permeability layer directly overlain by such a fractured or rubbly layer might cause the observed detections. Such geologic configurations would have to extend continuously over large distances to allow the observed fast, long-range transport. This situation may be common at the INEEL site and might be significant for long-range contaminant transport at sites such as Yucca Mountain, where the UZ is composed predominantly of fractured rock.

11.3.4.8.5 Radioisotope Migration Experiments Under Unsaturated Conditions: Results From an Experiment at a Scale of 30 cm.

Radionuclide migration experiments under unsaturated conditions have been completed by Atomic Energy of Canada Limited (AECL) on a scale of 30 cm in a block of non-welded tuff (Vandergraaf et al. 2001 [DIRS 155042]). This block was obtained from the Busted Butte UZ facility in the Calico Hills Formation. The results, obtained from elution profiles, showed that, relative to an ideal conservative tracer, tritiated water, transport of technetium (injected as an anionic TcO_4^- species) was approximately 15 percent faster, but that neptunium (injected as the neptunyl ion NpO_2^+) was retarded by a factor of approximately 3. Triay et al. (1996 [DIRS 101024], Appendix A) conducted column experiments with crushed tuff and found neptunium breakthrough curves indicating retardation coefficients always greater than 1 and ranging up to approximately 4, depending on rock type. The AECL findings fall within this range.

Retardation of sodium-22, cobalt-60, and cesium-137 by the geological material was higher than for neptunium. Post-experiment radiometric analysis of the tuff, which is currently underway, shows that the order of retardation is sodium-22 < cesium-137 < cobalt-60. This agrees qualitatively with the experimentally determined static batch sorption coefficients for these radioisotopes.

Radionuclide experiments under unsaturated and saturated conditions at a scale of 1 m in blocks of tuff from the Busted Butte UZ facility are currently underway.

11.3.4.9 Summary of Remaining Uncertainties

Table 11.3.4-2 summarizes the key uncertainties related to mountain-scale UZ radionuclide transport. These uncertainties are applicable to the baseline potential repository and to the potential extension of the repository to the south. The major differences for the southern extension are greater uncertainty in the stratigraphic and structural features, rock properties, and hydrologic conditions (such as perched water) caused by the paucity of site characterization information in this region. The uncertainties associated with flow and transport properties in the southern area, which are currently estimated by extrapolation of the baseline model, need to be studied further.

11.3.4.10 Summary and Conclusions

The effects of a potential southern extension to the baseline potential repository block on radionuclide transport in the UZ were investigated by conducting a sensitivity analysis with TOUGH2 V1.4. The results indicate that radionuclide transport between the potential repository emplacement horizon and the water table in the southern extension is slightly slower than in the baseline potential repository block. The magnitude of the other effects on radionuclide transport resulting from a southern extension of the potential repository block is insignificant.

11.3.5 Effects of Thermally-Driven Coupled Processes on Radionuclide Transport in the Unsaturated Zone

11.3.5.1 Introduction

In the previous sections, various aspects of radionuclide transport under ambient conditions were discussed. In this section, the effects of thermally driven coupled processes on radionuclide transport are considered, including TH, THC, and THM effects. Because radionuclide transport in the UZ starts at the bottom of the emplacement drifts, only flow and transport from this point to the water table is of concern. The hydrogeologic units that the radionuclides may encounter are the TSw, the CHnv (vitric and zeolitic), and a limited area of the Prow Pass unit.

This section focuses primarily on a qualitative discussion of TH, THC, and THM effects on radionuclide transport using models already described in Sections 3 and 4. TH effects are evaluated using the mountain-scale TH model described in Section 3.3.5 and the TH seepage submodel of the mountain-scale model described in Section 4.3.5.3. Results from the mountain-scale THC model described in Section 3.3.6 are used to discuss potential THC effects on radionuclide transport. Finally, results from the drift-scale continuum THM model described in Section 4.3.7 are used to infer THM effects on transport. The uncertainties associated with all of these models are described in detail in the individual sections already mentioned.

11.3.5.2 Goal of Models

The goals of the models used in this section were to evaluate the potential effects of thermally driven coupled processes on radionuclide transport. Of particular importance is the drying out of the fracture and matrix continuum in the shadow zone, an issue of much importance for repository performance. For an explanation of the shadow zone concept, refer to Section 11.3.1.

11.3.5.3 Discussion of Total System Performance Assessment-Site Recommendation Results

All effects of TH, THC, and THM coupled processes were excluded from the TSPA-SR (CRWMS M&O 2000 [DIRS 153246]) on the basis of low consequence. The screening arguments for exclusion of these coupled processes are presented in *Features, Events and Processes in UZ Flow and Transport* (BSC 2001 [DIRS 154826]). The screening arguments are based on process model analyses and qualitative reasoning.

TH coupled processes were investigated for mountain-scale UZ flow (CRWMS M&O 2000 [DIRS 144454]). The processes were found to have minimal effect on flow beneath the potential repository, indicating that only small increases in liquid flux due to TH effects should be expected below the potential repository. These findings were used as a basis for excluding the effects of TH processes on radionuclide transport.

THC coupled processes were investigated using process modeling at the drift scale in *Drift-Scale Coupled Processes (DST and THC Seepage) Models* (CRWMS M&O 2000 [DIRS 142022]; BSC 2001 [DIRS 154677]). This study found coupled THC processes have little effect on hydrogeologic properties in the vicinity of the emplacement drifts. Although some significant changes in aqueous and gas-phase compositions were predicted near the drift (see Section 6.3.1.3), most of these changes were found to dissipate within the modeled time period (100,000 years); others were found to be unrelated to the thermal perturbation (see Section 6.3.1.4). Because these interactions were studied at the emplacement drift boundaries, where thermal-chemical interactions are expected to be more severe, it was concluded that the effects of thermal-chemical interactions along the pathways of aqueous radionuclides in the UZ will be small and of limited duration. Therefore, coupled THC effects on radionuclide transport were excluded from the TSPA-SR (CRWMS M&O 2000 [DIRS 153246]).

THM coupled processes were not directly analyzed using process models. Instead, a sensitivity study was conducted that evaluated the effects of a range of fracture properties (resulting from changes in fracture aperture) in terms of radionuclide transport behavior (CRWMS M&O 2000 [DIRS 151953]). The study concluded that transport behavior is relatively insensitive to large variations in fracture aperture over the entire UZ domain and virtually insensitive to localized variations in fracture aperture. Therefore, the effects of THM coupled processes on radionuclide transport were excluded from the TSPA-SR (CRWMS M&O 2000 [DIRS 153246]).

11.3.5.4 Model Development since Total System Performance Assessment-Site Recommendation

11.3.5.4.1 Thermal-Hydrologic Models

The mountain-scale TH model presented in Section 3.3.5 evaluates the large-scale global effects of heat on UZ flow and transport; submodels are used to evaluate smaller-scale effects of heat, such as that on seepage (See Section 4.3.5). Of particular interest is how much the UZ flow below the drift is affected by heat and how this affects the radionuclide transport behavior of the system. The three-dimensional mountain-scale model computes transient changes in UZ flow as affected by heat and climate change. Figures 3.3.5-8 through 3.3.5-11 show, respectively, the liquid flux versus elevation for a typical location through an emplacement drift for (a) a higher-temperature case for thermal properties, without and with lithophysal cavities, and (b) a lower-temperature case for thermal properties, without and with lithophysal cavities. The drift is located at an elevation of approximately 1,100 m, as evidenced by the large liquid flux at this location for the higher-temperature case, caused by large capillary suction in the dryout zone (Figures 3.3.5-8) through 3.3.5-11. Boiling processes, climate change, and the effects of the shadow zone below the drift complicate the analysis of liquid fluxes below the drift. At 600 years, climate change is assumed to occur (see Section 3.3.1.3), with a subsequent increase in precipitation and infiltration; this is reflected in higher long-term liquid fluxes below the drift at late times (2,000 years) after other complications, such as liquid boiling, are over. The effects of boiling and shadow zone can be seen clearly in Figure 3.3.5-8 for the case of a higher-temperature operating mode. However, the main implication of Figures 3.3.5-8 through 3.3.5-11 is that the UZ flow does not drastically change with changes in heat for either the higher- or lower-temperature cases. Although boiling changes UZ flow slightly for some 1,000 years, especially in the higher-temperature case, the main lasting effect results from the climate change at 600 years (USGS 2000 [DIRS 136368]). Thus, it can be concluded that the global large-scale TH effects on UZ transport below the drifts are probably negligible.

In terms of more localized effects of heat on transport, the drying out of the shadow zone due to heat and the subsequent impact on transport through this zone must be evaluated. Of particular importance is whether fractures and the rock matrix totally dry out near the bottom of the drift, because this would result in total containment until either continuum starts to rewet. The reason is that diffusion of radionuclides from the EBS at the bottom of the drift to the rock cannot occur without liquid water being present in the rock, either in the matrix or the fractures. An exception to this is radionuclide releases in the gaseous phase, which are believed to be small and are therefore neglected in the TSPA-SR. A second important consideration is that of partial or total dryout of the fracture or matrix continuum, since this will affect the relative rate of diffusion into one continuum with respect to the other.

The submodel of the TH mountain-scale model, used to evaluate TH effects on seepage in Section 4.3.5, provides the results necessary to evaluate the effects of heat on dryout in the shadow zone for the higher- and lower-temperature cases. Figures 11.3.5-1 and 11.3.5-2 show the saturation distributions at various times for the higher-temperature case and the fracture and matrix continuum, respectively. These figures show complete dryout below the drift for both the fracture and matrix continua owing to boiling. The dryout zone expands with time below the drift and reaches a maximum thickness of some 70 m after about 1,000 years (Figure 11.3.5-3). After that, the dryout zone starts to contract; it disappears after approximately 2,500 to 3,000 years. During this entire period, there can be no radionuclide transport from the drift because of the total lack of liquid water for advective or diffusive transport.

In the case of the lower-temperature operating mode, only the fractures dry out below the drift because the heat source is not sufficient to boil a significant amount of the water residing in the matrix. Figure 11.3.5-4 shows the saturation distribution within the fractures for different times in the lower-temperature case. The figure shows that dryout in fractures will occur beneath the drifts for at least 2,000 years, during which time radionuclide releases can only occur into the matrix blocks below the drifts. This is not expected to improve repository performance significantly, since most of the radionuclides are expected to diffuse primarily into the matrix under ambient conditions because the matrix has a much higher liquid saturation (moisture content) than the fractures, as discussed in Section 11.3.1. The impact of changing water and gas chemistry on radionuclide transport is being evaluated as part of a study on the effect of alkaline plumes on the UZ below the potential repository drifts.

11.3.5.4.2 Thermal-Hydrologic-Chemical Models

Several model improvements were made to the THC seepage models (BSC 2001 [DIRS 154677]; see also Section 6.3.1.4), limiting the uncertainty of results compared to the predictions in *Drift-Scale Coupled Processes (DST and THC Seepage) Models* (CRWMS M&O 2000 [DIRS 142022]). Although there were still some important changes in aqueous and gas-phase compositions predicted near the drift, most of these changes were found to dissipate within 10,000 years, and no significant long-lasting THC effects were predicted around the drift.

A mountain-scale THC model is described in Section 3.3.6, which also discusses the results of this model regarding global UZ flow issues. These same results can be used to evaluate the potential effects of THC processes on UZ transport. The conclusions from Section 3.3.6 are that THC processes, primarily dissolution and precipitation processes, have only minor effects on UZ flow because a change in permeability of less than an order of magnitude is smaller than the natural variability of several orders of magnitude. Some enhanced THC processes result from gas convection and increased condensation near the edges of the repository, but these are confined mostly to areas near and above the potential repository. Therefore, the long-term liquid fluxes of liquid and transport below the potential repository in the UZ were not affected significantly by gas convection. The mountain-scale THC model shows some dissolution in the zeolitic rocks in the CHnv, which results in some relatively small enhancement in porosity (less than 10 percent) and permeability (less than an order of magnitude). These enhancements may lead to higher water flow through the matrix of these zeolitic units, resulting in an increased sorption of radionuclides that will enhance performance. Consequently, it is concluded that THC processes will not affect transport in the UZ more than natural variability in hydrologic properties. The possibility for an alkaline plume from the EBS to affect transport has not been evaluated in this report, but this work is currently in progress.

11.3.5.4.3 Thermal-Hydrologic-Mechanical Models

The development of a mountain-scale THM model is described in Section 3.3.7, and that of a drift-scale model in Section 4.3.7. The results from both models can be used to qualitatively discuss potential THM effects on radionuclide transport from the near field to the water table. The results from these models indicate that a change in permeability of only 10 percent to 40 percent will occur in the lower lithophysal unit because of THM effects (Figures 4.3.7-15 and 4.3.7-16). Permeability changes from THM effects in units underlying the lower lithophysal units are of the same order (Table 3.3.7-2). These are relatively small changes, so it is expected that THM effects will have a minor influence on localized flow close to drifts and global UZ flow patterns. Hence, THM effects on transport will be negligible.

11.3.5.5 Abstraction for Total System Performance Assessment

The work reported in this section is devoted to evaluating process model sensitivities and uncertainties. Consequently, simulation results from this study are not used to support any abstraction model that directly supports the TSPA. The results described in this section indicate that the process model and associated model abstractions used to represent this component in the TSPA-SR (CRWMS M&O 2000 [DIRS 153246]) are representative (or conservative) with respect to the effects of this component on total system performance. Therefore, any future changes in model abstractions for this component will not diminish the performance represented in the TSPA-SR.

11.3.5.6 Multiple Lines of Evidence

Multiple lines of evidence are provided for the thermally-driven coupled processes in Sections 3.3.5 through 3.3.7 and Sections 4.3.5 through 4.3.7.

11.3.5.7 Summary of Remaining Uncertainties

Two categories and several key uncertainty issues related to modeling the effects of thermally driven coupled processes on radionuclide transport in the UZ are summarized in Table 11.3.5-1.

11.3.5.8 Summary and Conclusions

This section evaluates the effects of thermally driven coupled processes on radionuclide transport in the UZ. TH effects on the shadow zone may have considerable beneficial effects on transport. For the higher-temperature case, model calculations show that both the rock matrix and fractures immediately below the drifts will remain totally dry because of boiling for 2,500 to 3,000 years. As a result, there can be no radionuclide release from the EBS into the UZ except for radionuclides that are transported in the gas phase (such as carbon-14). For the lower-temperature case, the fracture network below the drifts is estimated to remain dry for about 2,000 years, but the liquid saturation of the rock matrix will remain near initial ambient values. As a result, radionuclides from the UZ could only migrate from the drift invert into the adjacent rock matrix in the UZ. The effects of THC and THM processes on radionuclide transport are therefore found to be negligible for the limited studies conducted.

INTENTIONALLY LEFT BLANK

Table 11.3.1-1. Summary of Uncertainty Issues Related to the Drift Shadow Transport Model

Category	Uncertainty Issue	Treatment of Uncertainty Issue	Affected Goals
Conceptual Uncertainties	Area reduction factor versus capillary equilibrium	Based on hydrologic and geochemical evidence (Section 11.3.1.7) Implemented through active fracture model (Section 11.3.1.1.1) Confirmed through calibration for hydrologic model and field transport testing (Section 11.3.1.1.3) Alternative conceptual models examined and rejected (Liu et al. 1998 [DIRS 105729])	Development of general understanding of transport process and basis for transport prediction models
	Effective area reduction in flow model	Effective area reduction in flow model due to flow weighting scheme used for fracture-matrix flow (Section 11.3.1.8) Not used in current drift shadow transport model for area reduction in matrix diffusion. Use of this factor would result in even greater isolation of fractures and matrix (Section 11.3.1.8)	Development of general understanding of transport process and basis for transport prediction models
	Significance of drift seepage.	Current process model calculations only performed for drifts without seepage (Section 11.3.1.1.1) Conservatively accounted for in PA model through assignment of advective releases from waste emplacement drift to fractures (Section 11.3.1.6)	Transport in the drift shadow under more widely varying flow conditions
	Representation of matrix diffusion in transport models	Current model abstraction for TSPA may underestimate matrix diffusion for fracture to matrix transfers (Section 11.3.2)	Development of general understanding of transport process and basis for transport prediction models
Parameter and Data Uncertainties	Total percolation rate and fracture-matrix flow distribution	Variations in total percolation rate included in PA model through the UZ site-scale flow model for various climate/infiltration scenarios (Section 11.3.1.8) Variations in fracture-matrix flow distribution included in PA model through site-scale flow model (Section 11.3.1.8)	Transport in the drift shadow under more widely varying flow conditions
	Formation-specific parameters	Flow parameters calibrated to site-specific measurements of water saturation and capillary pressure, with uncertainty developed in accordance with calibration under uncertain infiltration rates (Section 11.3.1.1.3) Transport parameters and parameter uncertainty developed from measurements using site-specific materials (CRWMS M&O 2001 [DIRS 154024])	Determination of flow and transport formation parameters
	Heterogeneity	Captured in drift seepage analyses (CRWMS M&O 2000 [DIRS 153314])	Distribution of flow and transport parameters
	Uncertainty propagation	Uncertainty accounted for in part through drift seepage uncertainty analysis (CRWMS M&O 2001 [DIRS 154291])	Distribution of inputs for TSPA calculation (CRWMS M&O 2001 [DIRS 154291])

Table 11.3.2-1. Summary of Key Uncertainty Issues Related to Calculating Flow and Transport between Fractures and the Matrix

Category	Uncertainty Issue	Treatment of Uncertainty Issues	Affected Goals
Conceptual uncertainty	Appropriateness of the continuum approach	Based on flow and transport behavior in the UZ, scale of the problem, data availability, and computational feasibility (CRWMS M&O 2000 [DIRS 122797], Section 6.4.2) Supported by modeling study of Alcove 1 tests (CRWMS M&O 2000 [DIRS 122797], Section 6.8.1)	Development of UZ flow and transport
	Appropriateness of active fracture model	Based on unsaturated flow theory and experimental observation regarding fingering flow (CRWMS M&O 2000 [DIRS 141187], Section 6.4.5) Consistent with field observations in the UZ (Liu et al. 1998 [DIRS 105729]) Supported by modeling study of Alcove 1 tests (CRWMS M&O 2000 [DIRS 122797], Section 6.8.1)	Description of flow in fractures and fracture-matrix interaction
Uncertainty related to numerical approaches	Appropriateness of matrix block discretization (DKM vs. MINC)	Demonstrate the inadequacy of the DKM in handling sharp gradients near fracture-matrix interfaces (Section 11.3.2.5) Make recommendations to resolve this issue (Section 11.3.2.9)	Model prediction of UZ flow and transport
	Appropriateness of upstream weighting scheme for the fracture-matrix connection	Partially accounted for through the model calibration against field observations in the *Calibrated Properties Model* (CRWMS M&O 2000 [DIRS 144426]) Needs further investigation	Calibration of UZ rock properties and model prediction of UZ flow and transport
Parameter uncertainty	Appropriateness of parameters used in the modeling study reported in this section	Used properties without considering perched water Used calibrated, base case, mountain-scale parameter set	Quantitative comparison between simulation results obtained with the DKM and the MINC in this study

Table 11.3.3-1. Parameters Used for the Transport Problem in a Parallel Fracture System

Parameter	Value
Molecular diffusion coefficient	2.5×10^{-11} m^2/s
Fracture spacing	1.0 m (Case 1) or 10.0 m (Case 2)
Retardation factor	30
Velocity in fracture	1.1574×10^{-5} m/s
Grid spacing	0.5 m
Matrix volume per cell	0.25 m^3 (Case 1) or 25.0 m^3 (Case 2)
Fracture volume per cell	0.5×10^{-5}
Fracture-matrix interface area	0.5 m^2
Domain length	36.75 m

Source: TerBerg 2001 [DIRS 155033].

Table 11.3.3-2. Summary of Key Uncertainty Issues

Category	Uncertainty Issue	Treatment of Uncertainty Issues	Affected Goals
Uncertainty related to numerical approach	Grid discretization - grid coarseness affects data resolution (i.e., an increase in grid coarseness will result in a decrease in resolution)	Partially accounted for through the model calibration against field observations in the *Calibrated Properties Model* (CRWMS M&O 2000 [DIRS 144426]) and comparisons with field measurements of tracer transport	Model prediction of UZ flow and transport
Conceptual model and model implementation uncertainty	Limited theoretical and experimental results to support dual continuum transport calculation methods in fractured porous media	Used dual–porosity model results for validation. Partially accounted for through the model calibration against field observations in the *Calibrated Properties Model* (CRWMS M&O 2000 [DIRS 144426]) and comparisons with field measurements of tracer transport	Quantitative comparison between simulation results obtained with FEHM V2.0, T2R3D V1.4, DCPT V1.0, and DCPT V2.0 in this study

Table 11.3.4-1. Stable Uranium and Stable Isotope Data from Peña Blanca

Sample	Uranium (mol/L)	delta-D (‰)	delta-Oxygen-18 (‰)	Notes
AS-1	2.8E-7	-11	-2.5	12 m from adit entrance on +00 level
AS-2	1.6E-7	-7	-3.4	15 m from adit entrance
AS-3	1.8E-8	-7	-3.6	23 m from adit entrance
AS-4	1.3E-8	-1	-2.8	8.5 m into north part of adit
AS-5	2.7E-8	-64	-9.3	Perched water from borehole at +10 level
AS-6	2.5E-8	-61	-8.7	Abandoned mining camp supply well

Source: Bodvarsson 2001 [DIRS 154669], Attachment 1, pp. 86 to 87.

NOTE: Water samples collected February 25, 2000.

Table 11.3.4-2. Summary of Key Uncertainty Issues

Category	Uncertainty Issue	Treatment of Uncertainty Issues	Affected Goals
Flow distributions and pathways	Uncertainty related to how large-scale flow variability and fracture-matrix flow exchange affect transport	Active fracture model accounts for fracture-matrix interface factors that affect flow and advective transport A range of flow models have been used to account for large-scale variability in flow fields and transport pathways, including perched water models and flow focusing into faults	Model prediction of UZ transport
Sorption coefficients	Large uncertainty ranges in K_d	Parameter ranges have been developed from laboratory experiments and scientific literature data for sorption	Model prediction of UZ transport
Matrix diffusion coefficients	Effects of fracture-matrix interface characteristics on matrix diffusion	Active fracture model accounts for fracture-matrix interface factors that affect flow and advective transport. These factors also affect matrix diffusion and are incorporated into transport calculations in terms of the active fracture model Parameter ranges have been developed from laboratory experiments on matrix diffusion	Model prediction of UZ transport

Table 11.3.5-1. Summary of Uncertainty Issues Related to the Effects of Thermally-Driven Coupled Processes on Transport in the Unsaturated Zone

Category	Uncertainty Issue	Treatment of Uncertainty Issue	Affected Goals
Conceptual uncertainties	Area reduction factor versus capillary equilibrium	Based on unsaturated flow theory, experimental observation regarding fingering flow (CRWMS M&O 2000 [DIRS 141187], Section 6.4.5), and field geochemical evidence (CRWMS M&O 2001 [DIRS 154426]) Supported by field observations from the UZ (Liu et al. 1998 [DIRS 105729]) Supported by modeling study of Alcove 1 tests (CRWMS M&O 2000 [DIRS 122797], Section 6.8.1)	Description of fracture-matrix interaction underneath the repository; development of basis for numerical transport models
Parameter and data uncertainties	Thermal operating modes	Sensitivity studies for range of environments representing both higher- and lower-temperature operating modes	Values of transport parameters near waste emplacement drifts; thermodynamic and kinetic databases and boundary conditions used in TH/THC/THM models
	Modification of porosity and permeability by chemical precipitation and dissolution	Sensitivity analyses performed in drift scale thermal tests with the DST THC model (CRWMS M&O 2001 [DIRS 154426]). Effects on mountain-scale radionuclide transport are expected to be small	Rates of advective transport; relative significance of fracture-matrix interaction
	Formation-specific radionuclide transport parameters and their thermal dependence	Transport parameters developed from laboratory measurements using site-specific materials and field tracer tests under ambient and thermal-loaded conditions Thermodynamic and kinetic databases were derived from various sources including YMP studies and other scientific literature. Sensitivity analyses were performed on thermodynamic and kinetic data (CRWMS M&O 2001 [DIRS 154426]) Radionuclides have not been explicitly simulated in the THC models yet; however, transport behavior of radionuclides may be inferred from the results presented in this section and Section 11.3.4. Diffusion and distribution coefficient ranges have been developed from laboratory experiments and scientific literature. Additional analyses on their thermal dependency would reduce uncertainty.	Determination of rates of radionuclide chemical reactions and transport through the UZ to the water table
	Heterogeneity	Captured in drift seepage analyses (Section 4.3); however, effects on mountain-scale radionuclide transport require further analyses	Spatial distribution of transport parameters

INTENTIONALLY LEFT BLANK

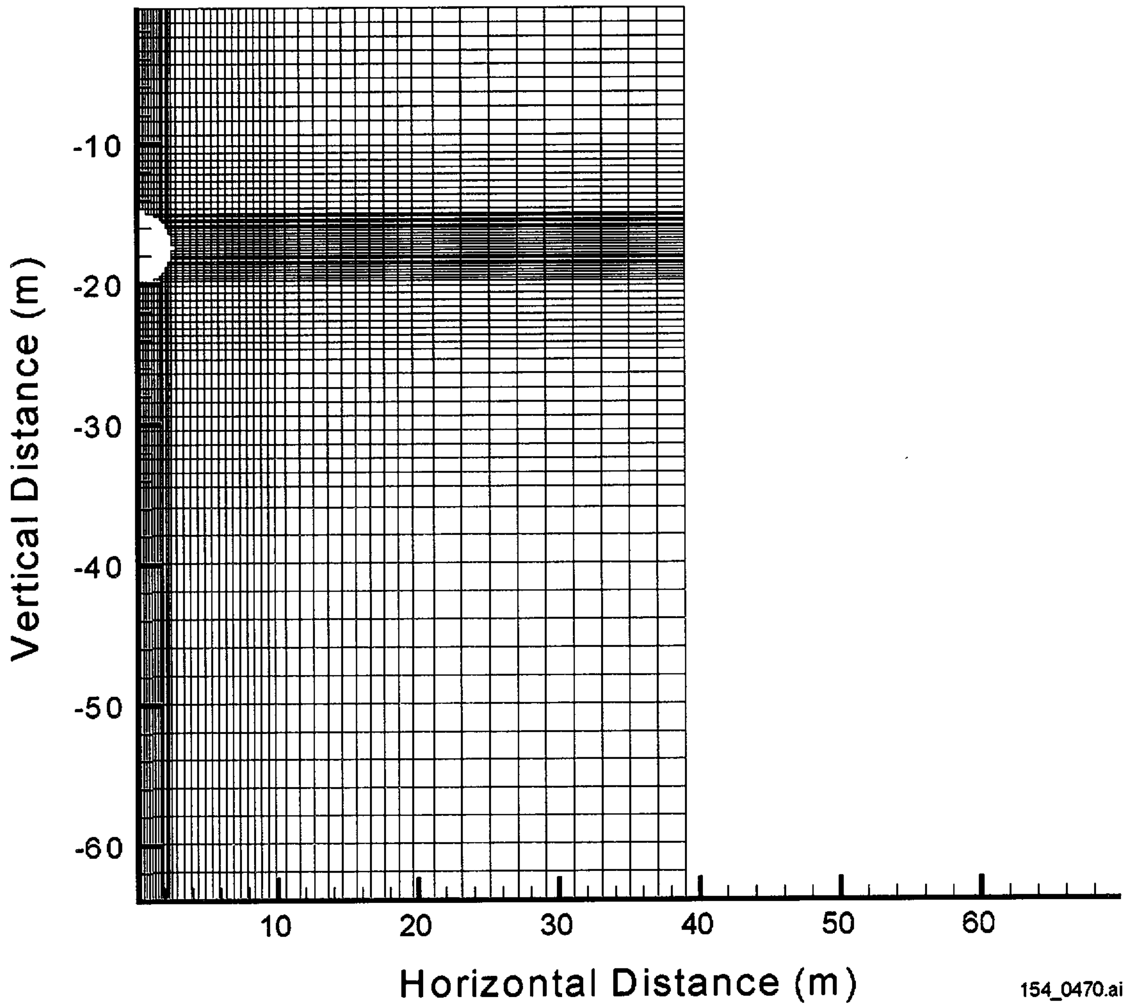

154_0470.ai

Source: Houseworth 2001 [DIRS 155144], p. 19.

NOTE: The water table is an average of 300 m below the potential repository horizon.

Figure 11.3.1-1. Model Grid with Waste Emplacement Drift used for Dual-Permeability Model

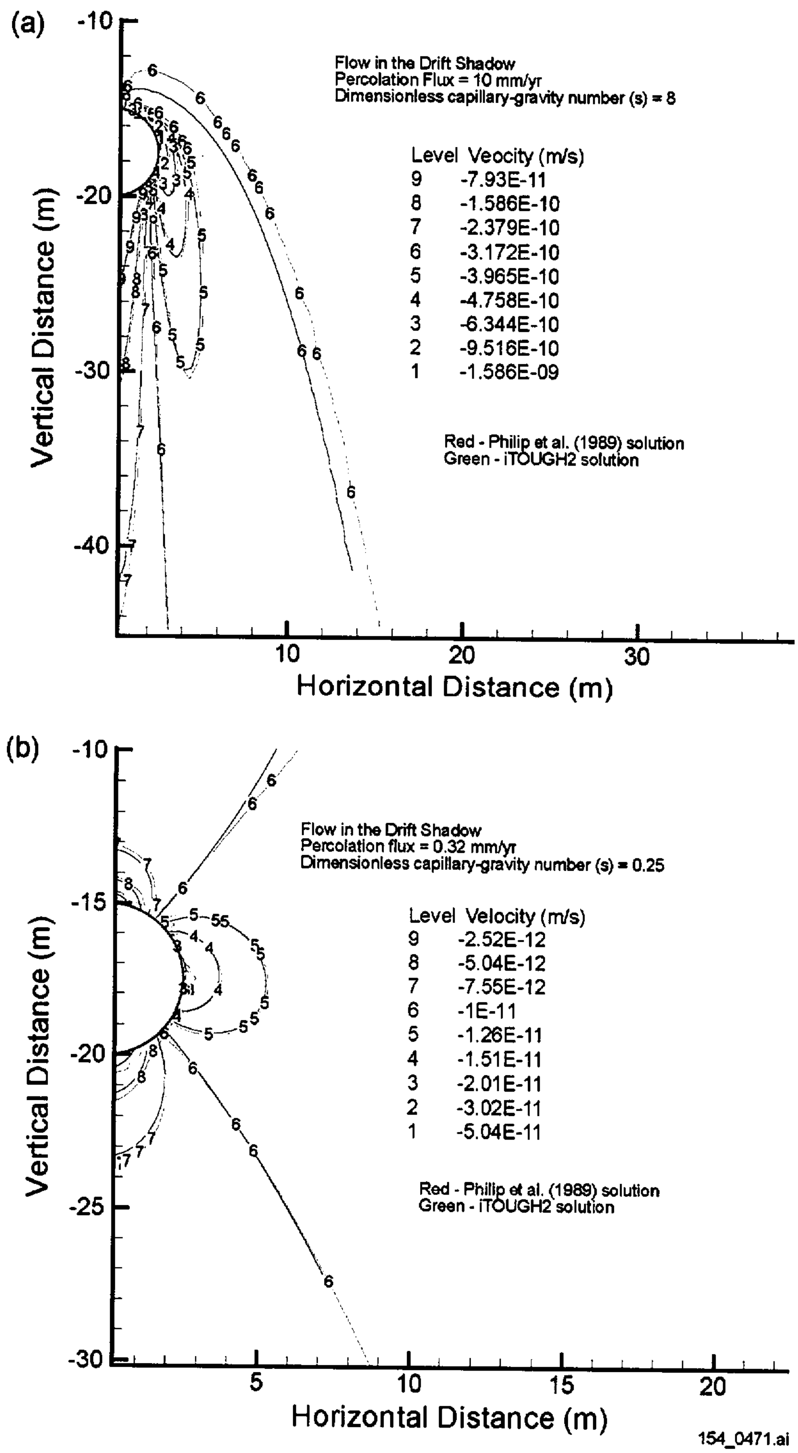

154_0471.ai

Source: Houseworth 2001 [DIRS 155144], pp. 7 to 13.

NOTE: Contours from iTOUGH2 and the analytical Philip solution for (a) percolation flux of 10 mm/yr and capillary coefficient of 8.0, and (b) percolation flux of 0.32 mm/yr and capillary coefficient of 0.25. Negative vertical flow velocities indicates downward flow.

Figure 11.3.1-2. Vertical Flow Velocity Contours for Flow in Drift Shadow

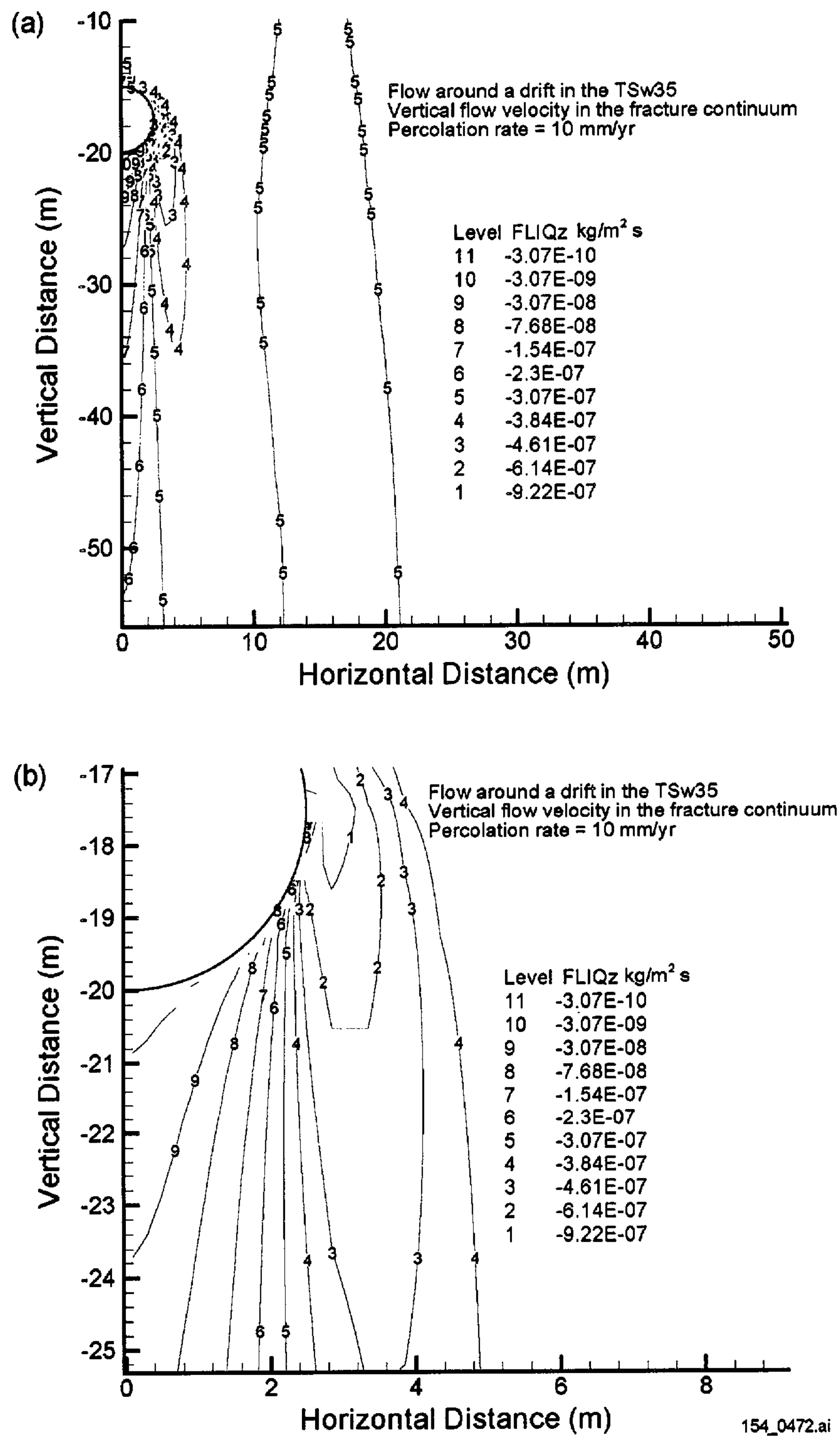

154_0472.ai

Source: Houseworth 2001 [DIRS 155144], pp. 14 to 19.

NOTE: Flow around a drift in the tsw35 fracture continuum at a percolation rate of 10 mm/yr (a) over a large area, and (b) detail near the base of the emplacement drift.

Figure 11.3.1-3. Vertical Flow Velocity Contours for Flow around a Drift in the tsw35 Fracture Continuum

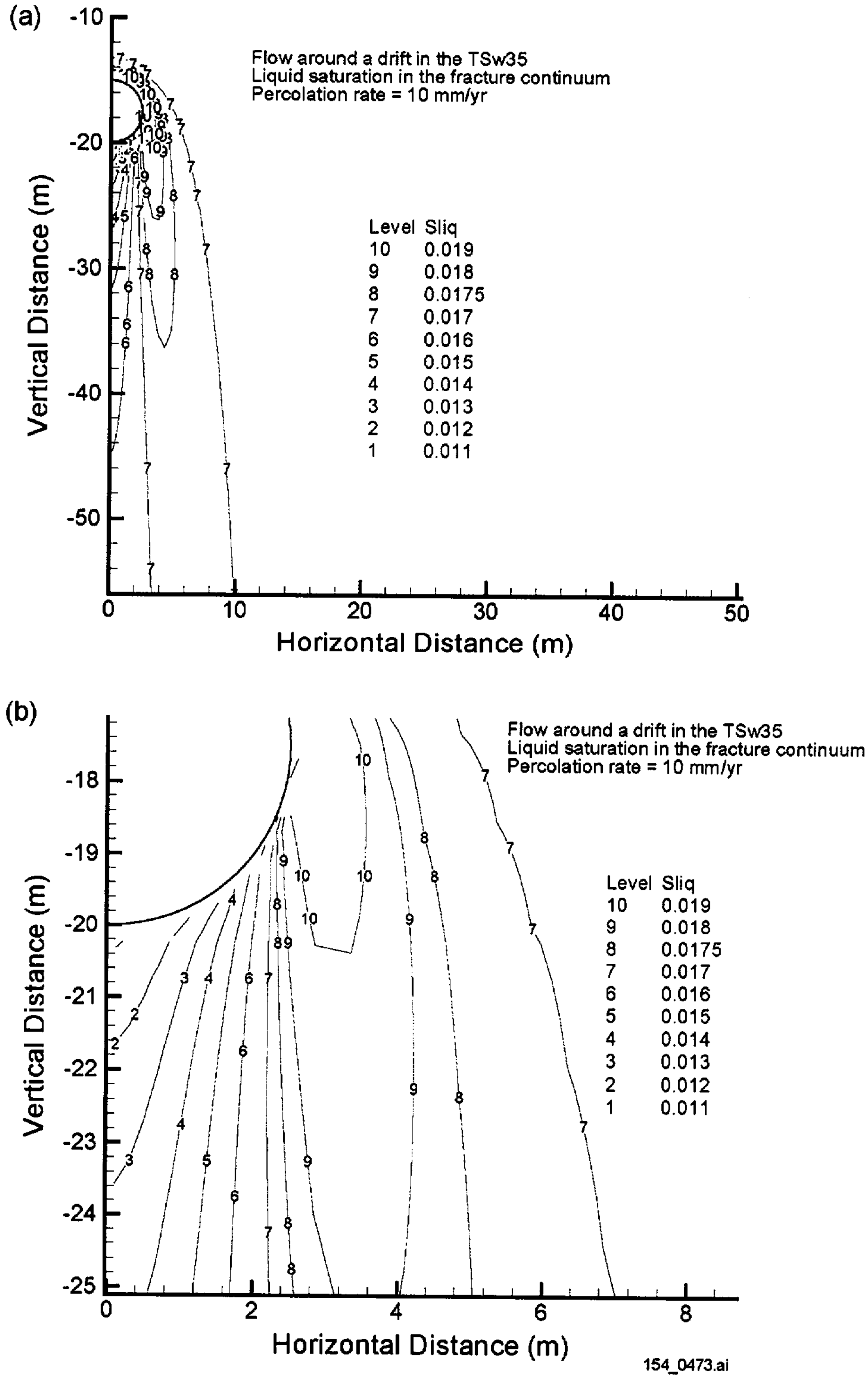

154_0473.ai

Source: Houseworth 2001 [DIRS 155144], pp. 14 to 19.

NOTE: Flow around a drift in the tsw35 at a percolation rate of 10 mm/yr (a) over a large area, and (b) detail near the base of the emplacement drift. Residual saturation is 0.01.

Figure 11.3.1-4. Water Saturation Contours for Flow around a Drift in the tsw35 Fracture Continuum

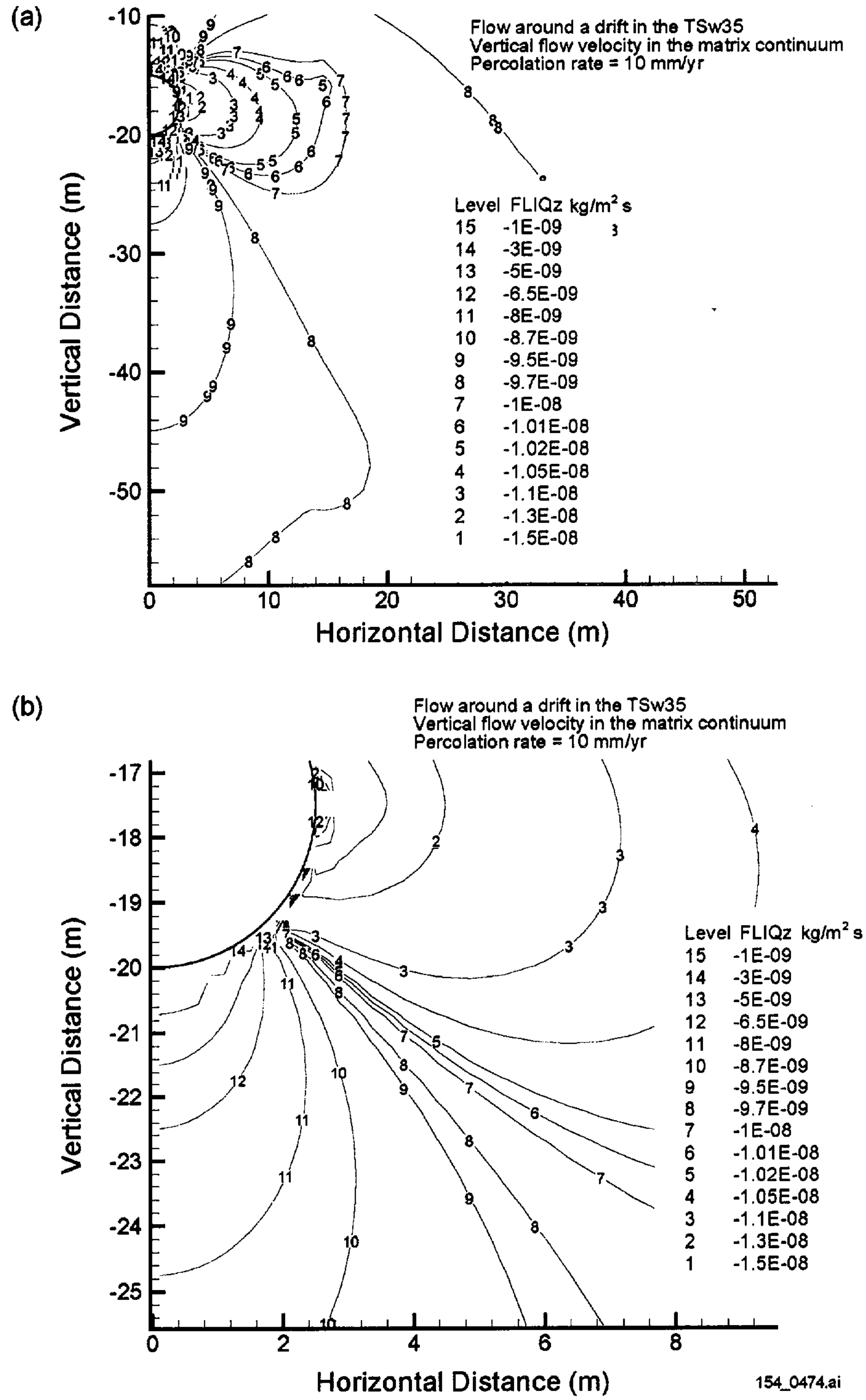

154_0474.ai

Source: Houseworth 2001 [DIRS 155144], pp. 14 to 19.

NOTE: Flow around a drift in the tsw35 at a percolation rate of 10 mm/yr (a) over a large area, and (b) detail near the base of the emplacement drift.

Figure 11.3.1-5. Vertical Flow Velocity Contours for Flow around a Drift in the tsw35 Matrix Continuum

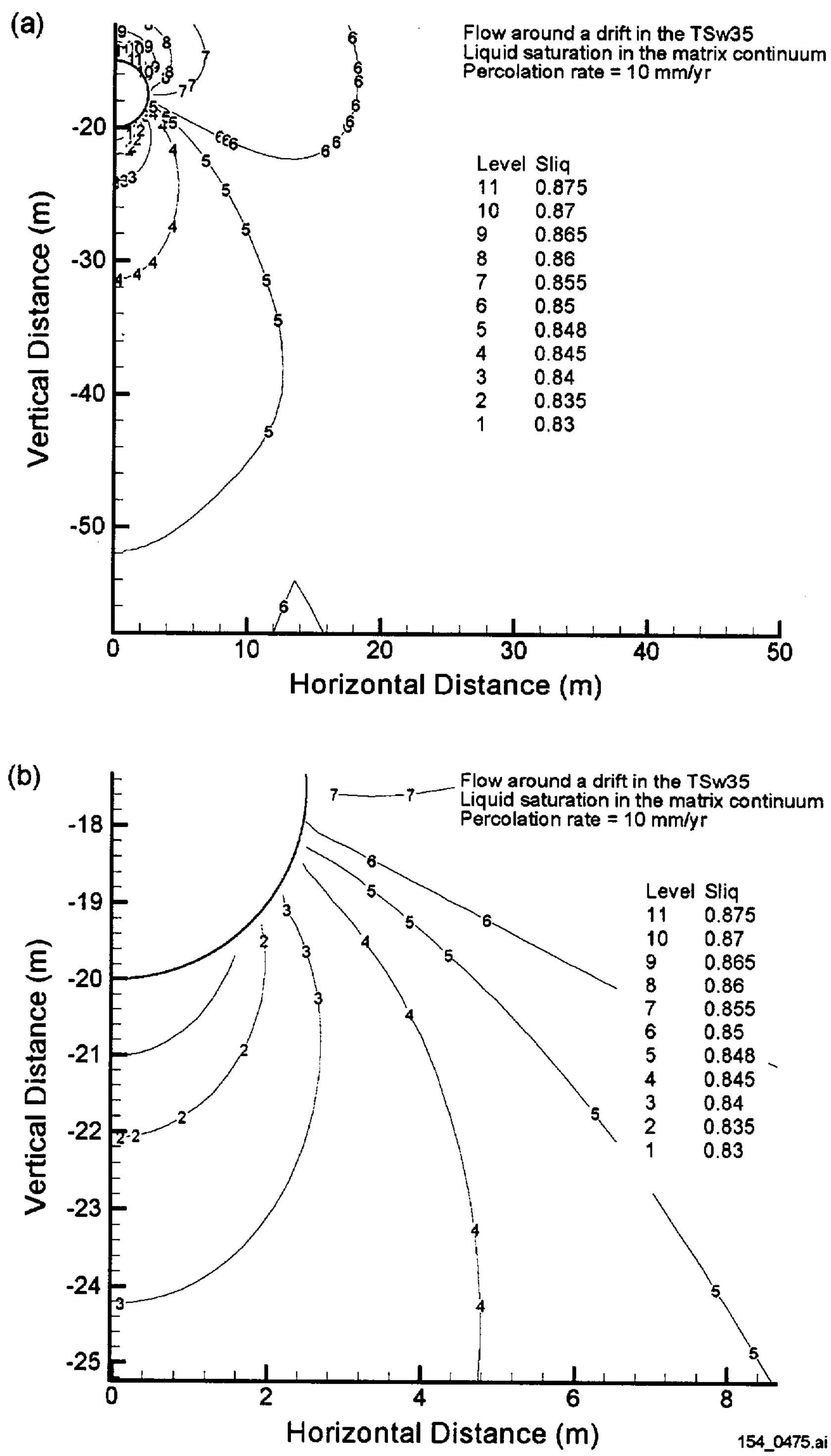

154_0475.ai

Source: Houseworth 2001 [DIRS 155144], pp. 14 to 19.

NOTE: Flow around a drift in the tsw35 at a percolation rate of 10 mm/yr (a) over a large area, and (b) detail near the base of the emplacement drift.

Figure 11.3.1-6. Water Saturation Contours for Flow around a Drift in the tsw35 Matrix Continuum

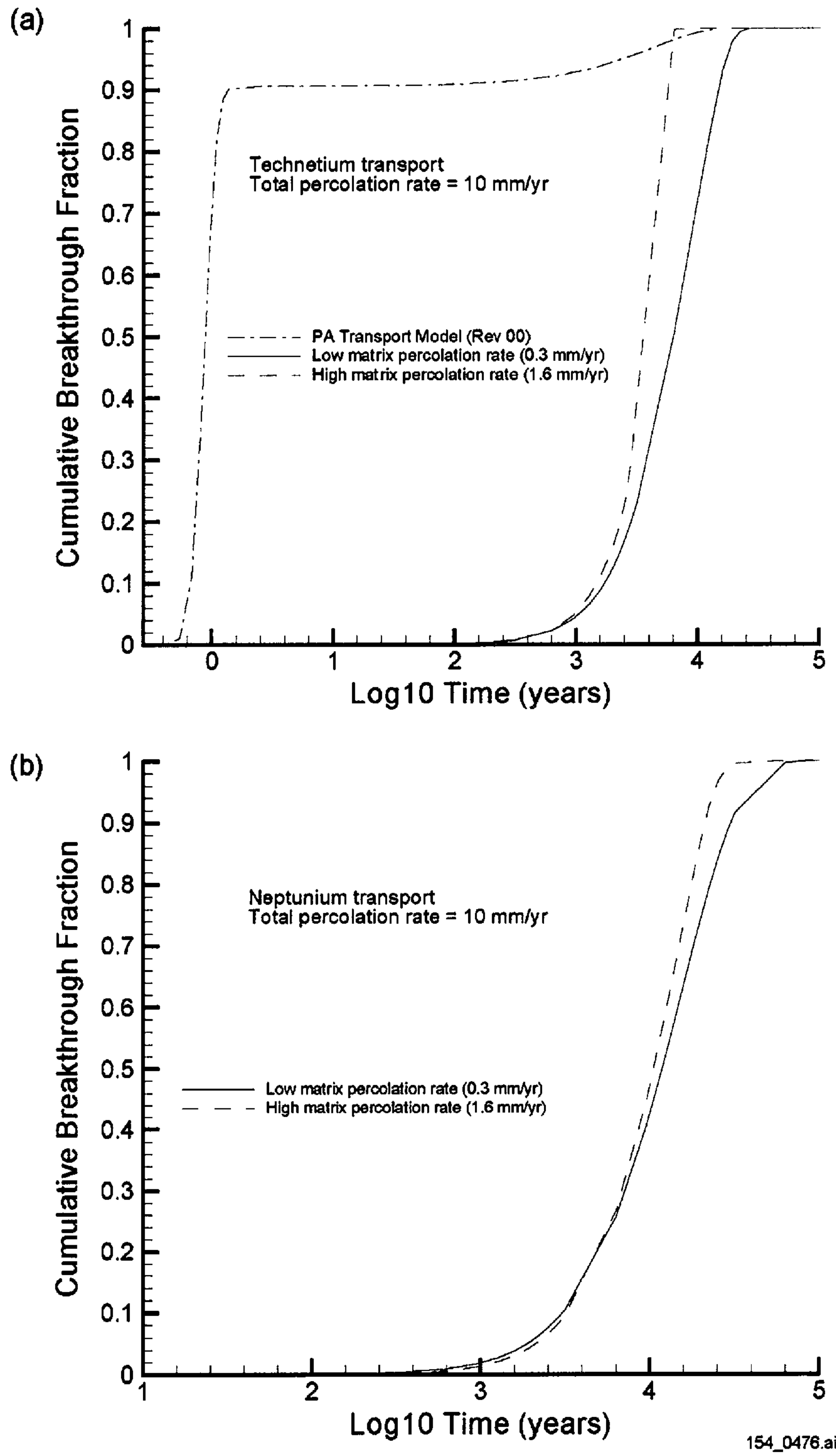

154_0476.ai

Source: Houseworth 2001 [DIRS 155144], pp. 19 to 23.

NOTE: Breakthrough is 45 m below the potential waste emplacement drift.

Figure 11.3.1-7. Technetium (a) and Neptunium (b) Transport with a Total Percolation Rate of 10 mm/yr

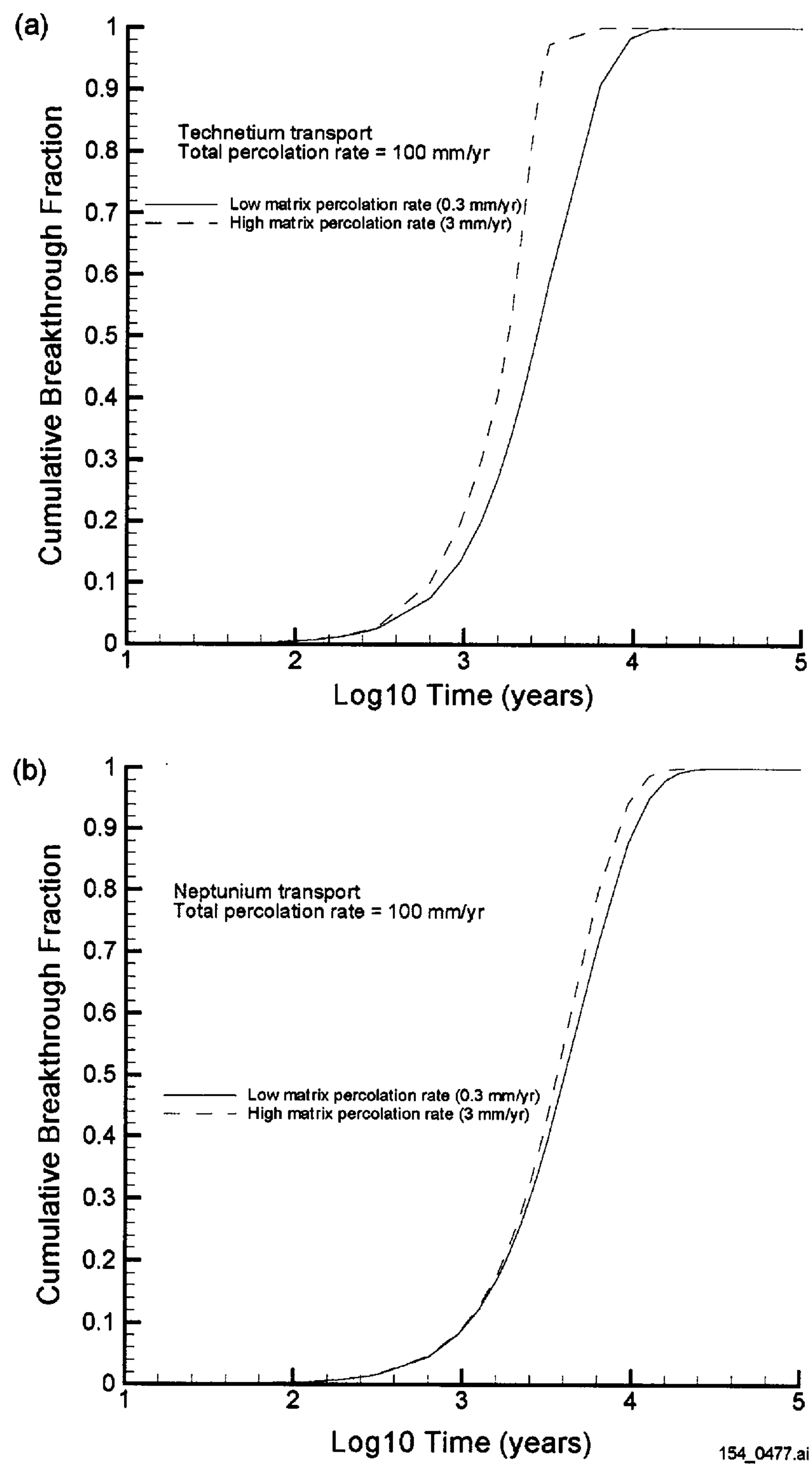

154_0477.ai

Source: Houseworth 2001 [DIRS 155144], pp. 19 to 23.

NOTE: Breakthrough is 45 m below the potential waste emplacement drift.

Figure 11.3.1-8. Technetium (a) and Neptunium (b) Transport with a Total Percolation Rate of 100 mm/yr

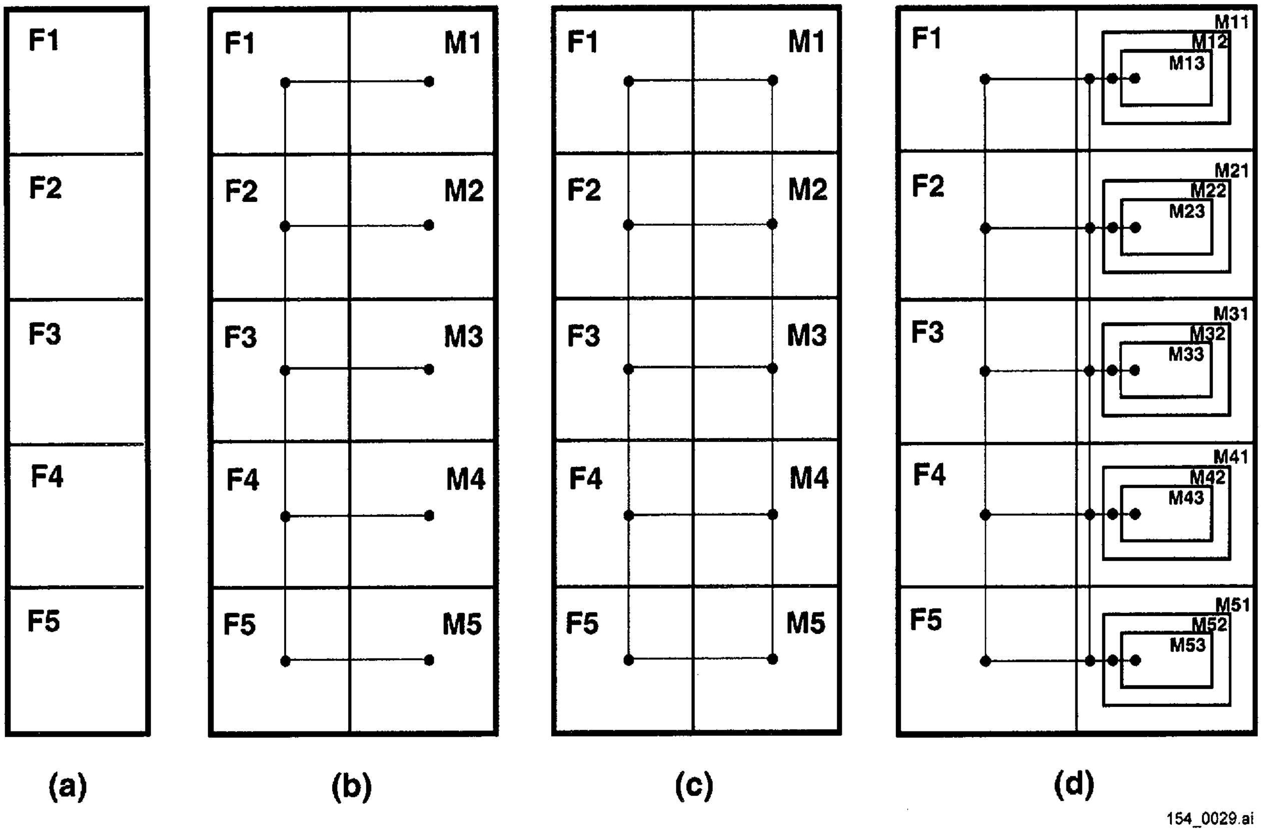

154_0029.ai

Source: Doughty 1999 [DIRS 135997], Figure 2.

NOTE: (a) Effective continuum model, (b) dual porosity model, (c) dual permeability model, and (d) multiple interacting continua model with three matrix continua (i.e., gridblocks). "F" refers to effective continuum model gridblocks in (a) and fracture gridblocks in (b), (c) and (d). "M" refers to matrix gridblocks.

Figure 11.3.2-1. Schematic Diagram of a One-Dimensional Column of Gridblocks and Four Models of Flow

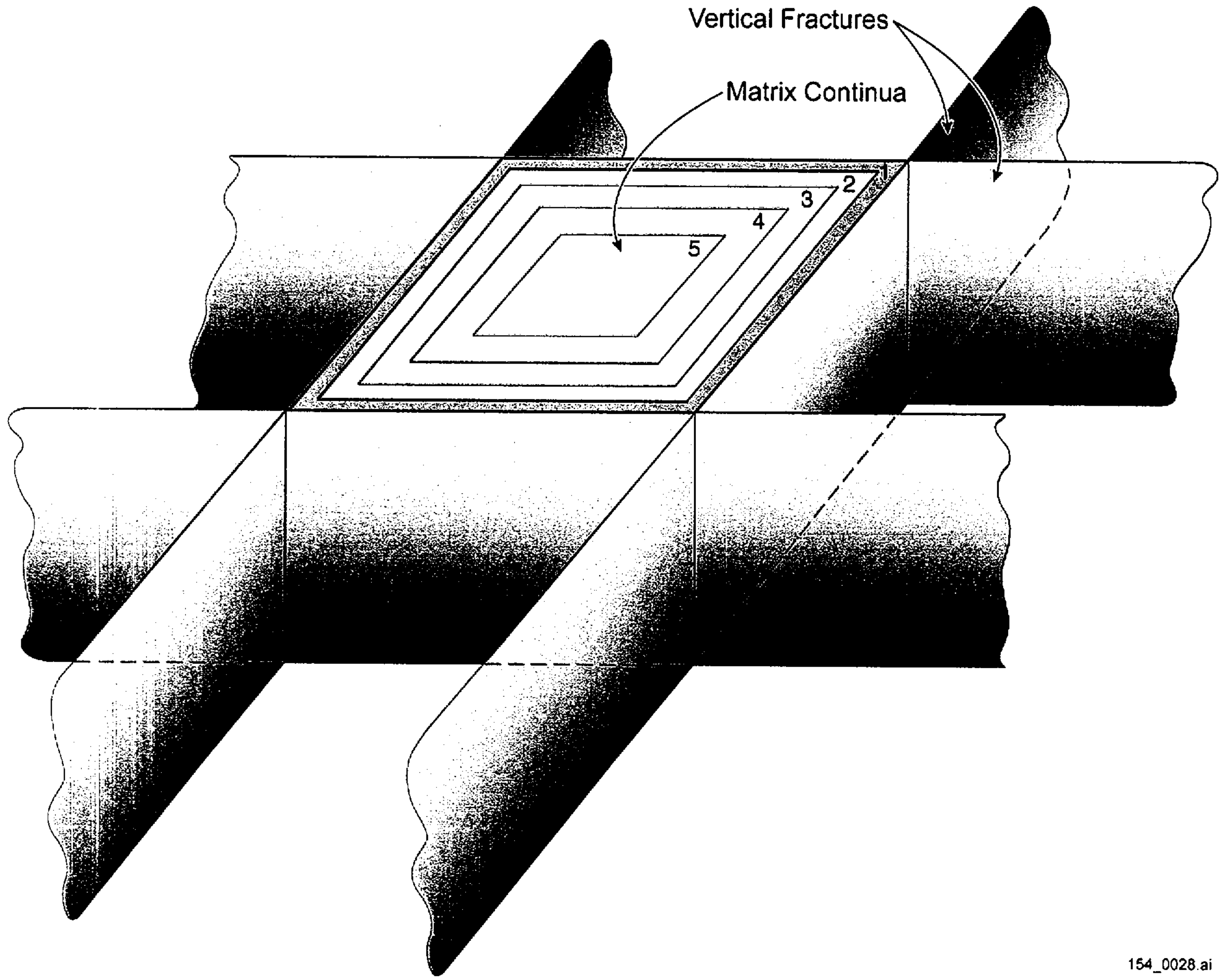

154_0028.ai

Source: CRWMS M&O 2000 [DIRS 141187], Section 6.4.

Figure 11.3.2-2. Matrix Discretization for the Multiple Interacting Continua Model Scheme

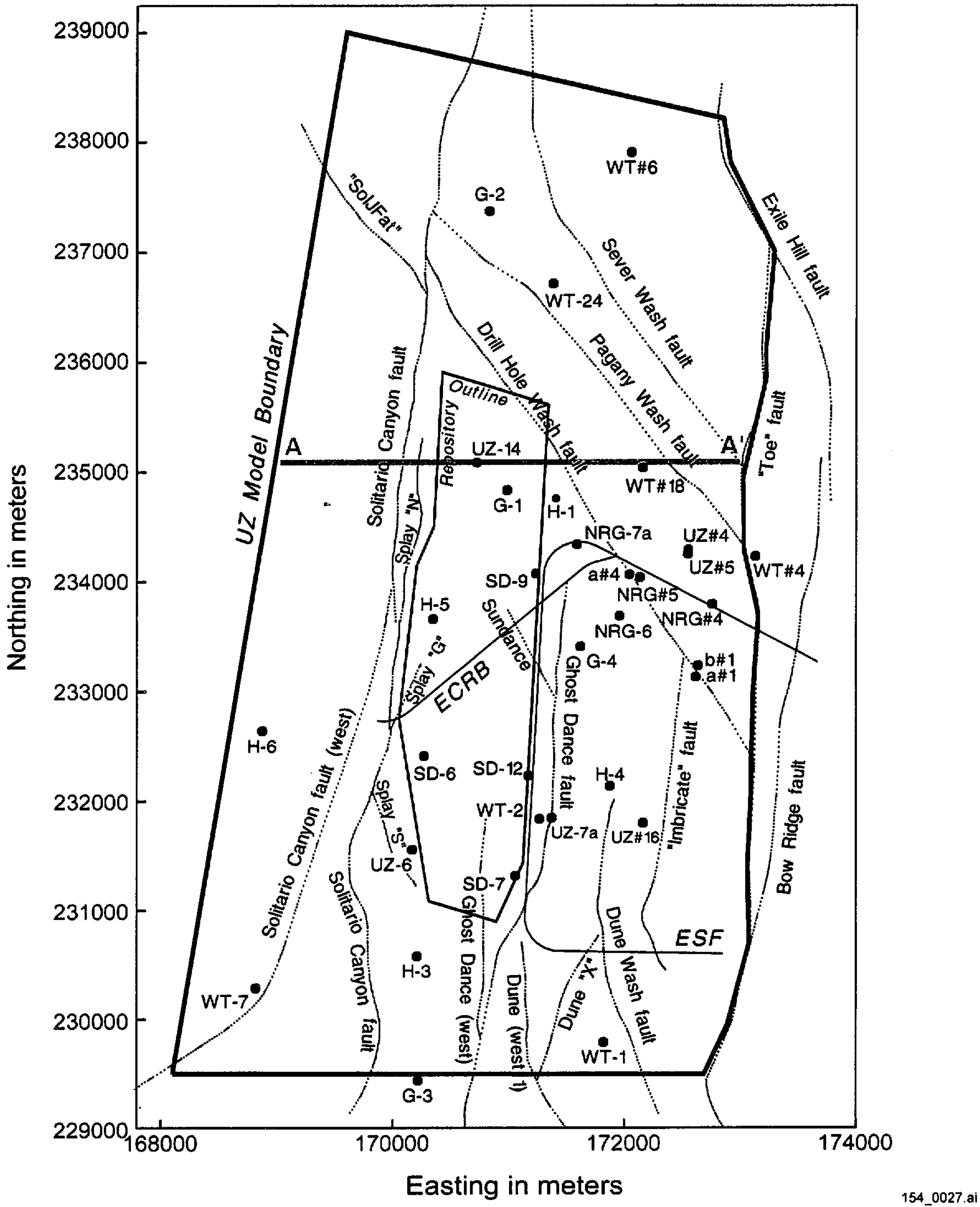

154_0027.ai

Source: CRWMS M&O 2000 [DIRS 141187], Figure 1.

NOTE: The East-West cross section (A-A') was used in numerical simulations.

Figure 11.3.2-3. Plan View of the Unsaturated Zone Model Domain and the East-West Cross Section

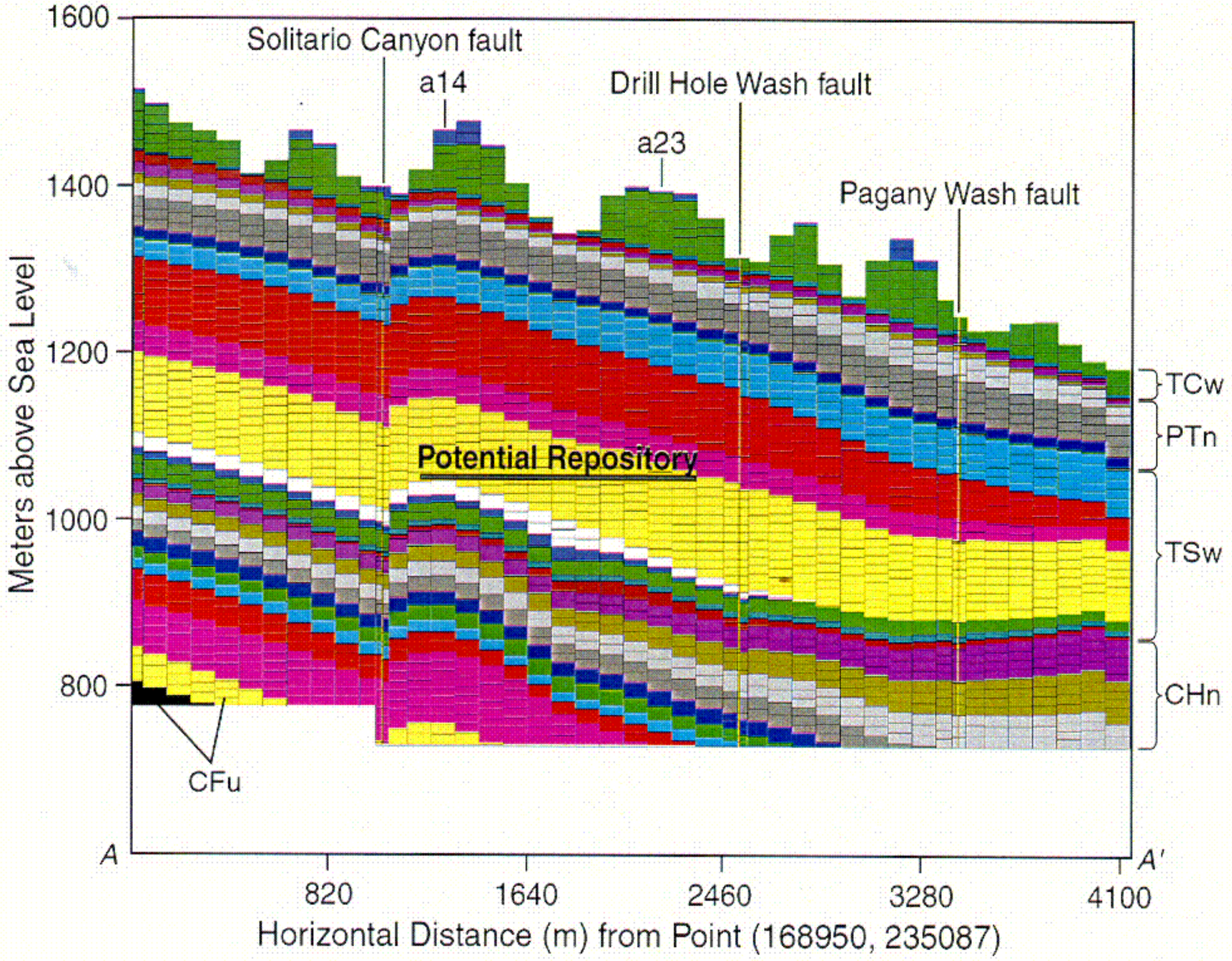

154_0026.ai

Source: TerBerg 2001 [DIRS 155111].

Figure 11.3.2-4. Two-Dimensional Numerical Grids for the East West (A-A') Cross Section

C01

(a)

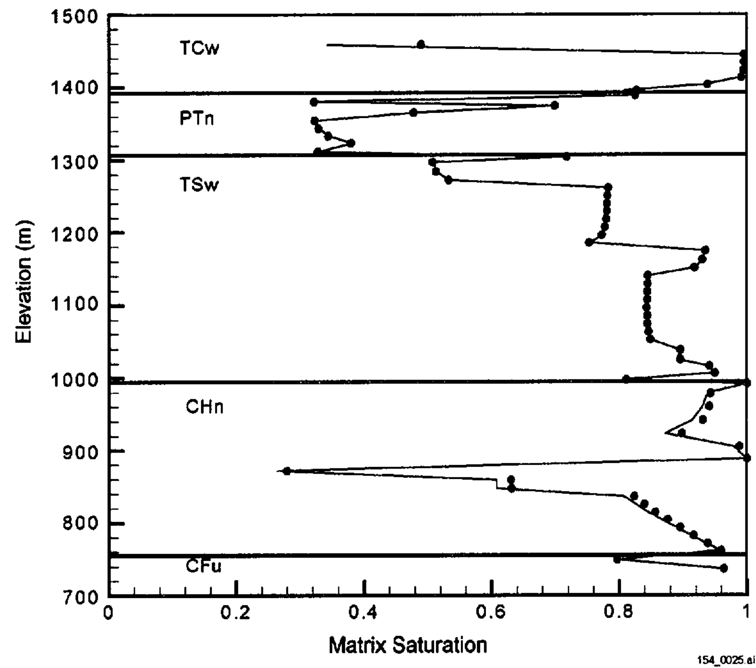

(b)

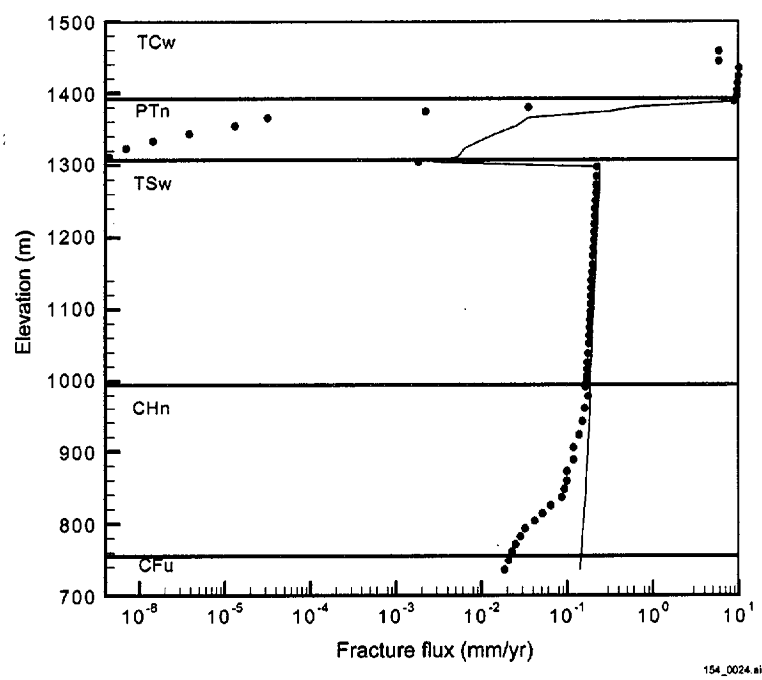

154_0025.ai / 154_0024.ai

Source: TerBerg 2001 [DIRS 155111].

NOTE: Dual permeability model (solid line); multiple interacting continua model (circles).

Figure 11.3.2-5. Comparison of (a) Saturation and (b) Fracture-Flux Output from Two Simulation Models for Vertical Column a14

(a)

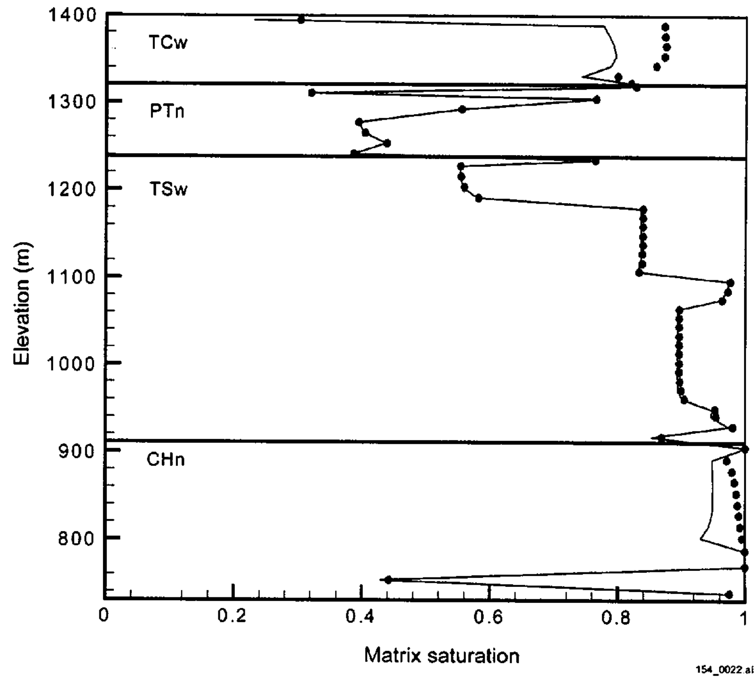

(b)

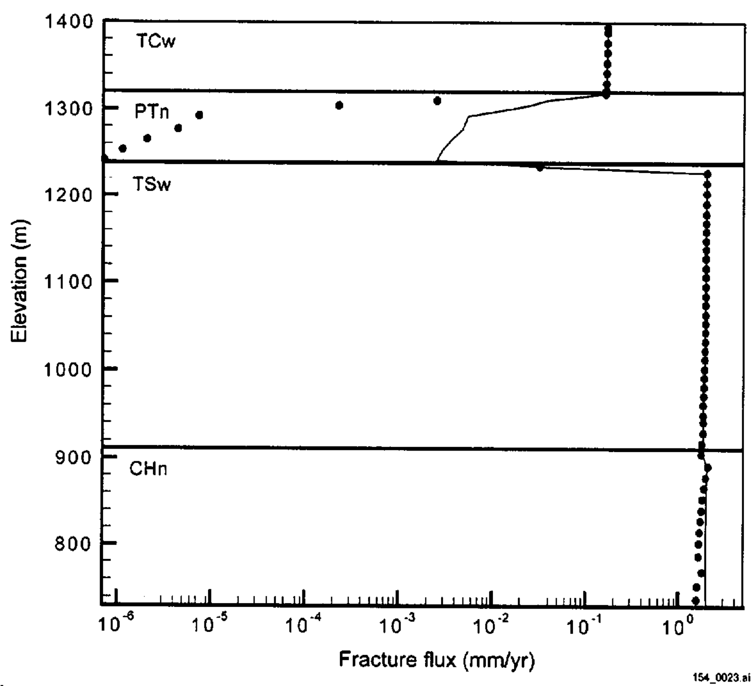

154_0022.ai / 154_0023.ai

Source: TerBerg 2001 [DIRS 155111].

NOTE: Dual permeability model (solid line); multiple interacting continua model (circles).

Figure 11.3.2-6. Comparison of (a) Matrix-Saturation and (b) Fracture-Flux Output from Two Simulation Models for Vertical Column a23

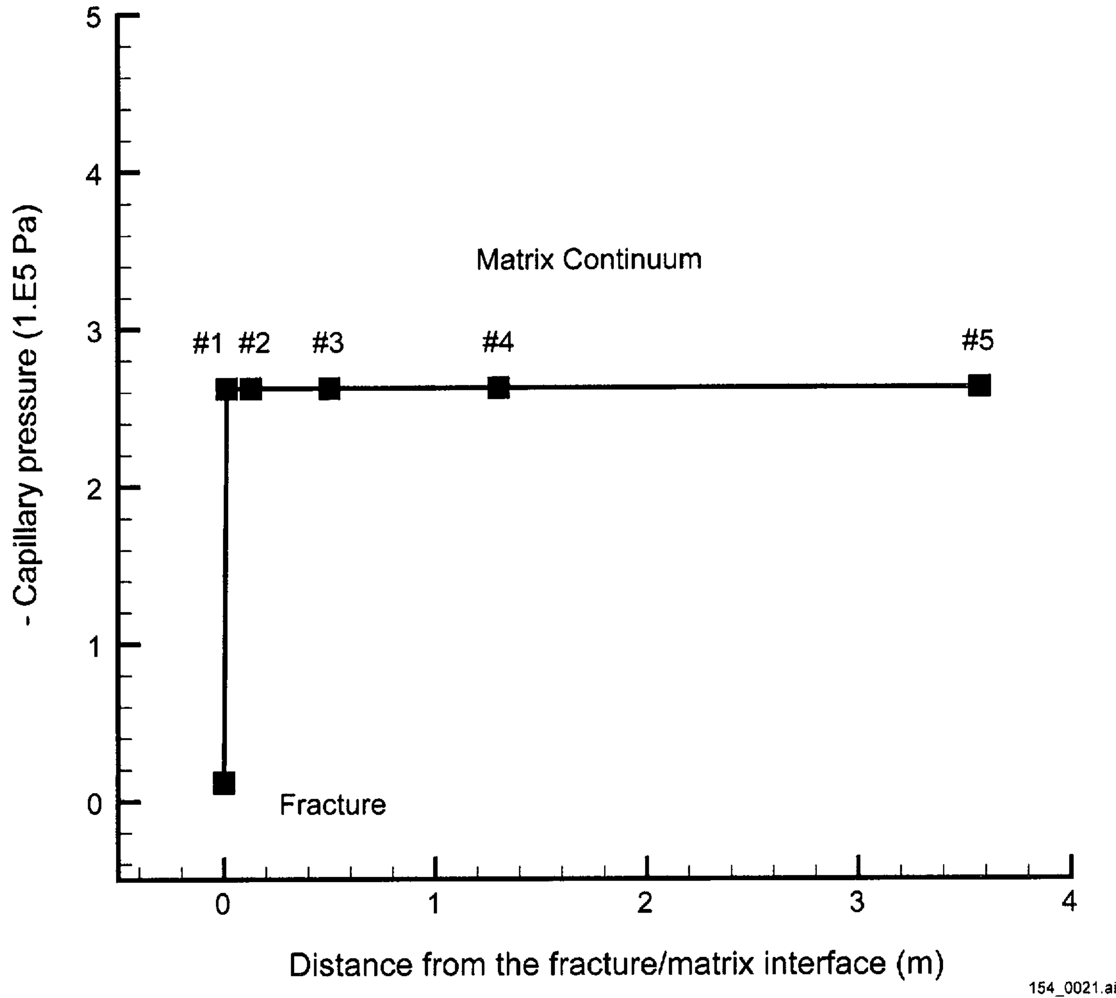

154_0021.ai

Source: TerBerg 2001 [DIRS 155111].

NOTE: Data for column a14 and a matrix block are located at an elevation of 923 m.

Figure 11.3.2-7. Distribution of Capillary Pressures Within a Matrix Block

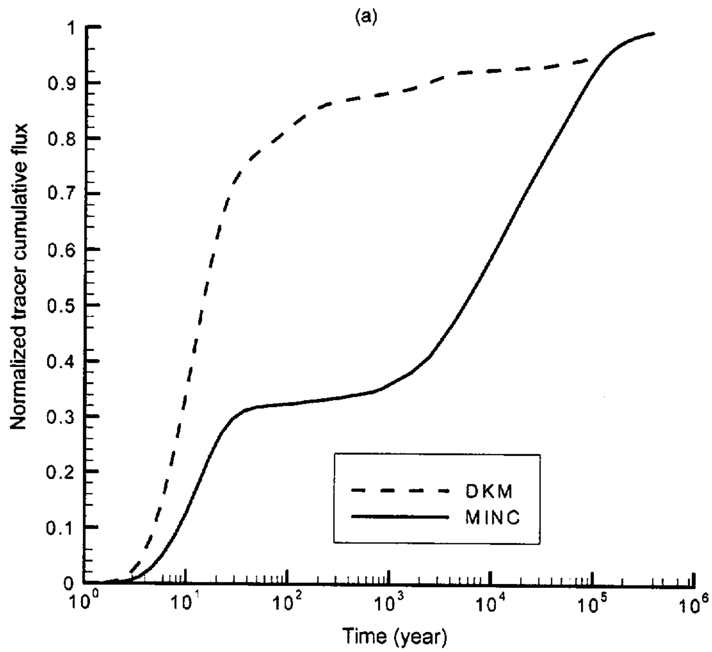

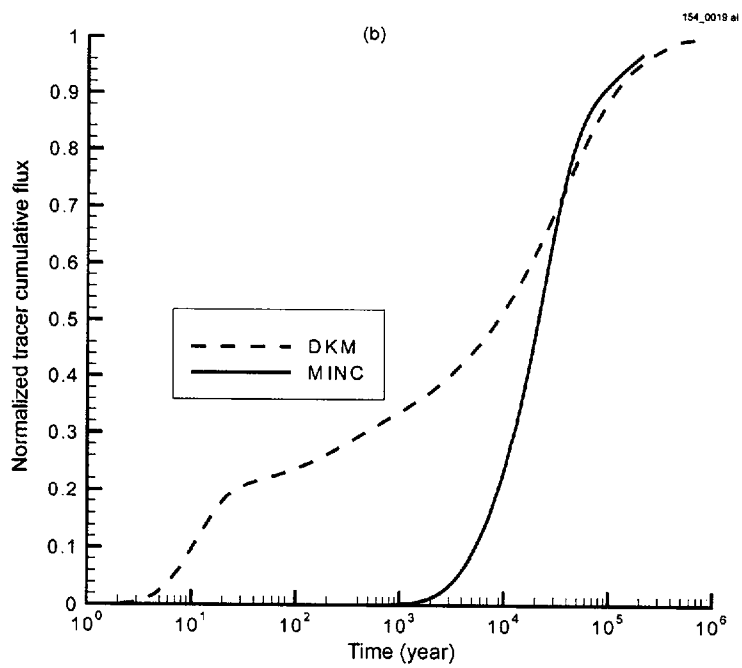

154_0019.ai / 154_0020.ai

Source: TerBerg 2001 [DIRS 155111].

NOTE: Dual permeability model (DKM); multiple interacting continua model (MINC). Model run with molecular diffusion coefficient set at (a) 3.2×10^{-11} m^2/s and (b) 0 m^2/s.

Figure 11.3.2-8. Normalized Tracer Cumulative Flux at Water Table as a Function of Time

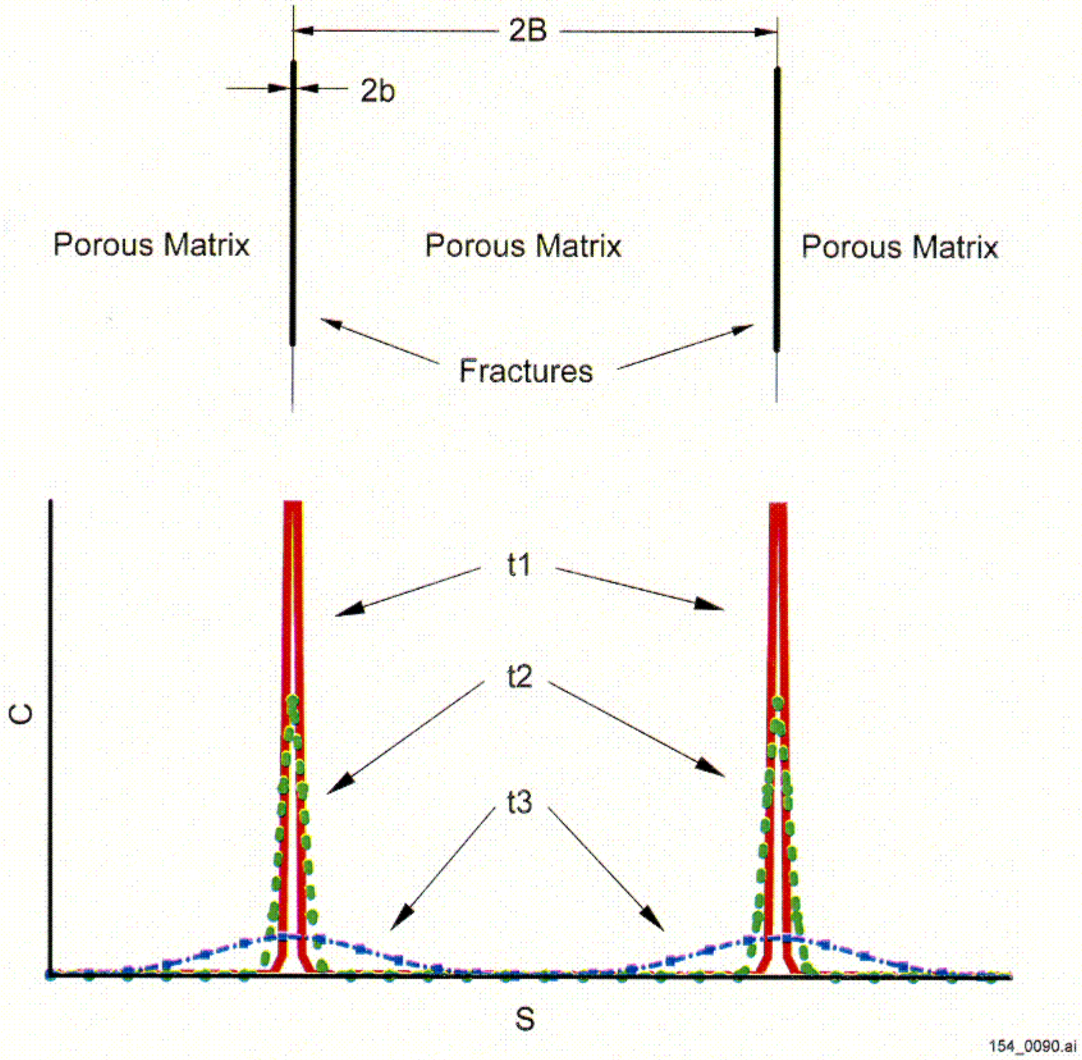

154_0090.ai

Source: TerBerg 2001 [DIRS 155033].

NOTE: C can be interpreted as the probability density function of the particles t3>t2>t1. S = distance, B = fracture spacing, and b = fracture aperture.

Figure 11.3.3-1. Schematic of the Propagation of a Pulse in Fracture-Matrix System with Time

C02

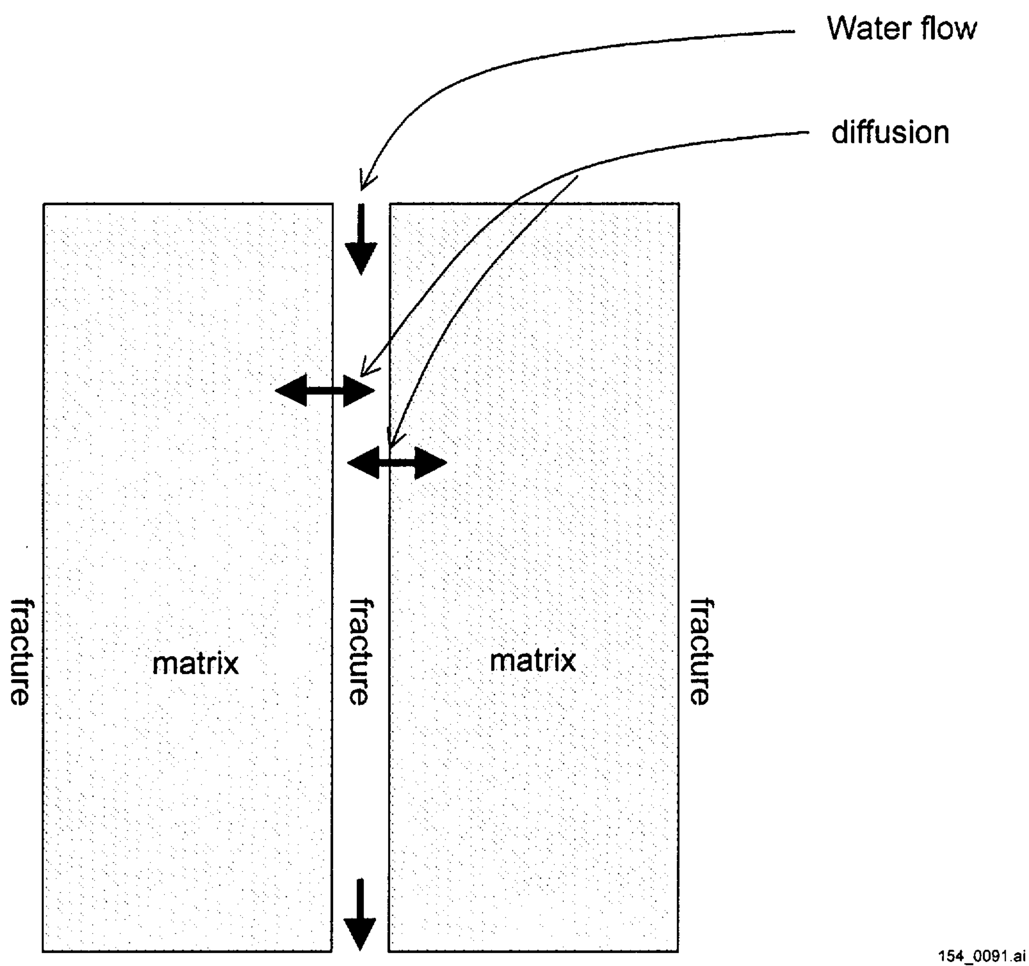

154_0091.ai

Source: TerBerg 2001 [DIRS 155033].

Figure 11.3.3-2. Schematic of a Parallel Fracture System without Water Flow between the Fractures and the Matrix

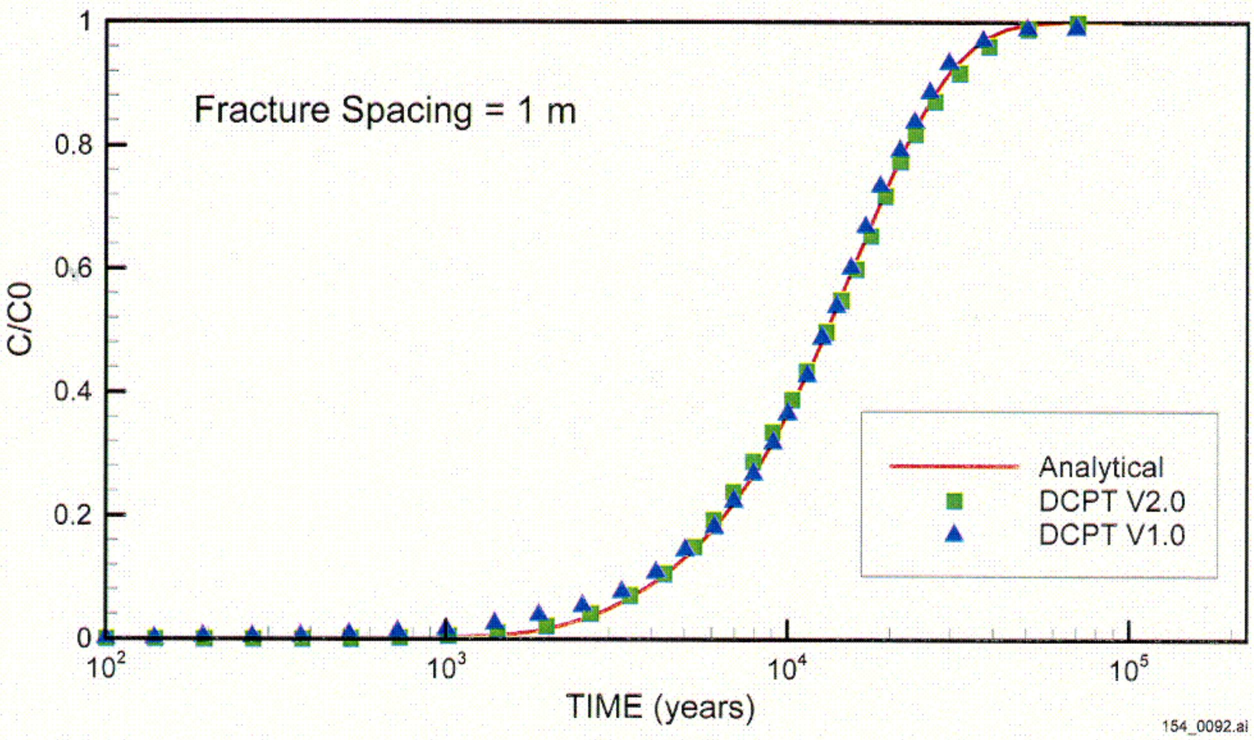

154_0092.ai

Source: TerBerg 2001 [DIRS 155033].

NOTE: The current model uses DCPT v1.0; DCPT v2.0 is a more-refined version. C is the concentration of tracer, and CO in the concentration at inlet.

Figure 11.3.3-3. Predicted Breakthrough of the Current Model, a More-Refined Model, and the Analytical Solution using 1 m Fracture Spacing

C03

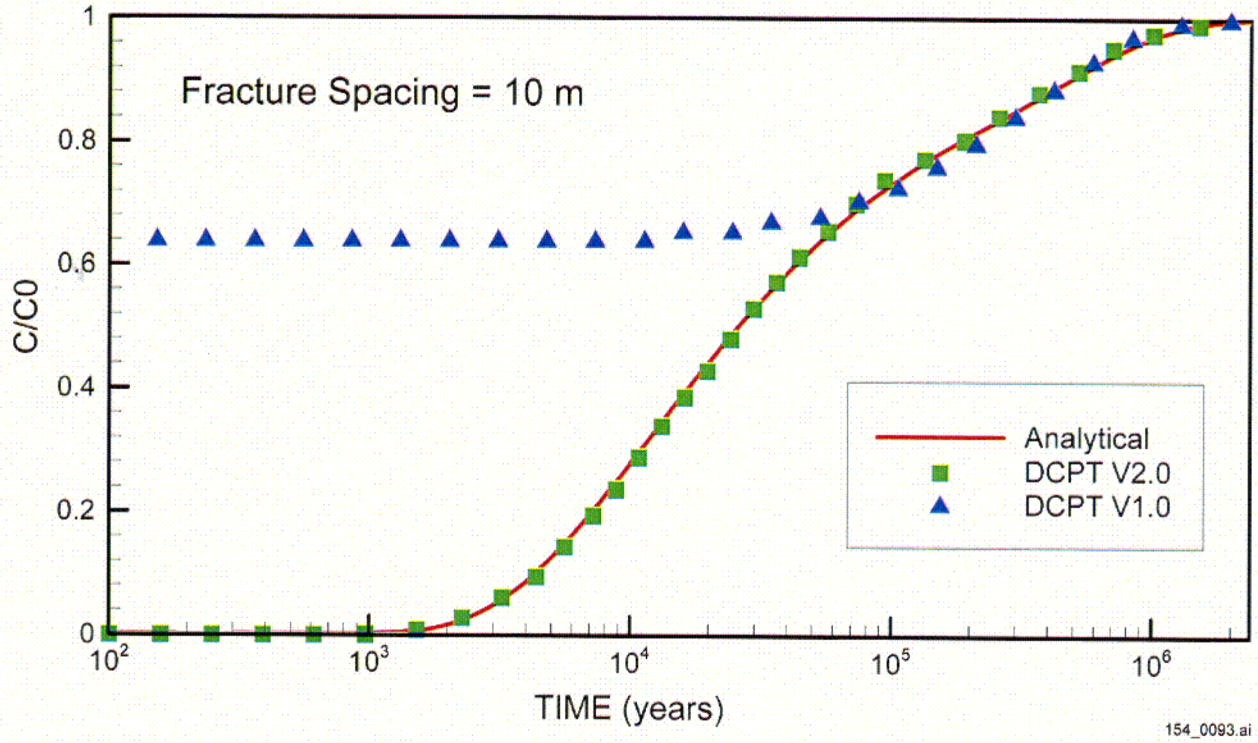

154_0093.ai

Source: TerBerg 2001 [DIRS 155033].

NOTE: The current model uses DCPT v1.0; DCPT v2.0 is a more-refined version. C is the concentration of tracer, and CO is the concentration at inlet.

Figure 11.3.3-4. Predicted Breakthrough by the Current Model, a More-Refined Model, and the Analytical Solution using 10 m Fracture Spacing

C04

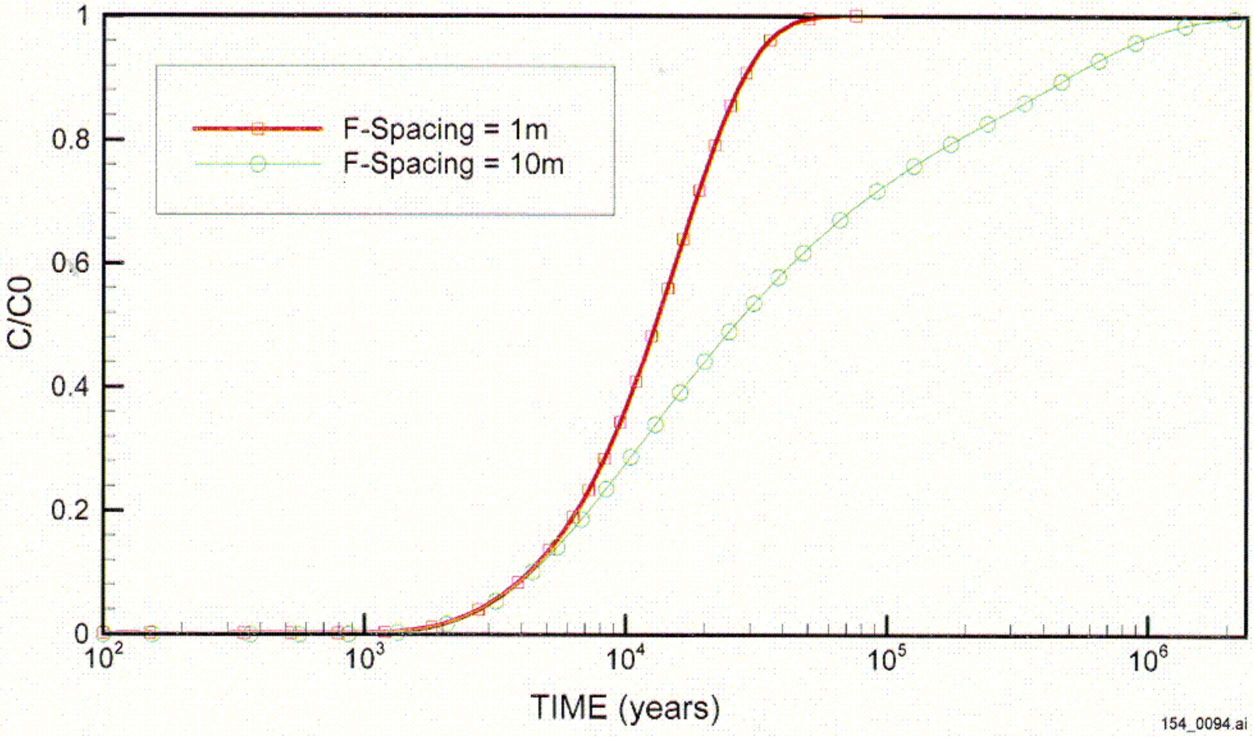

154_0094.ai

Source: TerBerg 2001 [DIRS 155033].

NOTE: C is the concentration of tracer, and CO is the concentration at inlet.

Figure 11.3.3-5. Effect of Fracture Spacing on Breakthrough as a Function of Time

C05

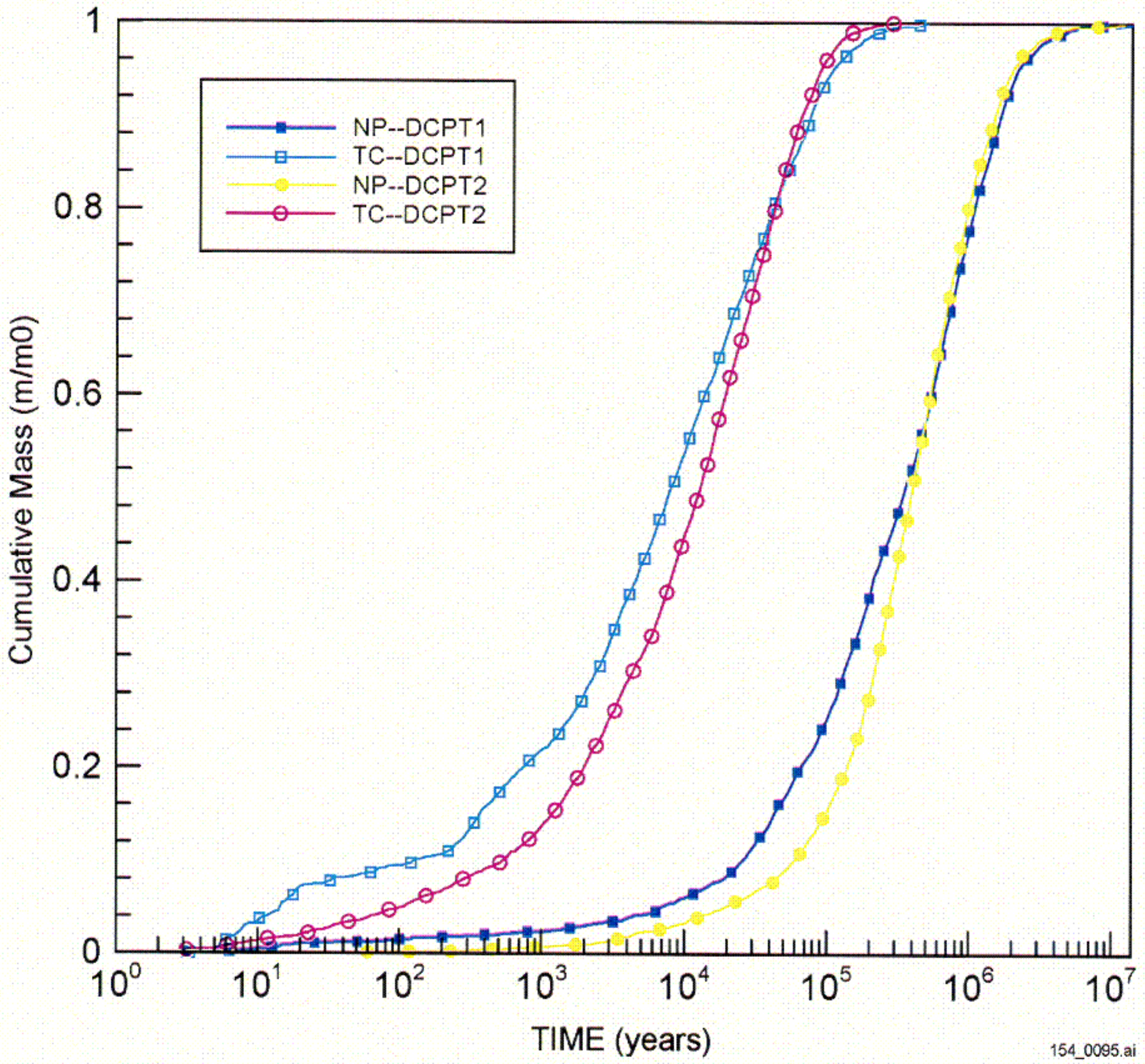

154_0095.ai

Source: TerBerg 2001 [DIRS 155033].

NOTE: The current model uses DCPT v1.0; DCPT v2.0 is a more-refined version. The base case is TSPA-SR (CRWMS M&O 2000 [DIRS 153246] with present-day mean infiltration. NP = neptunium, TC = technetium.

Figure 11.3.3-6. Predicted Cumulative Breakthrough Curves for the Base Case of the Unsaturated Zone Transport System, the Current Model, and the More-Refined Model

C06

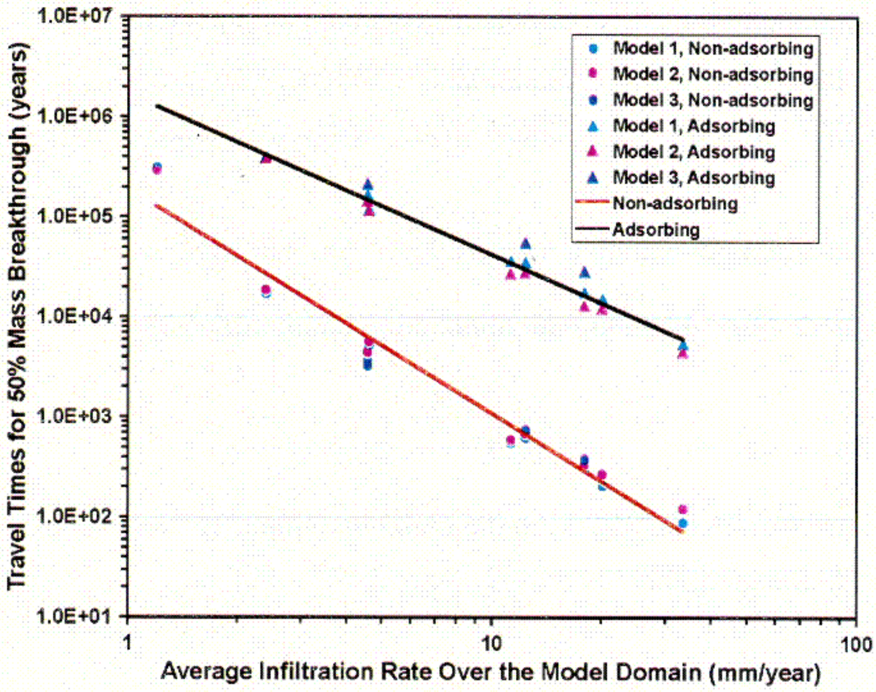

154_0049a.ai

Source: CRWMS M&O 2000 [DIRS 122797], Figure 6-57, Tables 6-29, 6-30, and 6-31.

NOTE: Transport times at 50 percent mass breakthrough for 42 simulation scenarios (model 1, 2, and 3 denote three types of perched water models).

Figure 11.3.4-1. Correlations of Average Infiltration Rates and Groundwater Travel or Tracer Transport Times

C07

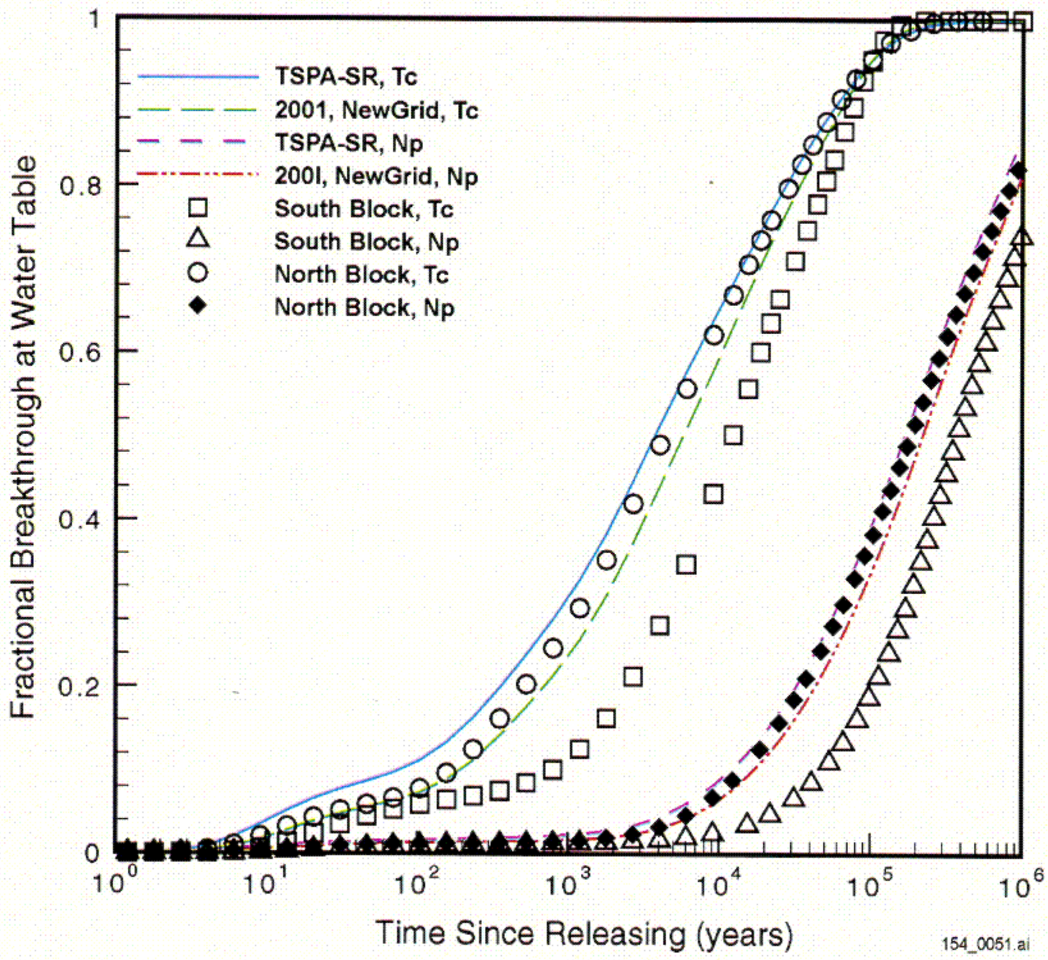

154_0051.ai

Source: Bodvarsson 2001 [DIRS 154669], Attachment 13, p. 27.

NOTE: TSPA-SR refers to results presented in CRWMS M&O (2000 [DIRS 153246]). TSPA-SR data were taken from CRWMS M&O (2000 [DIRS 122797], Section 6.7.3). Other data are from TerBerg (2001 [DIRS 155032]. Time since releasing from the potential repository using the new unsaturated zone flow field and TSPA-SR flow field for different releasing scenarios.

Figure 11.3.4-2. Simulated Breakthrough Curves of Cumulative Tracer and Radionuclide Mass Arriving at the Water Table

C08

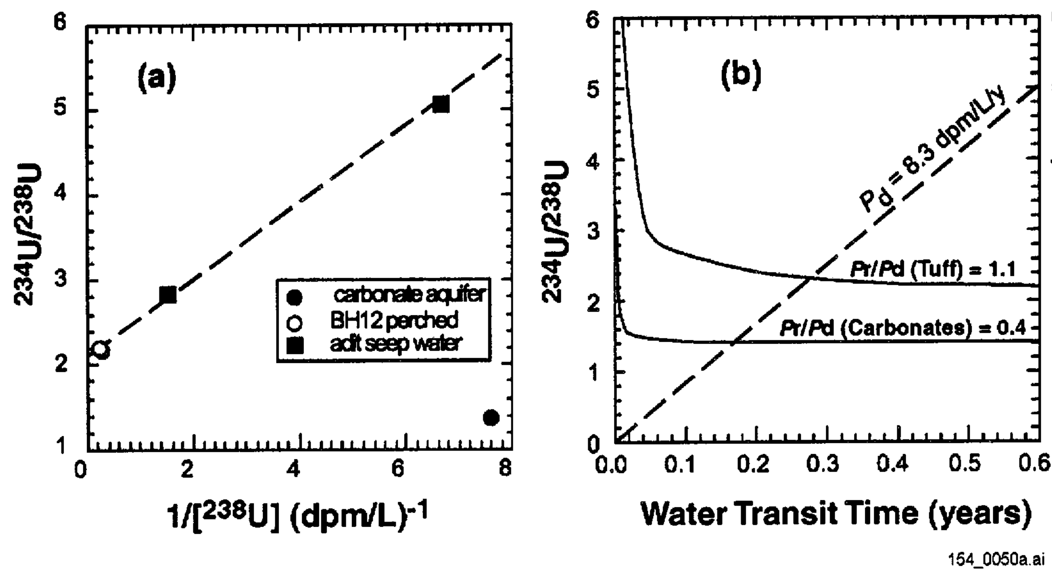

154_0050a.ai

Source: Pickett and Murphy 1999 [DIRS 110009], Figure 5) for (a); (b) derived from (a) as discussed below.

NOTE: Dashed line shows a positive linear correlation for waters sampled from the unsaturated zone. P is the supply rate of the dissolved nuclide through rock dissolution (P_d) and alpha recoil (P_r). The slope and intercept obtained through linear regression in (a) were used to derive P_d and P_r. shown in (b) (b) uranium-234/uranium-238 (solid lines), and uranium-238 activity (dashed line) as a function of water transit time in the unsaturated zone, showing a rapid decrease of uranium-234/uranium-238 to a relatively constant level within a couple of weeks after the water enters the unsaturated zone. To account for the low uranium-234/uranium-238 ratio of 1.39 in the carbonate-aquifer as shown in (a), the P_r/P_d ratio would be about 0.4, a ratio about three times smaller than that of unsaturated zone.

Figure 11.3.4-3. Uranium Activity Ratios in Peña Blanca Waters

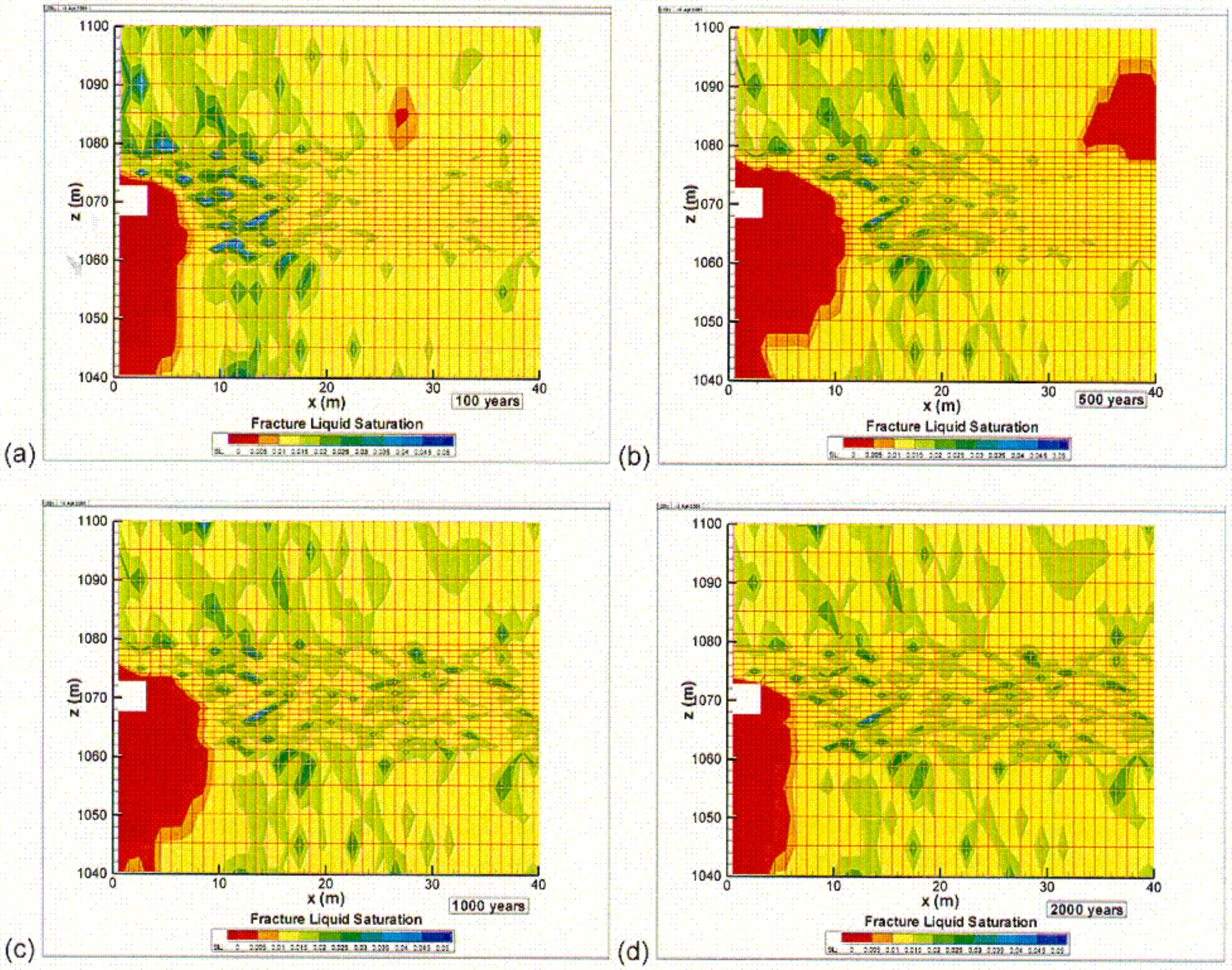

154_0258.ai

154_0258.ai

Source: Derived from data presented in Bodvarsson (2001 [DIRS 154669], Attachment 17, pp. 56 and 62).

NOTE: Four cases depict liquid saturation at (a) 100 years, (b) 500 years, (c) 1,000 years, and (d) 2,000 years.

Figure 11.3.5-1. Liquid Saturation Distributions in the Fracture Continuum for the Higher-Temperature Case

C09

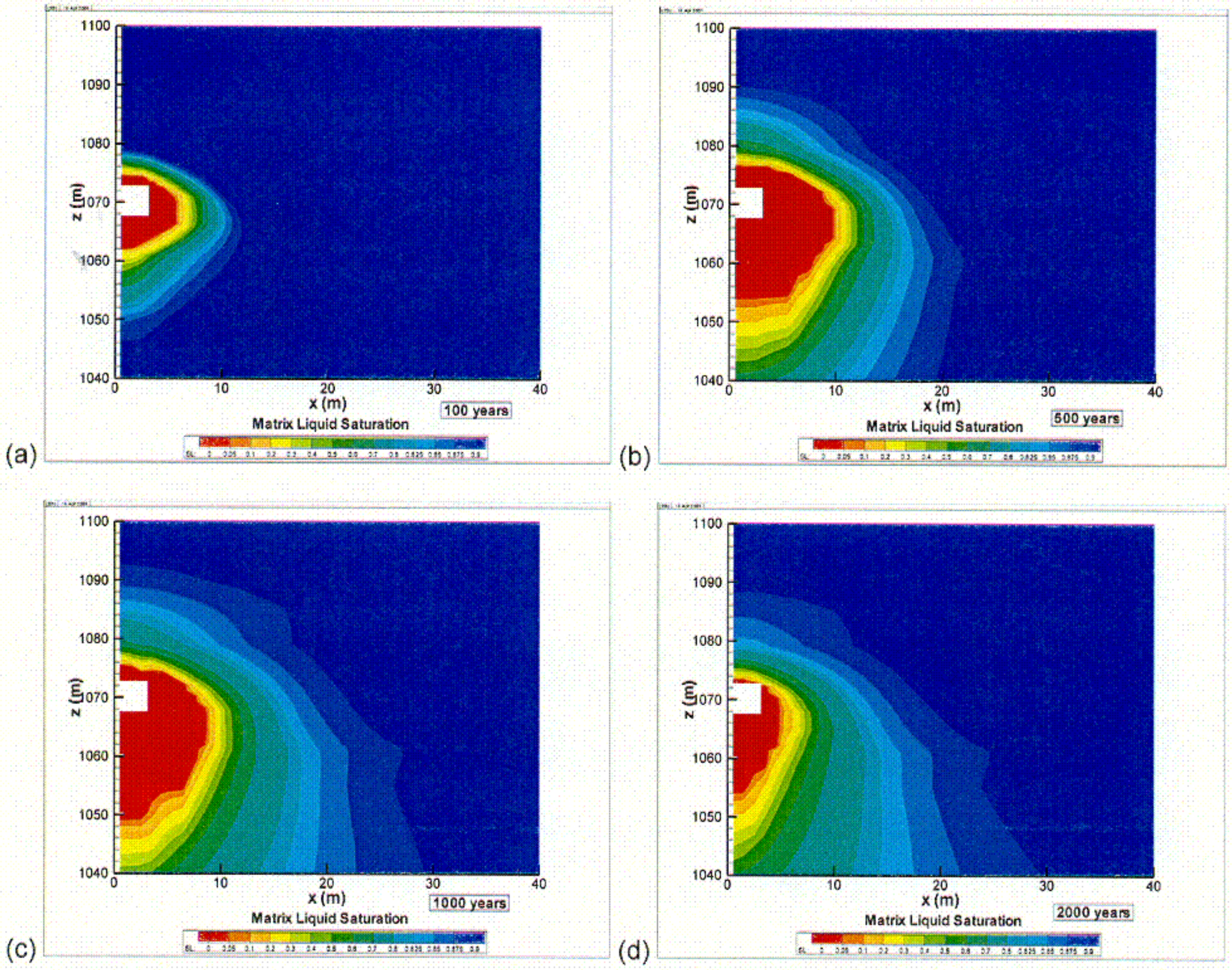

154_0257.ai

154_0257.ai

Source: Derived from data presented in Bodvarsson (2001 [DIRS 154669], Attachment 17, pp. 56 and 61).

NOTE: Four cases depict liquid saturation at (a) 100 years, (b) 500 years, (c) 1,000 years, and (d) 2,000 years.

Figure 11.3.5-2. Liquid Saturation Distributions in the Matrix Continuum for the Higher-Temperature Case

C10

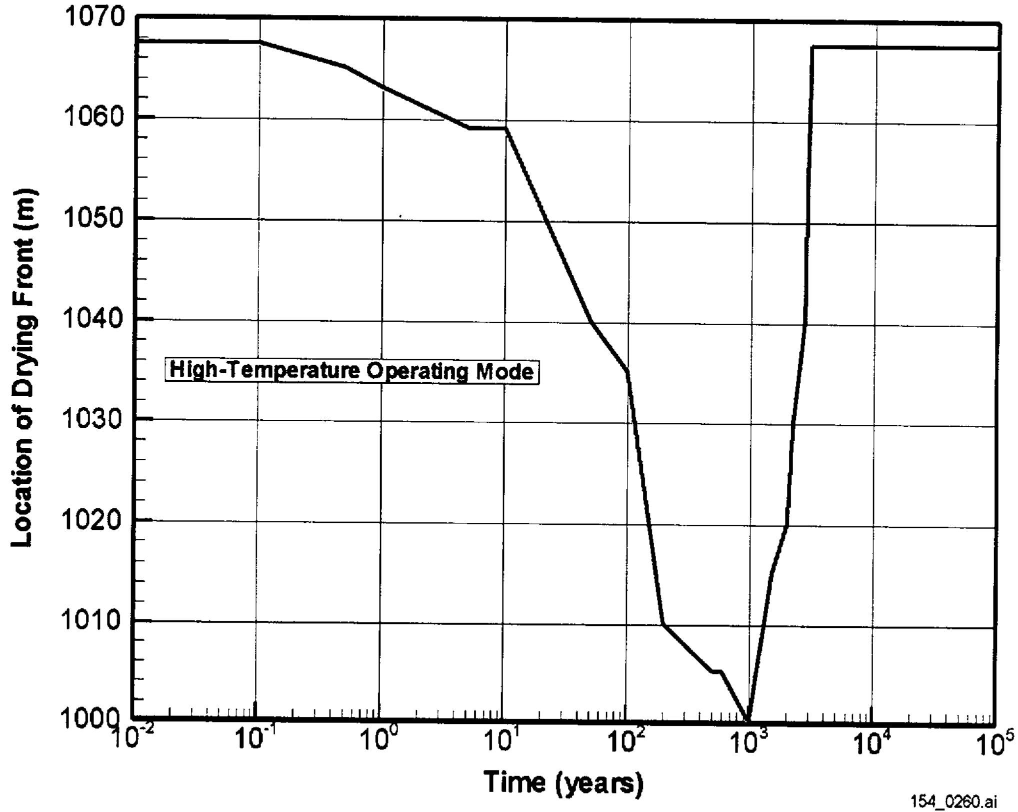

154_0260.ai

Source: Bodvarsson 2001 [DIRS 154669], Attachment 17, p. 77.

Figure 11.3.5-3. Changes in the Depth of the Dryout Zone over Time for the Higher-Temperature Case

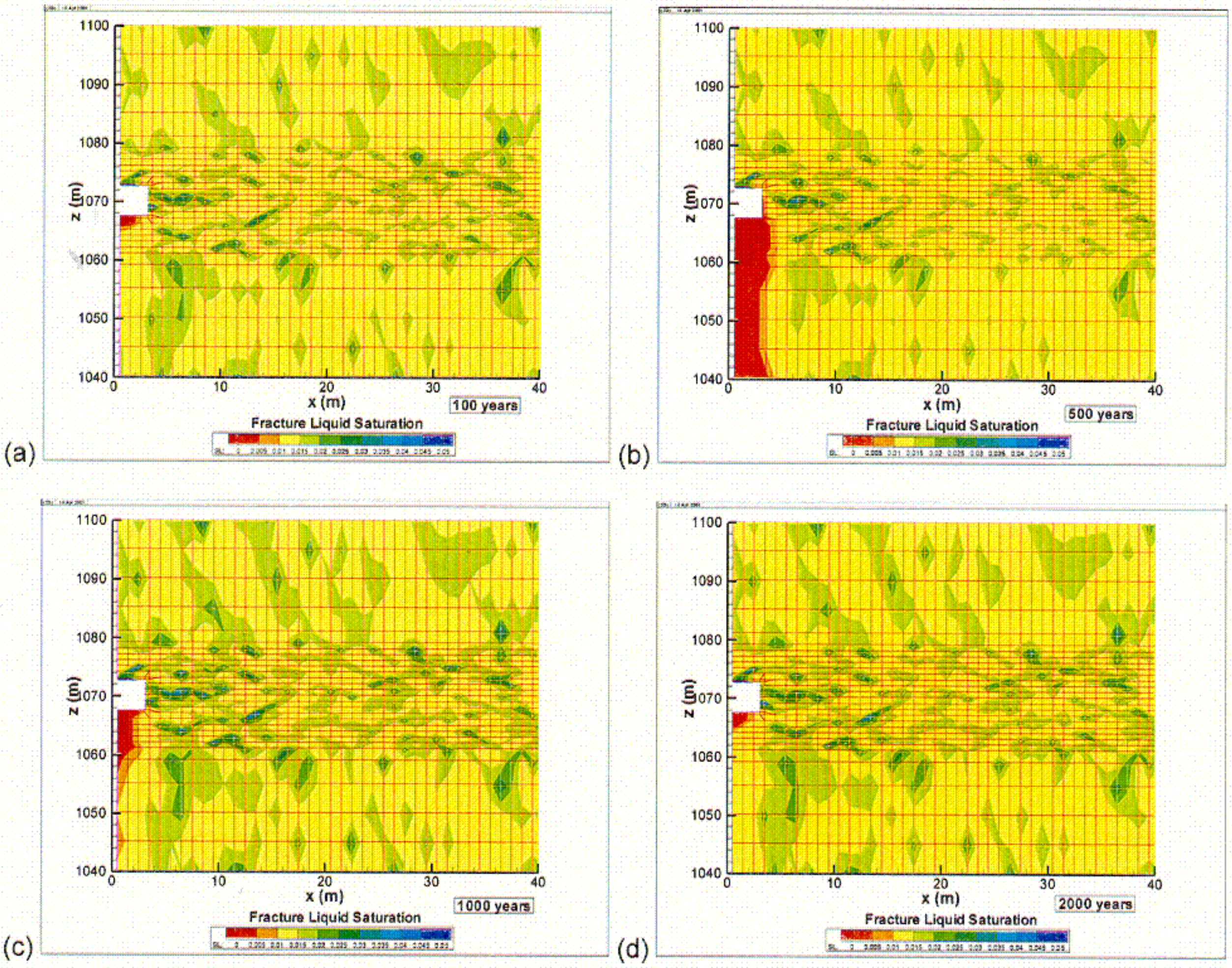

154_0259.ai

154_0259.ai

Source: Derived from data presented in Bodvarsson (2001 [DIRS 154669], Attachment 17, pp. 69 and 71).

NOTE: Four cases depict liquid saturation at (a) 100 yrs, (b) 500 yrs, (c) 1,000 yrs, and (d) 2,000 yrs.

Figure 11.3.5-4. Liquid Saturation Distributions in the Fracture Continuum for the Lower-Temperature Case

c 11

INTENTIONALLY LEFT BLANK